Szklarska Poręba, Poland
9–12 June 2024

9th International Symposium on Applied Electromagnetics SAEM 2024

SAEM 2024
Szklarska Poręba, Poland

BOOK OF DIGESTS SAEM'24

Organised by

PTZE Polish Society of Applied Electromagnetics, Poland

University of Maribor
Faculty of Energy Technology, Slovenia

Ss. Cyril&Methodius University in Skopje
Faculty of Electrical Engineering & Information Technologies, North Macedonia

PTZE POLISH SOCIETY OF APPLIED ELECTROMAGNETICS

9th INTERNATIONAL SYMPOSIUM ON APPLIED ELECTROMAGNETICS SAEM'24

9–12 June 2024, Szklarska Poręba, Poland

BOOK OF DIGEST SAEM'24

Co-organizers

Polish Society of Applied Electromagnetics, POLAND

Ss. Cyril & Methodius University of Skopje
Faculty of Electrical Engineering & Information Technologies, NORTH MACEDONIA

University of Maribor, Faculty of Energy Technology, SLOVENIA

Warszawa, 2024

PTZE POLSKIE TOWARZYSTWO ZASTOSOWAŃ ELEKTROMAGNETYZMU

Title: Book of digest SAEM’24

Cover graphic designed by: Włodzimierz Mazerant

Warszawa 2024

ISBN 978-83-88131-07-3

9th International Symposium on *APPLIED ELECTROMAGNETICS* SAEM'24

Szklarska Poręba, 9–12 June 2024

INTERNATIONAL SCIENTIFIC COMMITTEE

Chairperson:

Andrzej Krawczyk
Polish Society of Applied Electromagnetics, POLAND

Vice-chairs:

Goga Cvetkovski
University of Skopje, Faculty of Electrical Engineering & Information Technologies, NORTH MACEDONIA

Bojan Štumberger
University of Maribor, Faculty of Energy Technology, SLOVENIA

Members:

Željko Hederić, CROATIA
Maria Evelina Mognaschi, ITALY
Vesna Arnautovski-Toseva, NORTH MACEDONIA
Maja Celeska-Krstevska, NORTH MACEDONIA
Lidija Petkovska, NORTH MACEDONIA
Jovica Vuletić, NORTH MACEDONIA
Anna Koziorowska, POLAND
Ewa Korzeniewska, POLAND
Roman Kubacki, POLAND
Marek Lis, POLAND
Tomasz Rymarczyk, POLAND
Rastko Fišer, SLOVENIA
Miralem Hadžiselimović, SLOVENIA
Damijan Miljavec, SLOVENIA
Zdravko Praunseis, SLOVENIA
Sebastijan Seme, SLOVENIA
Gorazd Štumberger, SLOVENIA
Mladen Trlep, SLOVENIA
Mykhaylo Zagyrniak, UKRAINE

LOCAL ORGANISING COMMITTEE

Chairperson:

Ewa Korzeniewska, POLAND

Members:

Andrzej Jąderko, POLAND
Leszek Kasprzyk, POLAND
Anna Zielińska, POLAND

CONTENTS

Welcome address

The International Scientific Committee of SAEM'24 and the Local Organizing Committee are pleased to welcome all the participants of both conferences.

The SAEM'24 Symposium continues the tradition of joint conferences, organized by the countries of Macedonia, Poland and Slovenia in previous years: Ohrid (Macedonia, 2006), Zamość (Poland, 2008), Ptuj (Slovenia, 2010), Sopron (Hungary, 2012), Skopje (Macedonia, 2014), Wrocław (Poland, 2016), Podcetrtek (Slovenia 2018) and Struga (North Macedonia 2022). The SAEM'20 conference, planned to be held in Osijek, Croatia had to be skipped because of COVID-19 pandemic. This year it is going to be held in Poland, in Szklarska Poręba, the mountain city, placed in the Lower Silesia, near the joint point of Poland, Czech Republic and Germany borders. The conference will be organized simultaneously with XXXIII PTZE Symposium.

Open to researchers from all over the world, it hosted people from such countries as Ukraine, Japan, Hungary, Finland, Turkey, Belgium, Bulgaria and Croatia, not to mention the researchers from the main organising countries.

The Organizers of SAEM'24 cordially invite all the participants to the city of Szklarska Poręba which is a picturesque town located in the heart of the Karkonosze Mountains close to the joint point of three borders, namely those of Poland, German and Czech Republic. The city is known for its breathtaking natural landscapes, rich history and exciting tourist attractions. Whether you are a nature lover, history enthusiast or adventure seeker, Szklarska Poręba has something for everyone.

We do hope that all the participants of the SAEM'24 conference will have very scientifically fruitful time and a lot of positive feelings in Szklarska Poręba. We wish you satisfactory conferences and quiet and happy journeys to and from the conference venue.

Chairpersons
of the International Scientific Committee
Andrzej Krawczyk
Goga Cvetkovski
Bojan Štumberger

Chairperson
of the Local Organizing Committee
Ewa Korzeniewska

Modeling and experimental evaluation of an iron core inductor

Iztok Brinovar[1], Klemen Sredenšek[1], Bojan Štumberger [1,2], Sebastijan Seme[1, 2], Amor Chowdhury[1,3], Miralem Hadžiselimović [1,2]

[1] Faculty of Energy Technology, University of Maribor, Hočevarjev trg 1, Krško, Slovenia, iztok.brinovar@um.si

[2] Faculty of Electrical Engineering and Computer Science, University of Maribor, Koroška cesta 46, Maribor, Slovenia

[3] Faculty of Mechanical Engineering, University of Ljubljana, Aškerčeva cesta 6, Ljubljana, Slovenia

Abstract

This article deals with modeling and experimental evaluation of an iron core inductor. Measurements are conducted to assess the impact of residual magnetic flux density in the iron core on the transient response during the energization of the iron core inductor with alternating voltage. The article also addresses different experimentally based methods for determining magnetic flux linkage characteristics and discusses different approaches to defining and modeling the magnetic nonlinearity of an iron core inductor. Nonlinear dynamic models, which include static or dynamic inductances, are experimentally evaluated to confirm their accuracy and applicability.

1. Introduction

Electromagnetic devices and electric machines typically feature magnetic cores made from ferromagnetic materials known for their magnetically nonlinear properties. One of the simplest electromagnetic devices with a magnetic core is an iron core inductor. The magnetically nonlinear behaviour of the iron core inductor can be described in the form of current dependent magnetic flux linkage characteristics $\psi(i)$. Several methods appropriate for determining magnetic flux linkage characteristics of electromagnetic devices and electric machines are shown in [1] and [2]. In this paper two experimentally based methods for determining magnetic flux linkage characteristics are presented and evaluated. The paper also presents different approaches of defining and modeling the magnetic nonlinearity of an iron core inductor. Definitions of magnetically nonlinear parameters of the model in terms of static ($L_s(i)$) and dynamic inductances ($L_d(i)$) are presented (Fig. 1) together with their influence on calculated currents during transient and steady state.

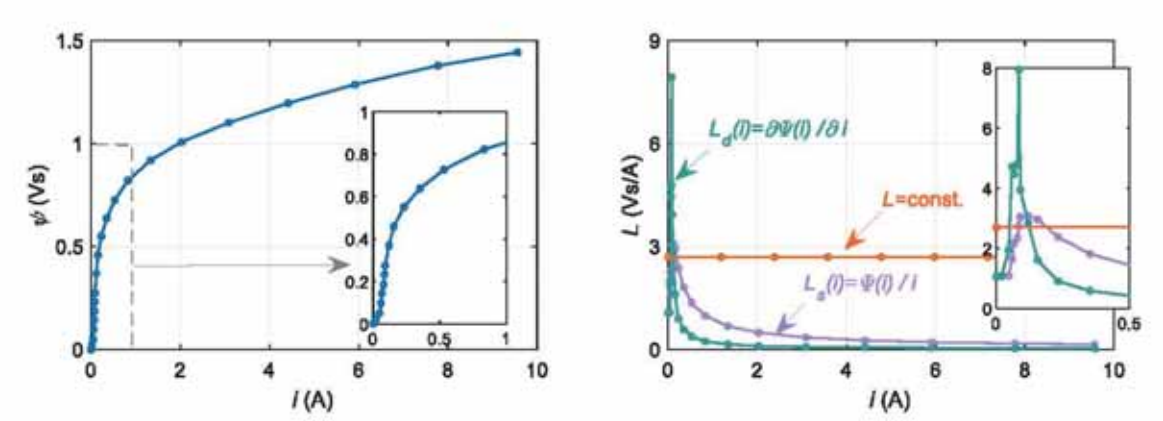

Fig. 1: Magnetic flux linkage characteristic $\psi(i)$, static inductance $L_s(i)$, dynamic inductance $L_d(i)$.

2. Experimental and simulation results

During transients, such as switch-on modes, AC machines and devices may draw several times their rated current when first energized, for several cycles of the input waveform. Worst-case inrush currents occurs when the iron core inductor is switched on at or near zero crossing of the applied voltage and if the polarity of the voltage half cycle has the same polarity as the residual flux density (B_r) in the iron core. Fig. 2 is showing measured voltage and currents during the switch-on of the iron core inductor for the cases when the residual flux density in the core is: a) zero (B_r=0), b) positive (+B_r) and c) negative (-B_r). Also, the results in Fig. 3 show substantial differences between currents calculated with static and dynamic inductances and calculated currents where magnetic nonlinearity is neglected.

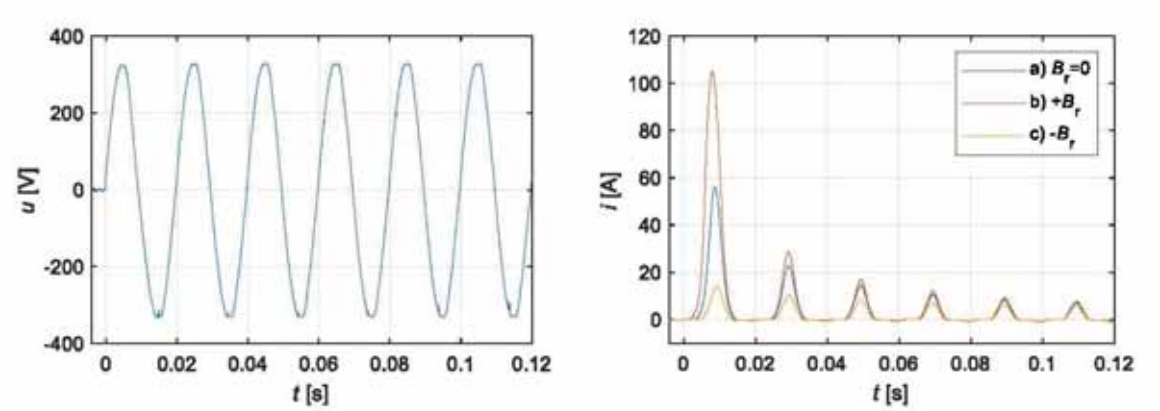

Fig. 2: Applied voltage and responding current during the switch-on of the iron core inductor.

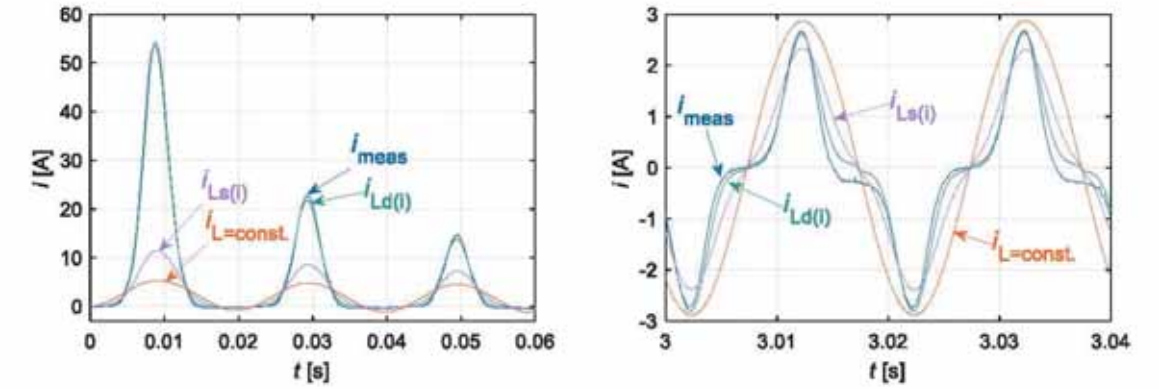

Fig. 3: Measured current i_{meas} and currents calculated using static inductance $i_{Ls(i)}$, dynamic inductance $i_{Ld(i)}$, and constant inductance $i_{L=const.}$ during a) transient and b) steady state.

3. Conclusion

In electric machines and electromagnetic devices in which inductances vary significantly throughout the range of operation, the knowledge of static and dynamic inductances is essential. Although both the static and dynamic inductances are current dependent, it was shown that only their proper use can lead to the correct results.

References

[1] G. Štumberger, B. Polajžer, B. Štumberger, M. Toman, D. Dolinar: "Evaluation of experimental methods for determining the magnetically nonlinear characteristics of electromagnetic devices", *IEEE transactions on Magnetic*, 2005.

[2] G. Štumberger, Ž. Plantić, B. Štumberger, T. Marčič: "Impact of static and dynamic inductance on calculated time responses", *Przeglad Elektrotechniczny*, 2011.

Analysis of power quality parameters in networks supplying apartment blocks, single-family house, and industrial facility

Aleksander Chudy[1], Paweł Mazurek[1], Korneliusz Pawlak[2]

[1] Lublin University of Technology, Lublin

[2] Ball Packaging Europe Lublin Sp. z o.o.

Introduction

Nowadays, the necessity for reliable and high-quality electrical power is vital across varied sectors, ranging from residential to industrial settings. Ensuring the stability and efficiency of power supply networks is essential to satisfy the demands of occupants and sustain the productivity of industrial facilities. With this necessity in mind, this study gives an analysis of power quality parameters in networks providing apartment blocks, a single-family house, and an industrial facility.

For apartment blocks, the primary concern often revolves around managing diverse and fluctuating loads from multiple units within the same building. Issues such as harmonic distortion, voltage fluctuations, and power factor imbalance can arise due to the collective impact of various appliances and equipment used by residents [1].

In single-family houses, while the scale may be smaller compared to apartment blocks, similar concerns regarding load diversity and quality persist. Additionally, factors such as renewable energy integration, electric vehicle charging, and smart home technologies further complicate the energy quality landscape. Addressing these complexities requires tailored approaches to monitoring, analysis, and mitigation strategies [2].

Industrial facilities present a distinct set of challenges, often characterized by high-power loads, sensitive equipment, and stringent reliability requirements. Energy quality issues such as voltage sags, transients, and power interruptions can have significant operational and financial implications for these establishments. Therefore, comprehensive analysis of power quality parameters Is essential to minimize downtime, enhance productivity, and ensure regulatory compliance.

Furthermore, advancements in technology and regulatory frameworks play a crucial role in shaping the landscape of power quality management. Integration of renewable energy sources, deployment of smart grid technologies, and adherence to stringent quality standards are integral components of modern power supply networks.

Methodology and selected results

The Sonel PQM-711 power quality analyser (Sonel F-2 current clamps) was used for power quality parameters measurements in the apartment blocks and the industrial facility. For the assessment of power quality parameters in the single-family house, the Chauvin Arnoux 8336 power quality analyser was utilized (Chauvin Arnoux MA193 current clamps). The averaging times have been configured as 10 minutes for industrial facility, 3 seconds for the apartment blocks and 1 minute for single-family house.

Figure 1 and Figure 2 show phase voltage variation and voltage harmonic spectrum (95th percentile) concerning apartment blocks, respectively. The measurements revealed an exceedance of the 15th voltage harmonic in the third phase. The 95th percentile reached 0.55%, exceeding the limit of 0.5%.

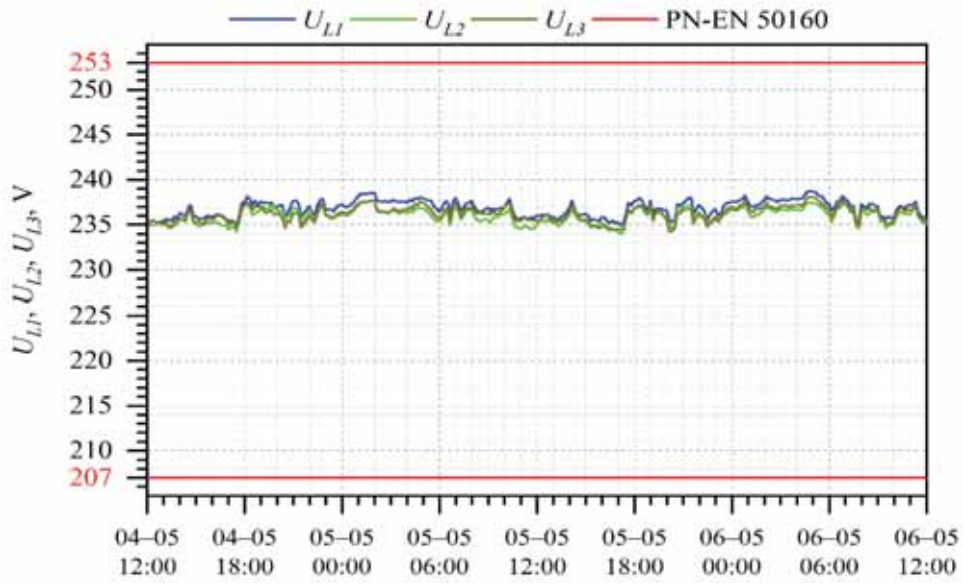

Figure 1. Phase voltage values – apartment blocks

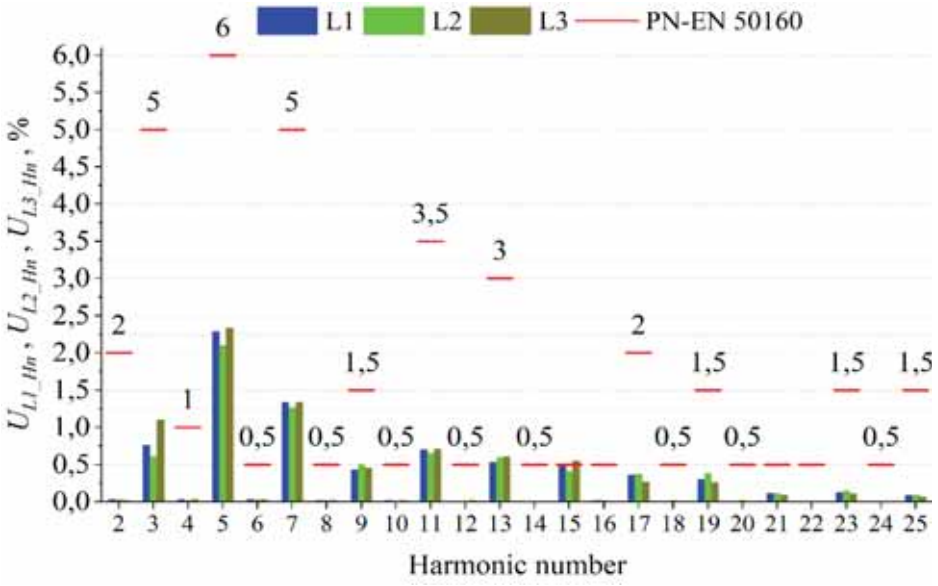

Figure 2. Voltage harmonic spectrum (95th percentile) – apartment blocks

Conclusions

The measurements of power quality parameters across different settings underscores the significance of monitoring and analysis. Utilizing advanced instrumentation tailored to specific environments provides valuable insights to address challenges and improve overall energy efficiency. These results will be compared with regulatory standards to assess compliance and identify areas for improvement.

References

[1] Thentral T. T., Palanisamy R., Usha S., Bajaj M., Zawbaa H. M., Kamel S., Analysis of Power Quality issues of different types of household applications, *Energy Reports*, 8 (2022), 5370-5386

[2] Garabitos Lara E., Electrical dataset of household appliances in operation in one apartment, *Data in Brief*, 51 (2023)

Efficiency maximization of PMSM using equilibrium optimizer algorithm

Goga Cvetkovski

Ss Cyril and Methodius University,
Faculty of Electrical Engineering and Information Technologies,
Rugjer Boskovic 18, P.O. Box 574, 1000 Skopje, North Macedonia,
gogacvet@feit.ukim.edu.mk

Abstract
This paper presents a novel approach to the efficiency improvement of permanent magnet synchronous motor using equilibrium optimizer algorithm (EOA) as an optimisation tool. This algorithm belongs to the so called meta-heuristic optimisation group of algorithms, which so far have proven to be quite suitable for optimisation of standard mathematical functions. The idea is to implement this novel optimisation algorithm for the efficiency improvement of permanent magnet synchronous motor, where the objective function in the optimisation process is the efficiency of the investigated motor. Comparative analysis of the initial and the optimal solutions gained from the optimisation is performed and a number of results will be presented.

1 Introduction

The optimal design of electrical machines has been a challenge for a long period of time. The optimal design is a time consuming process and therefore a number of investigations have been realised in order to implement optimization algorithm in order to speed up the process and make it more reliable. In that manner in this work a novel optimization algorithm named equilibrium optimizer algorithm that belongs to the meta-heuristic group of algorithms or more widely to the group of stochastic methods. Those methods can be divided in four groups: evolutionary algorithms, swarm based algorithms, natural sciences based algorithm and human behaviour based algorithms. The equilibrium optimizer algorithm belongs to the natural sciences methods together with: simulated annealing, gravitational force algorithm, multi-verse algorithm and many other methods. All those methods are based on the theory of a low that belongs to a certain natural science (physics, chemistry mathematics etc.). The investigated optimization method named equilibrium optimizer algorithm [1] is inspired by the equation (1) that describes the control volume mass balance in certain models that is used to estimate both dynamic and equilibrium states.

$$V\frac{dC}{dt} = Q\left(C_{eq} - C\right) + G \tag{1}$$

In equation (1) $V{\cdot}(dC/dt)$ is the rate of change of mass in volume (V), C is the concentration inside the volume (V), V is the control volume, Q is the volumetric flow rate into and out of the control volume, C_{eq} is the concentration at an equilibrium state, and G is the mass generator rate inside the control volume. In the EOA, each particle (solution) is defined with its concentration (position) and it acts as a search agent. The search agents randomly update their concentration with respect to the best-so-far solutions, namely equilibrium candidates, to finally reach to the equilibrium state (optimal result). A well-defined "generation rate" term is proved to invigorate the equilibrium optimizer's ability in exploration, exploitation, and local minima avoidance. The presence of exploration and exploitation features in the EOA ensures a good quality optimization in which the exploration gives to the algorithm an ability to globally search the space. This ability is associated with escaping from local optima and preventing local optima stagnation. Conversely, exploitation is the ability to locally search around

promising solutions in an effort to increase their quality. Similar to other metaheuristic methods the search starts with an initialization where initial population of solutions-concentrations is randomly generated. Each particle in each iteration updates its concentration with random selection among candidates chosen with the same probability. For instance, in the first iteration, the first particle updates all of its concentrations based on $C_{eq(1)}$; then, in the second iteration, it may update its concentrations based on $C_{eq(ave)}$. Until the end of the optimization process, each particle will experience the updating process with all of the candidate solutions receive approximately the same number of updates for each particle. In the full version of the paper a more detailed presentation of the algorithm will be given.

2 Model description and optimization results

The investigated object in this work is a brushless three-phase permanent magnet synchronous motor (PMSM) that has a laminated stator with 36 slots and a rotor with 6-skewed $SmCo_5$ surface-mounted permanent magnets with B_r = 0.95 T. The rated data of the motor are: I=18 A, T=10 Nm and n=1,000 rpm at frequency of 50 Hz.

The goal in this optimization process is to improve the efficiency of the investigated synchronous permanent magnet motor. Since the EO algorithm is defined as a minimization process the objective function is defined as an inverse function of the efficiency of the motor. The following motor parameters have been selected as optimisation parameters in the optimization procedure realised with the EO algorithm: outside radius of the rotor iron core R_{ro}, permanent magnet fraction f_m, permanent magnet radial height h_m, air-gap g, and axial active length of the motor L, as presented in Fig. 1. The results of the optimisation procedure realised with the investigated optimisation algorithm are presented in Table 1, while the objective function and efficiency change during the iterations is presented in Fig. 2. The objective function used for the optimisation is shown below:

$$Objective\ function = \frac{1}{efficiency(R_{ro}, f_m, h_m, g, L)} = \frac{T \cdot \omega_m + P_{Cu} + P_{Fe} + P_{wf}}{T \cdot \omega_m} \tag{2}$$

Table 1 Optimization results

Optimization parameters	Initial motor	EOA solution
R_{ro} (m)	0.042	0.0378
f_m (/)	0.9	0.91483
h_m (m)	0.002	0.0022
g (m)	0.0008	0.00072
L (m)	0.09	0.099
Objective function (pu)	1.177995	1.1358091
Efficiency (pu)	0.8489	0.88043

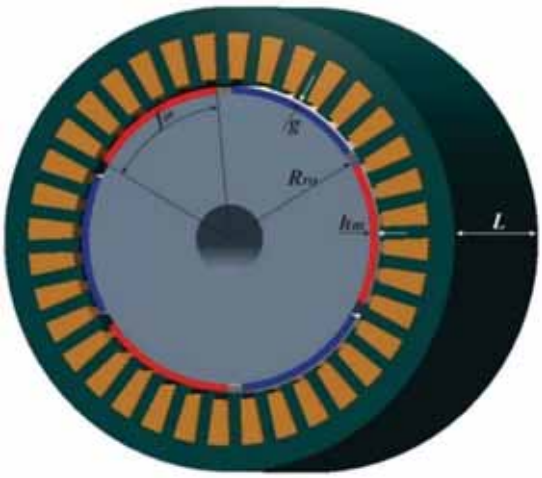

Fig. 1 PMSM optimization parameters

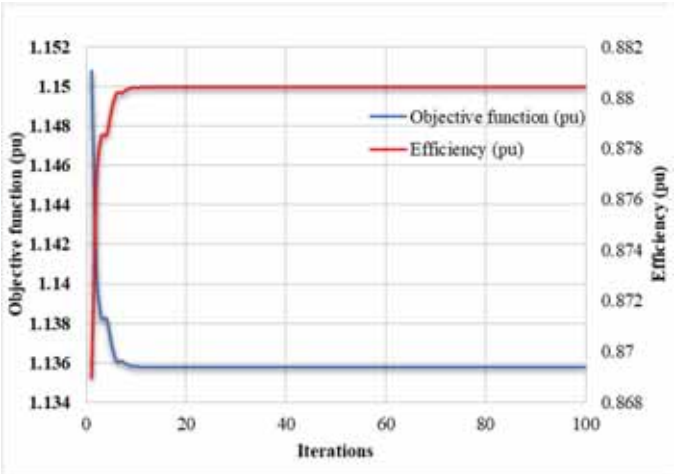

Fig. 2 Objective function and efficiency presentation

In the full version of the paper a detailed comparative analysis of the objective solutions obtained with the equilibrium optimizer based on different motor parameters will be presented. A FEM based comparative analysis of the initial model and the EOA optimized solution will be also presented.

References

[1] A. Faramarzi, M. Heidarinejad, B. Stephens, M. Seyedali, "Equilibrium optimizer: A novel optimization algorithm", *Knowledge Based Systems*, **Vol. 191**, (2020), e105190, pp. 1-39. doi.org/10.1016/j.knosys.2019.105190.

The Scientific Legacy of Professor Lidija Petkovska

Goga Cvetkovski

Ss Cyril and Methodius University,
Faculty of Electrical Engineering and Information Technologies,
Rugjer Boskovic 18, P.O. Box 574, 1000 Skopje, North Macedonia,
gogacvet@feit.ukim.edu.mk

Abstract
In photovoltaic systems it has been always a challenge to determine the methodology for calculation of the maximum power point (MPP) for given system, location and atmospheric conditions. Therefore, many optimization methods are in use as well as different photovoltaic cell circuit presentations. The determination of the MPP in the process of design of a photovoltaic (PV) power plant for the dimensioning of all the applied equipment to determine is quite a challenge and can be of great importance. For that reason, in this paper the MPP will be determined using the teaching and learning optimization algorithm applied on an ideal single-diode cell model.

1. Biographic information

Professor Lidija Petkovska (maiden Šurležanoska) was born on June 13, 1943 in Resen, where she began her primary education. She continued her education in Skopje at Kočo Racin elementary school, and in 1962 she graduated from Josip Broz Tito high school. Then she enrolled in studies at the Technical Faculty in Skopje on the Electrical Engineering study programme. After completing the first year in 1963, she continued her studies at the Faculty of Electrical Engineering in Belgrade and in 1967 graduated in the field of power engineering.

After graduation, in 1967 Prof. Lidija Petkovska got a job as a responsible engineer in the electrical department for maintenance of the Alumina factory in Skopje and remained in this position for almost three years. On February 1, 1970, she was elected as a teaching and research assistant at the Department of Electrical Machines at the Faculty of Electrical Engineering in Skopje. She was elected in the same position in 1973, 1977 and 1980, respectively. In 1972, she enrolled in postgraduate studies in the study programme of Electrical Machines at the Faculty of Electrical Engineering in Skopje. In 1981, she successfully defended her master's thesis entitled "Asynchronous Start of a Synchronous Motor with Silent Poles", and became Master of Electrical Engineering. In 1983, she was elected as a lecturer for the courses Micro-machines and Power Converters. She was elected in the same position in 1985, 1987 and 1991. In 1991, she successfully defended her doctoral thesis entitled "Contribution to the Analysis of the Influence of the Shape of the Excitation Field from Permanent Magnets on the Characteristics of an Electronically Controlled Synchronous Motor with a Three-Dimensional Calculation of the Magnetic Field" and obtained the academic degree of Doctor of Technical Sciences. After defending her doctorate dissertation in the same year, professor Lidija Petkovska was elected to the position of assistant professor. As a result of the exceptional results that Professor Lidija Petkovska achieves in the field of science, in early 1993 she was elected to the title of associate professor in the group of subjects in the field of electrical machines, transformers and devices. At the end of 1997, she was elected to the title of full professor and was re-elected to the same title in the middle of 2003 for the same group of subjects. In her career at the Faculty of Electrical Engineering and Information Technologies Professor Lidija Petkovska was the mentor of over 150 graduate theses, 7 master's theses and 4 doctoral theses. She was also a member of numerous committees for the defence of graduation theses, master's theses and doctoral dissertations.

She retired from the Faculty of Electrical Engineering and Information Technologies in 2008. She continued teaching on bachelor and master level at the Balkan University in Skopje until 2013, and on doctoral studies until the last day in 2023.

2. Teaching work

Her teaching work, as it happened with most of us, started as a teaching assistant on courses taught at the Department of electrical machines, transformers and apparatuses on graduate level. At that time most of the lectures, numerical exercises and laboratory exercises had to be prepared for the first time. During this period of her carrier she gave numerical exercises and laboratory exercises in the following courses: Electromechanical conversion of energy, Electrical machines 1, Electrical machines 2 and Design of electrical machines. In the study years 1978/79 and 1979/1980 she also gave lectures under supervision on the courses Electrical machines 1 and Electrical machines 2 on professional studies level. After becoming a lecturer, she individually prepared lectures and teaching materials for the courses on Micro-machines, Power converters and Non-symmetrical and transient regimes in electrical machines and transformers. In 1995 she published a book in Macedonian language under the title: Micro-machines for the purpose of the course with the same name on graduate studies. On postgraduate studies, as well as doctoral studies she gave lectures on several courses.

3. Scientific work

The scientific work of professor Lidija Petkovska is primarily related to her work done in the framework of her MSc and PhD thesis, as well as related to the theses work of her students on master and doctoral studies. Her scientific work is also related due to the cooperation with other colleagues from different Universities in the world and closely related to research investigation realised in many domestic and international projects. Those works are published in various journals and presented at a large number of conferences and symposia. She was the head of 3 scientific research projects and a participant in 7 funded by the Ministry of Education and Science. She was also the head of 5 development-research projects and a researcher in 6 projects funded by the Ministry of Education and Science of North Macedonia. She was also a head of a TEMPUS project.

Regarding scientific papers in international journals with an impact factor, she has published a total of 42, while in journals without an impact factor she has published over 21. She has also published 4 chapters in international books in the field of electrical machines. The number of published papers at international and domestic conferences is impressive and let’s say it is over 300. The high quality of the scientific papers is confirmed by the large number of citations of her papers by international and domestic authors in the field.

4. Organization of SAEM and ISEF

The history of SAEM is closely related to her enormous will and vision to be an organizer of a conference or symposia. Her idea was greatly supported by professor Andrzej Krawczyk and professor Bojan Štumberger that led to the organization of the first edition of SAEM in 2006 in Ohrid, Macedonia. The other editions followed: SAEM'2008, Zamosc, Poland, SAEM'2010, Ptuj, Slovenia, SAEM'2012, Sopron, Hungary, SAEM'2014, Skopje, Macedonia, SAEM'2016, Wroclaw, Poland, SAEM'2018, Podčetrtek, Slovenia, SAEM'2020, Beli Manastir (Croatia), unfortunately cancelled due to Covid-19 pandemic situation and finally SAEM’2022 in Struga, Macedonia.

Fig. 1. SAEM'2006 opening ceremony

Fig. 2. ISEF'2013 opening ceremony

On the other hand, ISEF'2013 was the conference that was organized in Ohrid, Macedonia in 2013 under the leadership of professor Lidija Petkovska and based on the previous experience in the organization of SAEM. The conference was held in Metropol Lake Resort in from 12-14 September 2013 at which 143 papers were presented by authors from 31 countries.

A data set of electrical energy consumption in sense of different service activities

Klemen Deželak

Environment and Energy Statistics Section, Statistical Office of the Republic of Slovenia (SURS), Litostrojska cesta 54, 1000 Ljubljana, Slovenia,
klemen.dezelak@gov.si

Abstract
Buildings in the service sector, such as offices, hospitals, hotels and schools, could represent a significant consumers of energy. Energy efficient building design, heating, ventilation, air conditioning systems and lighting can help reduce energy consumption in these facilities. With access to detailed energy usage data, consumers can identify areas where they can reduce consumption. Smart meters encourage energy conservation by empowering consumers with knowledge about their usage habits and the impact on their bills. Presented research deals with a monthly smart meters data set of electrical energy consumption in sense of different service activities within four year period in Slovenia.

1. Introduction

The service sector encompasses a wide variety of activities, each with its own energy requirements. For example, office buildings may primarily use electricity for lighting, heating, cooling and powering office equipment, while hospitals may have additional energy demands for medical equipment, ventilation systems, and other specialized facilities. To track the electricity consumption a traditional energy meters or smart meters could be used [1,2]. Traditional energy meters often rely on estimates or manual readings, which can result in inaccuracies in billing. Smart meters automatically track usage and transmit data to utility companies, ensuring accurate billing based on actual consumption. This transparency builds trust between consumers and providers. Smart meters provide real-time data on energy usage, allowing both consumers and utility companies to monitor usage patterns closely. This information can help consumers understand when and how they are using energy, enabling them to make informed decisions to reduce consumption during peak times or when rates are higher. Additionally, as renewable energy sources like solar and wind become more relevant, smart meters facilitate their integration into the grid by providing data on both sides, consumption and generation. This information could help balance supply and demand, ensuring a stable and sustainable energy system [2,3].

2. Smart meters in Slovenia

Back in 2014 a systemic law, called the Energy Act replaced some of the legislation valid in Slovenian energy area [4]. Basically legislation implemented several directives and determines the necessary elements for the implementation of EU Regulations. The Government of the Republic of Slovenia wanted to systemically regulate the three key energy pillars, as reliability, competitiveness and low carbon emissions. But firstly, the starting points are availability and accuracy of energy data. It is known that available, connected and digitized power meters provide large amounts of energy-related data, and their accuracy is highly important. In that sense within the article 49 of aforementioned energy act several paragraphs related to the advanced measurement systems could be founded. Advanced metering implementation plan within electrical distribution system of Slovenia from year 2016 [1] represented a document that provided a plan for the introduction of an advanced measurement system as specified in the measures and procedures regulation from year before [5]. Within aforementioned document Fig. 1, that shows cumulative status of embedded meters in advanced measurement system, plan by years (2017-2023) could be found [1].

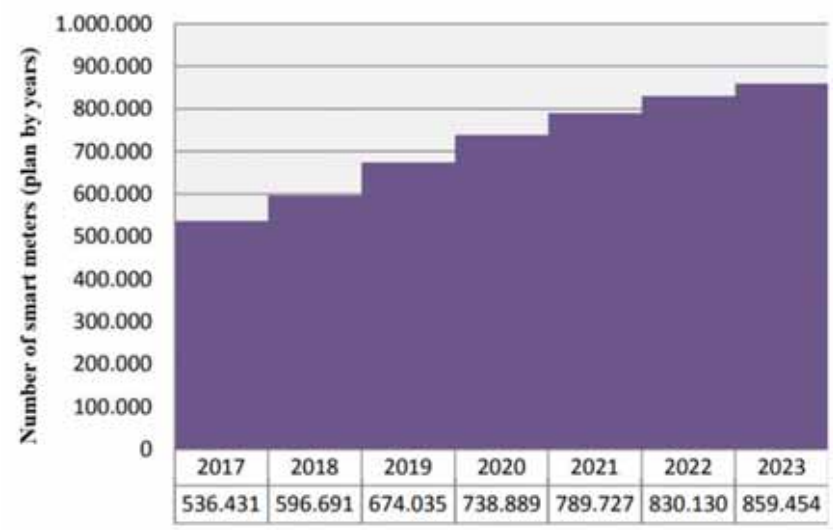

Fig. 1. Cumulative status of embedded meters in advanced measurement system, plan by years 2017-2023 [1]

Cumulative values of electrical energy consumption measurements by smart meters in Slovenia within education and human health and social work activities in four year period (2020-2023) are presented in Fig. 2. The Covid-19 pandemic has led to significant changes in energy consumption patterns. With many people working from home, there has been an increase in residential energy consumption during daytime hours, while commercial, educational and industrial energy usage has decreased due to closures and reduced operations. Smart meters provide real-time data on these shifting consumption patterns, allowing utility companies to adjust their operations and respond to changes in demand effectively.

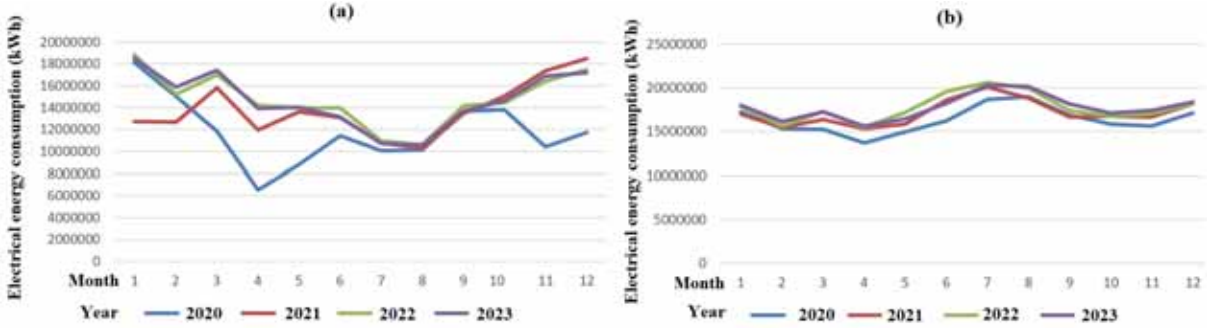

Fig. 2. Electrical energy consumption (kWh) within education (a) and human health and social work activities (b) in four year period (2020-2023)

References

[1] Načrt uvedbe naprednega merilnegasistema v elektrodistribucijskem sistemu Slovenije, SODO ID 1566, Sistemski operater distribucijskega omrežja z električno energijo, d.o.o., Maribor, (2016)

[2] M. Wali, H. K. Channi, (2024), "Smart Meter Infrastructure for Distributed Renewable Power", *AI Approaches to Smart and Sustainable Power Systems*, pp. 81-99.

[3] I. S. Bayram, T. S. Ustun, (2017), "A survey on behind the meter energy management systems in smart grid", *Renewable and Sustainable Energy Reviews*, Vol. 72, pp. 1208-1232.

[4] Energetski zakon (EZ-1), Uradni list RS, št. 17/14, dne 7. 3. 2014, https://www.uradni-list.si/glasilo-uradni-list-rs/vsebina/116549, (2014)

[5] Uredba o ukrepih in postopkih za uvedbo in povezljivost naprednih merilnih sistemov električne energije (Decree on measures and procedures for the introduction and interoperability of advanced electric power metering systems), Uradni list RS, št. 79/15 in 172/21 – ZOEE, (2015)

Electrical load operation identification system by using IOT

Bartosz Dominikowski

Lodz University of Technology,
Faculty of Electrical, Electronic, Computer and Control Engineering, Łódź

Introduction

The development of electronics and algorithms controlling the operation of electrical devices will affect the needs of remote communication. Client-server network architecture has become common in everyday use. The basic communication interfaces between electronic devices most often found in microcontroller systems are: *UART* (Universal Asynchronous Receiver Transmitter), *SPI* (Serial Peripheral Interface) or *I2C* (Inter-Integrated Circuit). The continued need for remote communication in measurement systems initiated the initiated appearance of network-distributed systems. Currently, devices communicating with the Internet or operating in a wireless local network are becoming increasingly important in the world of measurement systems. The Internet was used by computers and mobile devices until the appearance of the Internet of Things (*IoT*), i.e. a network of physical objects. Connecting electrical devices to the network allows to increase computing power by redirecting individual tasks to other computing systems. Computationally complex algorithms can be run on a system operating as a server communicating with the measurement module (other microcontroller). An important advantage of this solution is the possibility of using a large memory capacity in the system acting as a server for measurement data. Remote access to measurements in the client's application reduces the chances of losing measured data in the event of a failure in the measurement module.

In the proposed identification system, the author of the article monitors the current and voltage signals at the output terminals of the load power supply (electrical loads). For this purpose, electronically supported transducers of the *c/l* (closed loop) type were used. These systems are connected to the measurement module using an appropriately selected operational amplifier. This system is designed to maintain accuracy at a high level of reading resolution. Such measurement precision allows to accurately estimate the operating status and parameters of the analyzed electrical circuits. Data in the measurement module are transferred to the communication device (server). In this system, http get and post queries are implemented. Using a *Wi-Fi* connection, the client can view data from the identification system in a web browser or after running the application (original program). This application determines the parameters of the tested signals, such as phase shift with power factor, power spectral density of the main current and supply voltage. Based on the determined current and voltage data, the active power resulting from the load of the power supply system is determined. Various electrical energy load operating in parallel are connected to the power supply system. The algorithm then estimates which loads are operating in the power system. There are three operating states of the electrical load: connected to the power supply network or not, and operation with a failure. The condition for the correct operation of the electrical load identification system is their different rated powers.

Literature review

Digital systems using *IoT* technology with the *Wi-Fi* communication protocol are described in [1-5]. The issue is current, as evidenced by the large number of publications dealing with it. The method for identifying electrical circuits is given in [6].

Materials & Methods

A properly selected operational amplifier system with attached electronic components allows for maintaining the measurement properties. Using shielded cables, this system is connected to a high bit resolution *ADC*. These systems constitute a separate measurement module in the identification system, which allows for achieving better measurement parameters. The algorithm controlling the flow of measurement data is a program implemented in the *ESP32* microcontroller system acting as a server. Electrical power is determined based on current and voltage measurement signals. Measurement data is saved on a *microSD* memory card with a date and time stamp in text files at the moment of appearance a change in the electrical power of the load. This function increases security against loss of measurement data. After connecting as a client to the server, the system allows to view the measurements in a table and visualize them. The article compares various communication protocols such as *LoRa* (Long Range) with *Wi-Fi*.

Identification of the states of devices connected in parallel to the supply voltage is performed by using the method of summing the power of individual loads and artificial neural networks. In the case of an problem of determination the number of working devices, the neural network estimates which devices work in the analyzed power network.

Results

The achieved results proved the correct operation of the identification system. The test verifying the operation of the proposed system consisted in switching on and off individual devices connected in parallel to the power supply network. The measured electrical power is analyzed by an algorithm based on the sum of the power and using a neural network. In the case of the problem of identifying devices by using the method of summing the power of individual devices, the neural network estimates the state of electrical loads connected to the supply voltage.

Discussion

The use of the proposed method allows for the analysis of the load on the supply voltage source. This data allows to verify the operation of individual loads. This analysis is important for energy efficiency reasons. Data archiving is very important in the event of a failure. The proposed system allows to remotely determine which device is operating in the supply voltage network.

References

[1] Yara Alghofailim, Murad A. Rassam.: A Trust Management Model for IoT Devices and Services Based on the Multi-Criteria Decision-Making Approach and Deep Long Short-Term Memory Technique, Sensors 2022

[2] Víctor Sámano-Ortega, Omar Arzate-Rivas, Juan Martínez-Nolasco, Juan Aguilera-Álvarez, Coral Martínez-Nolasco, Mauro Santoyo-Mora: Multipurpose Modular Wireless Sensor for Remote Monitoring and IoT Applications, Sensors 2024

[3] Dimitrios Serpanos, Marilyn Wolf.: Internet-of-Things (IoT) Systems Architectures, Algorithms, Methodologies, Springer, 2018

[4] Shafique, K.; Khawaja, B.A.; Sabir, F.; Qazi, S.; Mustaqim, M. Internet of Things (IoT) for Next-Generation Smart Systems: A Review of Current Challenges, Future Trends and Prospects for Emerging 5G-IoT Scenarios. IEEE Access 2020

[5] Atzori, L.; Iera, A.; Morabito, G. The internet of things: A survey. Comput. Netw. 2010

[6] Dowalla K., Winiecki W., Łukaszewski R., Kowalik R.: Identyfikacja odbiorników energii elektrycznej z wykorzystaniem przekształcenia falkowego sygnałów napięcia zasilającego, Przegląd Elektrotechniczny, R. 94 NR 11/2018.

Design of a portable electric energy storage system

Jernej Frangež[1], Marko Jesenik[2]

[1] University of Maribor, Faculty of Electrical Engineering and Computer Science, Koroška cesta 46, 2000 Maribor, SLOVENIA;
jernej.frangez@um.si,

[2] University of Maribor, Faculty of Electrical Engineering and Computer Science, Koroška cesta 46, 2000 Maribor, SLOVENIA;
marko.jesenik@um.si

Abstract
In a world where energy demands are increasing, we are looking forward to the sustainable use of electric energy storage systems coming into place. From traditional stationary battery systems to small and portable. Our vision is to design a portable energy storage system with many options to extend its usage and perform in more scenarios, such as mobile storage, uninterruptible power supply, numerous options for output direct current voltages and more. In our work, we will focus on the design of a hybrid frugal, fast-response, uninterruptible power supply and present its working with measurements.

1. Introduction

Energy storage systems are devices used to store energy, which is, in our case, electric energy. With the higher demand for electric energy through the years and more dynamic production units such as solar power plants, it is necessary to have some dynamic storage units. There are already many solutions available in different categories, such as small portable electrical storage units, medium-sized home units, local distribution units, and big ones for high-voltage and power distribution [1]. Energy can be stored in different ways, such as batteries, kinetic, potential, chemical energy and so on [2, 3]. In our work, we will focus on portable electric energy storage systems with battery energy storage. Portable storage systems must be compact, light, and practical to transport between locations or to some remote areas without constant power from other sources.

For versatility, users are looking forward to products with many different input and output options. Most practical inputs and outputs are grid alternating voltage (AC) sources (230 V), input for solar modules, 12 V direct current (DC) output and 5 V DC output for mobile devices. Converters between voltage levels can be integrated or separated, where both have some advantages [4]. We will separate it to increase modularity, extend options for upgrades, and use it as a learning system for students.

2. Design of the energy storage system with an uninterruptible power supply function

Battery storage systems are composed of two main items: battery packets and power inverters. DC inputs and outputs are also essential for a broader range of applications. Fig. 1 presents a schematic of our input and output design of the portable electric energy storage design. Our hybrid uninterruptible power supply (UPS) function for grid consumers is designed for fast switching when detecting grid shortages. For example, lighting, consumers with electric motors, power inverters, etc. That function is usable, especially for devices where a slight shortage does not affect their working. We wanted a tremendous DC input voltage range from a few volts to a full-charge battery voltage level. For that purpose, we used an adaptive direct current converter (DC/DC) with the option to upgrade it for maximum power point tracking (MPPT) for solar panels. The same goes for the DC output to have a variety of output voltage levels till the battery output voltage. Universal Serial Bus (USB) provide 5 V and also supports fast charging for mobile devices.

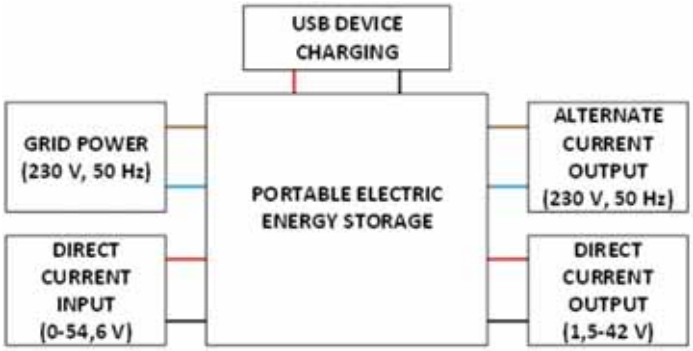

Figure 1: Schematic diagram of the inputs and outputs

When grid voltage is below the critical value, or it completely disappears, the electronic unit in the storage system detects it fast and switches on the inverter (Fig. 2). Left cursor line on the oscilloscope screenshot presents a grid shortage on the yellow signal which is grid voltage input and pink colour when the electronic circuit detected shortage and turn on inverter logical input. The signal with the turquoise colour presents the AC current to the consumer, and the blue colour presents the battery packet output voltage. The time between grid shortage to fully operational supply from storage is 16 ms.

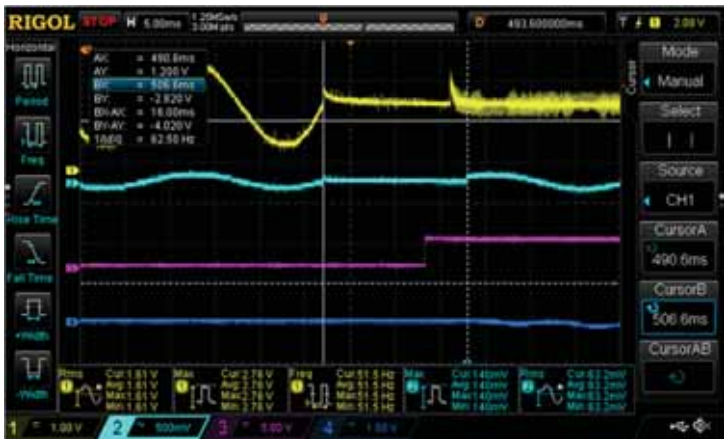

Figure 2: Fast switching response of hybrid unlimited power supply

3. Conclusion and submission of the paper

In the digest, we present portable electric energy storage systems and our proposal to use fast response hybrid UPS. The final paper will present the whole process of designing and testing. Our research will continue in the way we add as many components as we designed to the system.

Acknowledgements
The work was supported by the Slovenian Research Agency under grants P2-0114.

References

[1] J. Dugan, S. Mohagheghi, and B. Kroposki, "Application of Mobile Energy Storage for Enhancing Power Grid Resilience: A Review," *Energies,* vol. 14, no. 20, 2021, doi: 10.3390/en14206476.

[2] J. Cho, S. Jeong, and Y. Kim, "Commercial and research battery technologies for electrical energy storage applications," *Progress in Energy and Combustion Science,* vol. 48, pp. 84-101, 2015, doi: 10.1016/j.pecs.2015.01.002.

[3] C. Zhang *et al.*, "Mobile energy storage technologies for boosting carbon neutrality," *Innovation (Camb),* vol. 4, no. 6, p. 100518, Nov 13 2023, doi: 10.1016/j.xinn.2023.100518.

[4] L. Dorn-Gomba, E. Chemali, and A. Emadi, "A novel hybrid energy storage system using the multi-source inverter," in *2018 IEEE Applied Power Electronics Conference and Exposition (APEC)*, 2018: IEEE, pp. 684-691.

Portable ultrasound-impedance tomograph for long-term monitoring lower urinary tract in view of electromagnetic compatibility

Michał Gołąbek[1], Tomasz Rymarczyk[1,2], Piotr Bożek[1], Daria Stefańczak[1], Dariusz Wójcik[1,2]

[1] Netrix S.A. Research and Development Center, Lublin

[2] WSEI University, Lublin

Introduction

This article delineates the development procedure of an ultrasonic tomography apparatus coupled with an impedance tomography setup for monitoring bladder functions. The amalgamation of these tomographic methodologies enhances the precision of urinary tract imaging. The device incorporates ultrasound beamforming technology and conducts measurements utilizing a phased array ultrasonic transducer. The paper elucidates practical principles for crafting electronic circuits while considering electromagnetic radiation and presents the outcomes of compatibility assessments carried out at an accredited Laboratory of Electromagnetic Compatibility (LKE) located at Wrocław University of Science and Technology.

Hardware Construction

The design of the measuring device for dual diagnosis of the urinary tract is divided into several PCB boards. It consists of the mainboard, four ultrasound measurement cards (UST), one impedance measurement card (EIT), a WiFi communication module, a connectors module and an LED board for operation status indication and battery pack.

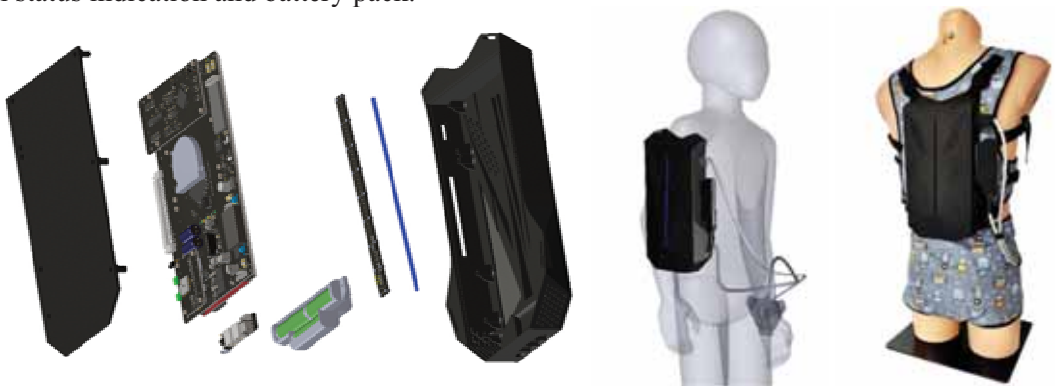

Figure 1. UST-EIT dual tomograph for bladder monitoring

The mainboard was based on the STM32H7 microcontroller. It supports parallel FMC data transmission operating at 100MHz clock from ultrasonic measurement cards and provides communication with the impedance measurement card using UART and QUAD SPI. In addition, the motherboard has USB 1.0 and USB 2.0 communication ports and a WiFi module for connection to the image reconstruction system. The motherboard also provides the appropriate supply voltage levels to the individual modules.

The four eight channels UST cards has synchronized for 1ns accurate excitation control, featuring a MAX2082 circuit and an Intel FPGA. The EIT card employs 16 textile electrodes with an LTC2203 ADC system (25 msps) for impedance measurements. It uses DAC8830 converters controlled by the FPGA for precise amplitude control.

The urinary tract diagnostic device has a backpack-style housing for comfort, stability, and adjustability. Durable, hygienic materials enable easy cleaning, effectively combining comfort, functionality, and hygiene.

Electromagnetic compatibility

The imaging device designed for observing the lower urinary tract underwent evaluation at the Accredited Laboratory of Electromagnetic Compatibility, located at Wroclaw University of Science and Technology in Poland. The tests aimed to verify whether the device can be safely used in "Professional healthcare facility environment and Home Healthcare Environment" according to PN-EN 60601-1-2 [1]. Initial evaluations took place during the device's development stage to preemptively detect any potential issues and ensure readiness for last certification assessments. Due to the large number of tests performed, only a few selected ones are presented.

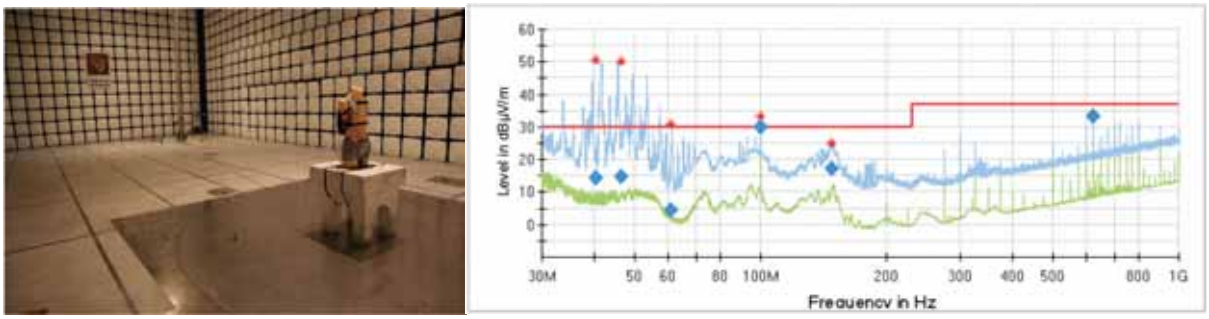

Figure 2. Results from radiated emissions tests in the frequency range from 30 MHz to 1 GHz, radiated at a distance of 10 meters according to PN-EN 55016-2-3 [2]

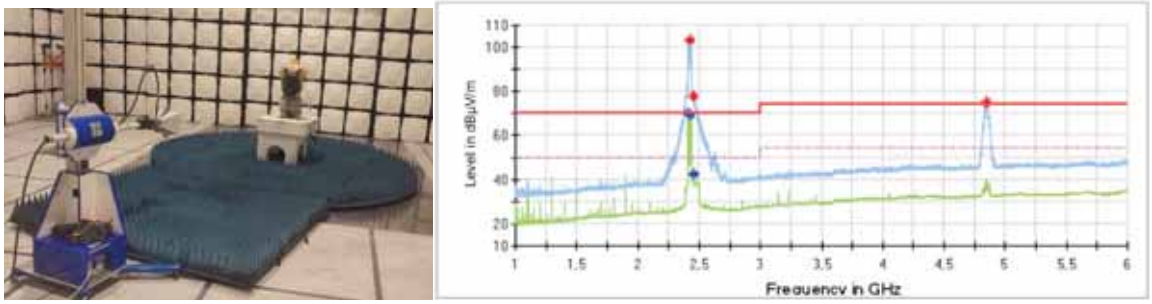

Figure 3. Results from radiated emissions tests in the frequency range from 1 GHz to 6 GHz, radiated at a distance of 3 meters according to PN-EN 55016-2-3 [2]

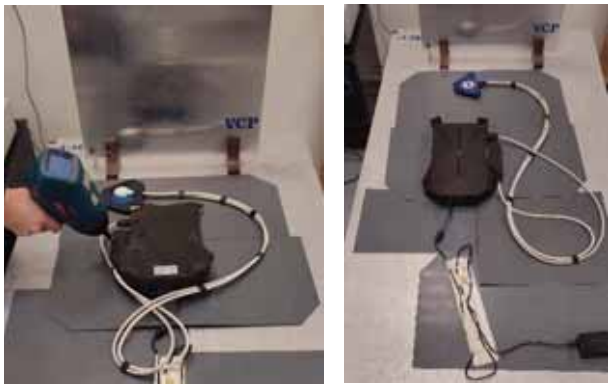

Figure 4. UST/EIT tomograph during ESD immunity tests according to PN-EN 61000-4-2 [3]

References

[1] PN-EN 60601-1-2:2015-11 (EN 60601-1-2:2015) Standard Medical Electrical Equipment - Part 1-2: General Requirements for Basic Safety and Essential Performance - Collateral Standard: Electromagnetic Disturbances - Requirements and Tests.

[2] PN-EN 55016-2-3:2017-06 + A1:2020-01 (EN 55016-2-3:2017 + A1:2019) Standard Specification for Radio Disturbance and Immunity Measuring Apparatus and Methods - Part 2-3: Methods of Measurement of Disturbances and Immunity - Radiated Disturbance Measurements.

[3] PN-EN 61000-4-2:2011 (EN 61000-4-2:2009) Standard Electromagnetic Compatibility (EMC) - Part 4-2: Testing and Measurement Techniques - Electrostatic Discharge Immunity Test

Effect of electromagnetic field on plants

Tomasz Jakubowski

Faculty of Production and Power Engineering,
University of Agriculture in Krakow,
Balicka 116B, 30-149 Krakow, Poland

Abstract

The impact of electromagnetic field on living organisms should be considered from the point of view of phenomena such as magnetoreception and magnetoactivity or electroreception and electroactivity, indicating the relationship between the ecosystem and its biocenosis and electric, magnetic and electromagnetic fields. Research shows that virtually all known biological objects are equipped, to a greater or lesser extent, with specific sensors whose task is to identify natural sources of electricity and magnetism.

In the opinion of most researchers, experiments that have been conducted for many years do not provide a clear answer to the question about the mechanism of this identification - this also applies to the issue of plants' reaction to artificially generated electromagnetic field. The above-mentioned phenomena of activity and reception are the subject of research on the response of plant objects to EMF in the context of increasing their biomass, yield generation and storage possibilities.

The paper reviews and synthesizes existing research results on the impact of electromagnetic fields on crop plants. The possibility of applying the proposed solutions to business practice was taken into consideration.

Effect of electromagnetic field on plants – selected examples

Subject of research and experiment	***Authors, year***	***Obtained results***
Exposure of Plants to a MF Intensity Lower than the Geomagnetic Field (intensities from 100 nT to 0.5 mT).	*Pittman, 1963* *Belov and Bochkarev, 1983* *Belyavskaya, 2004*	*It was found that a MF of relatively low intensity could be effective in stimulating or initiating plant growth responses.*
Effects fo MF on plant development, sunflower (Helianthus annuus) seedlings exposed to 20 μT.	*Fischer et al., 2004*	*Showed small, but significant increases in total fresh weights, shoot fresh weights, and root fresh weights, whereas dry weights and germination rates remained unaffected.*
Effects on Transition to Flowering	*Xu et al., 2012*	*Near-null MF can be produced by three mutually perpendicular couples of Helmholtz coils and three sources of high-precision direct current power, which can counteract the vertical, north–south and east–west direction components of the geomagnetic field (GMF).*

Subject of research and experiment	***Authors, year***	***Obtained results***
Exposure of plants to MF intensities higher than the geomagnetic filed (intensities higher than GMF relate to values higher than 100 μT). Seed germination of wheat, rice and legumes (however, many other physiological effects on plants of high MF described plant responses in terms of growth, development, photosynthesis, and redox status)	*Mahajan and Pandey, 2014*	*In seeds of mung bean (Vigna radiata), exposed in batches to static MFs of 87 to 226 mT intensity for 100 min, a linear increase in germination magnetic constant with increasing intensity of MF was found. Calculated values of mean germination time, mean germination rate, germination rate coefficient, germination magnetic constant, transition time, water uptake, indicate that the impact of applied static MF improves the germination of mung beans seeds even in off-season.*
Effects on cryptochrome	*Izmaylov et al., 2009*	*Arabidopsis seedlings were grown in a 500 μT MF and a near-null MF it was found that the 500 μT MF enhanced the blue light-dependent phosphorylations of CRY1 and CRY2, whereas the near-null MF weakened the blue light-dependent phosphorylation of CRY2 but not CRY1.*
Effects on roots and shoots	*Florez et al., 2007*	*Increased growth rates have been observed in different species when seeds where treated with increased MF. Treated corn plants grew higher and heavier than control, corresponding with increase of the total fresh weight. The greatest increases were obtained for plants continuously exposed to 125 or 250 mT.*

Short narrative biography

Tomasz Jakubowski currently works as a asossiate professor at the University of Agriculture in Krakow. He holds the title of M.Sc. Eng. (2005), doctoral degree (2009) in environmental engineering and Ph.D hab. Eng. agricultural engineering (agrophysics). He is the author of over 100 scientific publications in the areas of: the impact of physical methods on plants, food quality and safety, and sustainable development. For over 15 years he has been a member of the technical professional organization - Association of Agricultural Engineers and Technicians - Scientific Technical Organization (SITR-NOT) and the Polish Society of Agricultural Engineering (PTIR).

Parameters determination of the drive driven by a DC Motor

Marko Jesenik, Anton Hamler, Mislav Trbušić

University of Maribor, Faculty of Electrical Engineering and Computer Science,
Koroška cesta 46, Slovenia,
marko.jesenik@um.si

Abstract
A method is presented for the determination of the direct current (DC) motor and drive. The basis for the parameters` determination are speed and current startup responses. The method can be used in the case of controlled drive. Differential Evolution (DE) is used for the parameters` determination. The motor's model simulation, which is used for the Objective Function calculation, is described with two coupled Differential Equations. The Runge-Kutta fourth order method is used for the solving of the system of two coupled Differential Equations. The calculated results show good agreement between the known and calculated parameters.

1. Introduction

Drives with Direct Current motors (DC motors) are used widely in industrial applications. They are often used for industry control systems, because they are easy to control. Often DC motor's and also a drive's parameters are not known, or the motor's parameters provided by the motor manufacturer could have relatively large tolerances [1], especially for the cheaper DC motors. Also important are the drive's parameters, such as the inertia of the drive and friction. Usually the inertia and friction of all the drive's parts are not known.

2. DC motor's model

The DC motor is presented schematically in Figure 1. A working machine may, or may not, also be connected to the motor.

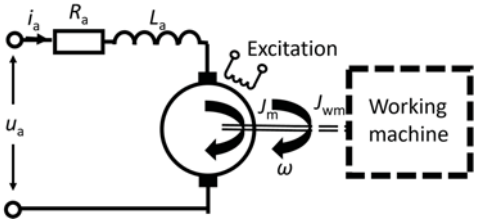

Fig. 1. DC motor and working machine

R_a is the ohmic resistance of the DC motor, L_a is the inductance of the DC motor (we assume it is constant, which is a simplification of the model), u_a is the voltage at the DC motor, i_a is the current of the DC motor, J_m is the inertia of the motor ω angular speed at the axis of the motor, and J_{wm} is the inertia of the working machine.
Drive operation can be simulated using two coupled Differential Equations, written as (1) and (2). It is assumed that excitation is present before the connection of the motor's armature.

$$u_a = i_a \cdot R_a + L_a \cdot \frac{di_a}{dt} + e \tag{1}$$

$$T_m - T_{load} = J \frac{d\omega}{dt} \tag{2}$$

Rewriting (1) and (2), considering $e = c_m \cdot \omega$, $T_m = c_m \cdot i_a$ and $T_{load} = T_{\mathrm{la}} + T_{\mathrm{lb}} \cdot \omega + T_{\mathrm{lc}} \cdot \omega^2$, we obtain (3) and (4), which are the basis for the mathematical model.

$$u_a = i_a \cdot R_a + L_a \cdot \frac{di_a}{dt} + c_m \cdot \omega \tag{3}$$

$$c_m \cdot i_a - \left(T_{\mathrm{la}} + T_{\mathrm{lb}} \cdot \omega + T_{\mathrm{lc}} \cdot \omega^2\right) = J \frac{d\omega}{dt} \tag{4}$$

Simulation of the motor's startup is made with numerical solving of the Differential Equations written in (3) and (4). A Runge-Kutta fourth-order method is used.

3. Method for Parameters` Determination

Parameters` determination (R_{a}, L_{a}, c_{m}, J, T_{la}, T_{lb} and T_{lc}) is based on the comparison of the measured current and speed response at startup with calculations based on the described mathematical model. We are using a direct approach for the inverse problem. Differential Evolution (DE) is used for parameters` determination [2,3]. The used strategy was DE/rand/1/exp, the used amplification of the differential variation was 0.6 and the used crossover probability was 0.8.

4. Results

The measured current and speed responses are made on a SIEMENS SIMOREG DC-Master drive. The measurement is made with the use of the "Trace" function, which is a part of the SIEMENS software. The startup of the motor is made using an n-control closed loop with the following data: $t_{\mathrm{speed\_up}}$=0 s, ω_{final}=126 s^{-1}, $i_{\mathrm{a\_limit}}$=11,44 A (110% of $I_{\mathrm{a\_rated}}$), no load, 87 measured points. To consider closed loop operation, voltage u_{a} is not a constant value, it is a measured value $u_{\mathrm{a}}(t)$, which is used as input to the motor's model. The calculated parameters are presented in Table 1.

Table 1. Known and calculated parameters

Parameter	Known value	Calculated value
R_{a} (Ω)	5.66	5.06
L_{a} (H)	not known	0.244
c_{m} (Vs)	not known	1.369
J (kgm^2)	≈ 0.04	0.0468
T_{la} (Nm)	≈ 0.9	0.799
T_{lb} (Nms)	≈ 0	$7.70 \cdot 10^{-18}$
T_{lc} (Nms^2)	≈ 0	$8.00 \cdot 10^{-19}$

5. Conclusions

The calculated results presented in Table 1 show good agreement between the known and calculated parameters.

The differences between the known and calculated values are approximately 11% in the case of R_{a} and T_{la}, and approximately 17% in the case of J.

This work was supported by the Slovenian Research and Innovation Agency under Grant P2-0114.

References

[1] N.B. Shanmuga, A. Mythile, S. Pavithra, N. Nivetha, (2020), "Parameter Identification of A DC Motor", International journal of scientific & technology research, 2020, vol. 9 (2), pp. 5746-5755.

[2] R.J. He, Z.Y. Yang, (2012), "Differential evolution with adaptive mutation and parameter control using Levy probability distribution", Journal of Computer Science and Technology, vol. 27 (5), pp. 1035-1055.

[3] S. Chattopadhyay, S.K. Sanyal, (2011), "Optimization of Control Parameters of Differential Evolution Technique for the Design of FIR Pulse-shaping Filter in QPSK Modulated System", Journal of Communications, vol. 6 (7) pp. 558-570, 2011.

Improved LSTM networks with self-attention layer used for monitoring industrial reactors using EIT and ECT

Grzegorz Kłosowski[1], Tomasz Rymarczyk[2,3], Michał Oleszek[2,3], Dariusz Wójcik[2,3], Konrad Niderla[2,3]

[1] Faculty of Management, Lublin University of Technology, Lublin, Poland

[2] Institute of Computer Science and Innovative Technologies, WSEI University, Lublin, Poland

[3] Research & Development Center Netrix S.A., Lublin, Poland

Improved LSTM Neural Network

An enhanced Long Short-Term Memory (LSTM) network architecture is proposed, featuring a dual channel "cell" structural variable at the input stage for separate EIT and ECT measurement sequences. First channel corresponds to the EIT measurement sequence, and the second channel is dedicated to the ECT measurement sequence. This unique configuration allows for the independent and nuanced analysis of each type of tomographic measurement, thereby preserving their individual characteristics and potential interdependencies. Another groundbreaking feature of the enhanced LSTM architecture is the inclusion of a self-attention layer.

The neural network architecture under investigation is implemented in MATLAB and is specialized for sequence-to-sequence mapping tasks. The network is designed to handle an input signal consisting of 2 channels each and 96 time steps. Solving a simple problem, using the Gauss-Newton method and the finite element method implemented in the Eidors toolbox (an add-on to Matlab), over 30,000 training cases were generated. In the context of tomographic data analysis, raw EIT data comprises a vector of 96 voltage measurements, while ECT data consists of a vector containing 120 capacitance measurements (for 16 measurement channels). To apply LSTM networks to these data streams, both channels must possess the same number of time steps [1]. To harmonize the temporal dimensions of these two modalities, a decision was made to reduce the number of measurements in the ECT data from 120 to 96. LASSO (Least Absolute Shrinkage and Selection Operator) regularization was employed to accomplish this.

Each sequence is represented as a numChannels-by-numTimeSteps (2×96) numeric array, where numChannels signifies the number of channels and numTimeSteps indicates the number of time steps in the sequence. Channel 1 contains EIT measurements, and channel 2 contains the ECT measurement sequence. Table 1 shows the detailed architecture of the neural network used.

Table 1. Improved neural network architecture

No.	Layers
1	sequenceInputLayer(2,"Name","sequence")
2	bilstmLayer(512,"Name","bilstm_1")
3	layerNormalizationLayer("Name","layernorm")
4	dropoutLayer(0.5,"Name","dropout")
5	bilstmLayer(512,"Name","bilstm_2","OutputMode","last")
6	layerNormalizationLayer("Name","layernorm_1")
7	selfAttentionLayer(4,256,"Name","selfattention","NumValueChannels",256,"OutputSize",1024)
8	dropoutLayer(0.5,"Name","dropout_1")
9	fullyConnectedLayer(20445,"Name","fc_2")
10	regressionLayer("Name","regressionoutput");

The Adam optimization algorithm is utilized for the training regimen, with the maximum number of epochs set to 500 and a mini-batch size of 64. The training data is shuffled at the beginning of each epoch to prevent the model from learning any spurious correlations. Validation data is evaluated every 30 epochs, and the training will cease if no improvement is observed for six consecutive validation checks.

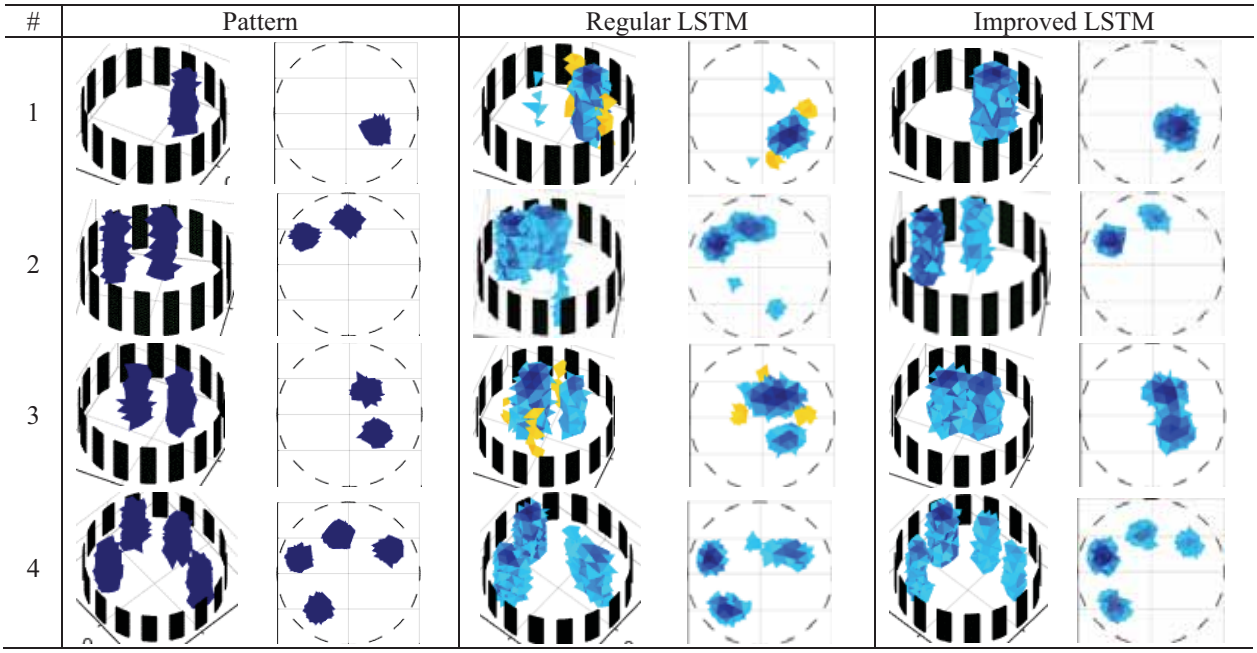

Figure 1: Comparison of regular and enhanced LSTM networks

Results

EIT and ECT measurements are treated as separate sequences but are encapsulated within a single "cell" structural variable {2×(96×1)}. This new architecture with separate sequence handling and self-attention capabilities is compared against the standard neural network model using the concatenated input vector. The comparative analysis aims to evaluate the efficacy and robustness of both approaches, specifically focusing on metrics like accuracy, precision, recall, and computational efficiency. Such an architecture accommodates the heterogeneity of the data and leverages advanced neural network capabilities to improve model performance potentially. A self-attention layer could further enhance the model's ability to recognize complex patterns and relationships between EIT and ECT measurements, thereby contributing to more accurate and reliable predictions. Figure 1 shows a comparison of the regular and improved LSTM networks. A subjective comparison using human perception allows us to judge that images taken with the improved LSTM are more accurate. Table 2 showcases the comparative results obtained through the computation of average values for four indices that are frequently employed to evaluate the quality of reconstructed images in tomography.

Table 2. Comparison metrics between regular and enhanced LSTM networks

Metric (mean)	**Regular LSTM**	**Enhanced LSTM**
MSE	0.044	0.039
PSNR	14.477	14.88
SIMM	0.505	0.520
ICC	0.626	0.679

These indices include the Mean Squared Error (MSE), Peak Signal-to-Noise Ratio (PSNR), Structural Similarity Index (SSIM), and Intraclass Correlation Coefficient (ICC) [2]. Each of these metrics serves

a distinct purpose and offers unique insights into the performance of the tomographic reconstruction methods under consideration. All metrics confirm the superiority of images reconstructed with the improved LSTM network.

References

[1] Kłosowski, G., Rymarczyk, T., Niderla, K., 2022. Use of the two-stage neural system in industrial electrical tomography - hybrid approach, in: UbiComp/ISWC 2022 Adjunct - Proceedings of the 2022 ACM International Joint Conference on Pervasive and Ubiquitous Computing and Proceedings of the 2022 ACM International Symposium on Wearable Computers. https://doi.org/10.1145/3544793.3560368

[2] Kłosowski, G., Rymarczyk, T., Niderla, K., Kulisz, M., Skowron, Ł., Soleimani, M. Using an LSTM network to monitor industrial reactors using electrical capacitance and impedance tomography – a hybrid approach. Eksploatacja i Niezawodność – Maintenance and Reliability 25, 2023. https://doi.org/10.17531/EIN.2023.1.11

Gustav Robert Kirchhoff – 200 Anniversary of his birth

Andrzej Krawczyk[1], Ewa Korzeniewska[2]

[1] Polskie Towarzystwo Zastosowań Elektromagnetyzmu,

[2] Politechnika Łódzka, Wydział Elektrotechniki, Elektroniki, Informatyki i Automatyki

This year (2024) electrical engineering world celebrates the 200 anniversary of the one of most famous German physicist, Gustav Robert Kirchhoff (Fig.1a). He was born on March 12, 1824, in Königsberg, Prussia (now Kaliningrad, Russia). His parents were Carl Friedrich Kirchhoff, a law counselor devoted to the Prussian state, and Juliane Johanna Henriette von Wittke. Kirchhoff's parents encouraged their children to serve the Prussian state as best as they were able. Kirchhoff was an academically strong student, so he planned to become a university professor, which was considered a civil servant role in Prussia at that time. Kirchhoff attended Kneiphofische High School with his brothers and received his diploma in 1842.

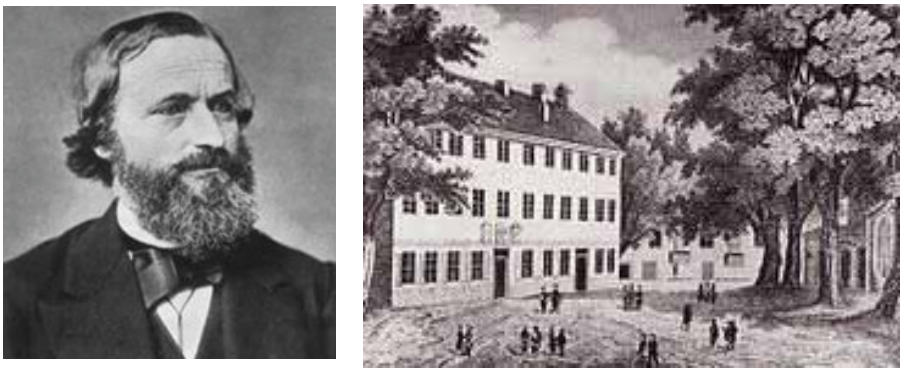

Fig. 1 a) Gustav Robert Kirchhoff b) University Albertina c. 1850

After graduating high school, Kirchhoff began studying in the Mathematics-Physics department at the Albertus University of Königsberg (Fig.1b). It was founded in 1544 as the world's second Protestant academy (after the University of Marburg) by Duke Albert of Prussia, and was commonly known as the Albertina. There, Kirchhoff attended a mathematics-physics seminar from 1843 to 1846 developed by the famous mathematicians Franz Neumann and Carl Jacobi. It is worth adding that, besides Gustav Kirchhoff, this university was graduated by the eminent people, e.g. Immanuel Kant, David Hilbert, Christian Goldbach, E. T. A. Hoffmann, Karl Weierstrass.

Neumann in particular had a profound impact on Kirchhoff, and encouraged him to pursue mathematical physics – a field which focuses on developing mathematical methods for problems in physics. While studying with Neumann, Kirchhoff published his first paper in 1845 at age 21. This paper contained the two Kirchhoff's laws, which allow for the calculation of the current and voltage in electrical circuits. Two Kirchhoff's laws were and are still now the first things in electrical engineering course to tackle with.

Kirchhoff's first law says that at a given junction in a circuit, the current going into the junction must equal the sum of the currents leaving the junction. **Kirchhoff's second law** says that if there is

a closed loop in a circuit, the sum of the voltage differences within the loop equals zero. It should be mentioned that the Kirchhoff laws were published 20 years before Maxwell launched his electromagnetic equations which are the differential form of the Kirchhoff ones. Hence, one can say that he generalized Ohm's law and prepared the ground for Maxwell's theory of electromagnetism. On the basis of Kirchhoff's two rules, a sufficient number of equations can be written involving each of the currents so that their values may be determined by an algebraic solution. Kirchhoff's rules are also applicable to complex variables of AC current circuits and with modifications to complex magnetic circuits.

In 1847 Kirchhoff became *Privatdozent* (unsalaried lecturer) at the University of Berlin and three years later accepted the post of extraordinary professor of physics at the University of Breslau (now Wrocław, Poland). In 1854 he was appointed professor of physics at the University of Heidelberg, where he joined forces with Bunsen (Robert Wilhelm Eberhard Bunsen, 1811-1899 – German physicist and chemist), and founded spectrum analysis. They demonstrated that every element gives off a characteristic coloured light when heated to incandescence. This light, when separated by a prism, has a pattern of individual wavelengths specific for each element. Applying this new research tool, they discovered two new elements, cesium (1860) and rubidium (1861).

Fundamental work by Kirchhoff on black body radiation (a term he introduced in 1862) was important in the development of quantum theory. Fraunhofer (Joseph von Fraunhofer (1787-1826 – German physician and astronomer) had observed bright lines in the spectrum produced by flames and noted that they appeared at similar frequencies to certain dark lines in the spectrum of the sun. To make further progress, however, required pure forms of substances, for if impurities were present then these confused the picture by producing lines. Kirchhoff was able to make his fundamental breakthrough by producing purer forms of substances than had been previously the case. He was then able to see, in 1859, that each element had a uniquely characteristic spectrum. He presented his law of radiation, stating that, for a given atom or molecule, the emission and absorption frequencies are the same.

With Clara, his first wife, Kirchhoff had three sons and two daughters and he was left to bring them up on his own in 1869 when Clara died. This was made harder by a disability which caused him to spend much of his life on crutches or in a wheelchair. He later married Luise Brömmel, who was from Goslar, in Heidelberg in 1872. Kirchhoff had been made offers by other universities but he was happy in Heidelberg and turned down such offers. However as his health began to fail he realized that the experimental side of the subject, one which he greatly enjoyed, was becoming increasingly difficult. Therefore, in 1875 when he was offered the chair of mathematical physics at Berlin, he accepted since it allowed him to continue to make a strong contribution to teaching and theoretical research without the problems that his poor health was giving him in carrying out experiments. His best known treatise, published after he took up the chair in Berlin, is the four volume masterpiece *Vorlesungen über mathematische Physik*, prepared together with his successor on the chair of the University of Berlin, Max Planck.

In 1864, he was elected as a member of the American Philosophical Society and in 1884, he became foreign member of the Royal Netherlands Academy of Arts and Sciences.
Gustav Kirchhoff died in 1887, and was buried in the St Matthäus Kirchhof cemetery in Schöneberg, Berlin.

Ultrasonic tomograph for industrial research

Krzysztof Król[1,2], Michał Gołąbek[1], Tomasz Rymarczyk[1,2]

[1] Research and Development Center, Netrix S.A., Lublin, Poland

[2] WSEI University, Lublin, Poland

Introduction

Ultrasonic tomography allows non-invasive imaging of the internal structure of objects [1,2,3] by exploiting the phenomenon of scattering and absorption of ultrasonic waves in the material. In this article we will focus on the construction of a new version and the operation of the ultrasonic tomograph in the context of industrial processes. Process tomography is an extremely useful tool in monitoring and optimising industrial processes [4,5,6].

Hardware

The purpose of this work is to present the design and implementation of a measurement module that enables the precise retrieval of a single measurement frame. The module aims to provide accurate and reliable parameter readings and enable further analysis and processing.
The main functionality of the measurement module is the retrieval of a single measurement frame, which consists of a 64x64 matrix (using all measurement channels). The module is responsible for communicating with the sensors, reading the measurement values and storing them in a format for further processing.

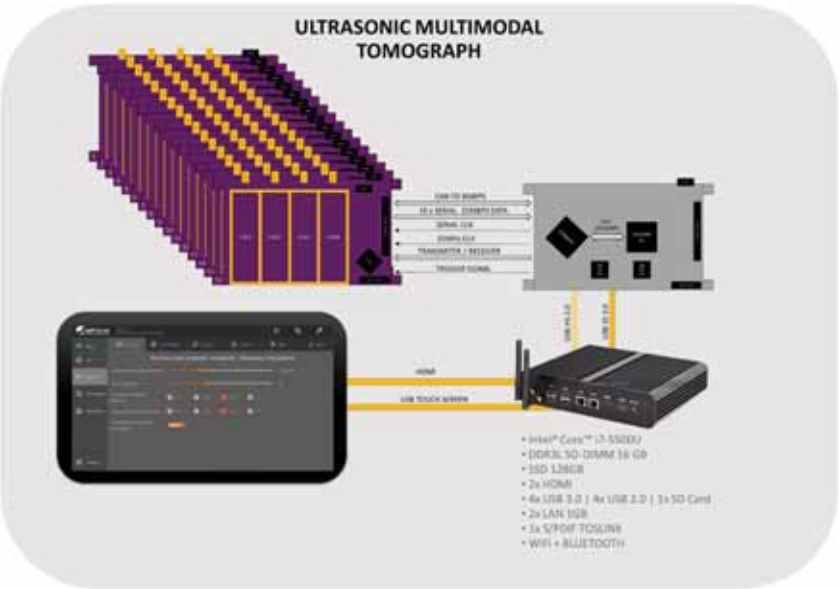

Figure 1: Block diagram of a multimodal tomograph

Theorem. Acoustic impedance is a parameter characterising the interaction of acoustic waves between different media. It is the ratio of the amplitude of the sound pressure to the velocity of the particles in

the medium propagating the wave. Acoustic impedance depends on the physical properties of the medium through which the acoustic wave travels and the frequency of the wave.
For a homogeneous medium, such as air, the acoustic impedance is constant for a given frequency and is equal to the product of the density of the medium and the speed of sound propagation through that medium. The acoustic impedance of the target medium may differ from that of the initial medium, leading to reflection or refraction of the wave at the boundary between the two.
In the case of acoustic boundaries between media with different acoustic impedances, some of the acoustic wave energy is reflected and some passes through the boundary. The ratio of reflection and transmission depends on the ratio of the acoustic impedances of the two media. When the impedance of the target medium is close to the impedance of the initial medium, the wave energy is effectively transmitted and a minimal part of the wave is reflected.
Acoustic impedance can be used to characterise the acoustic properties of materials, such as material density, elasticity or internal energy loss. Acoustic impedance tests are often performed using specialised equipment and measurement techniques, such as impedance tubes, impedance chambers or interferometric methods.
The formula for the acoustic impedance (often denoted as Z) in a homogeneous medium can be represented as the quotient of the acoustic pressure amplitude (denoted as P) to the particle velocity of the medium (denoted as V). Mathematically this is expressed as:

$$Z=P/V \tag{1}$$

The SI unit of acoustic impedance is Pa·s/m or kg/(m2·s).
The acoustic impedance of water depends on its physical properties and can vary with temperature and the presence of dissolved substances in the water. Under standard conditions, i.e. a temperature of 25°C, the acoustic impedance of water is approximately 1.48 × 106 kg/(m2·s).
The acoustic impedance value of water is related to its density and the speed of sound propagation. Water has a higher density than air, which translates into a higher acoustic impedance. In addition, the speed of sound in water is much higher than in air, which further affects the acoustic impedance value.
It is an approximate value and the actual acoustic impedance value of water may vary slightly depending on specific environmental conditions such as temperature, pressure, salinity or the presence of chemicals.
To determine the acoustic impedance of a second medium placed in a tank of water, the reflection coefficient formula can be used:

$$R=(Z\_1-Z\_2)/(Z\_1+Z\_2\ ) \tag{2}$$

where Z1 is the acoustic impedance of the water and Z2 is the acoustic impedance of the inclusion. The reflection coefficient can also be calculated as the ratio of the amplitude of the reflected wave to the transmitted wave:

$$R=I\_r/I\_0 \tag{3}$$

where Ir and I0 are the amplitude of the reflected and transmitted wave, respectively.

References

[1] Kłosowski G, Rymarczyk T, Niderla K, Kulisz M, Skowron Ł, Soleimani M. Using an LSTM network to monitor industrial reactors using electrical capacitance and impedance tomography – a hybrid approach. Eksploatacja i Niezawodność – Maintenance and Reliability. 2023;25(1):11. doi:10.17531/ein.2023.1.11.
[2] Kłosowski G., Rymarczyk T., Cieplak T., Niderla K., Skowron Ł., Quality Assessment of the Neural Algorithms on the Example of EIT-UST Hybrid Tomography, Sensors, 20 (2020), No. 11 3324
[3] T. Rymarczyk, G. Kłosowski, K. Kania, P. Rymarczyk, and M. Mazurek, "Tomographic ultrasonic sensors in industrial applications," Przegla˛d Elektrotechniczny, vol. 97, no. 1, pp. 166–169, 2020.
[4] Kozłowski E, Borucka A, Świderski A. Application of the logistic regression for determining transition probability matrix of operating states in the transport systems. Eksploatacja i Niezawodność – Maintenance and Reliability. 2020;22(2):192-200. doi:10.17531/ein.2020.2.2.
[5] P. Koulountzios, T. Rymarczyk and M. Soleimani, "A 4-D Ultrasound Tomography for Industrial Process Reactors Investigation," in IEEE Transactions on Instrumentation and Measurement, vol. 71, pp. 1-14, 2022, Art no. 4502714, doi: 10.1109/TIM.2022.3164166.
[6] Rymarczyk, T.; Król, K.; Kozłowski, E.; Wołowiec, T.; Cholewa-Wiktor, M.; Bednarczuk, P. Application of Electrical Tomography Imaging Using Machine Learning Methods for the Monitoring of Flood Embankments Leaks. Energies 2021, 14, 8081. https://doi.org/10.3390/en14238081

Navigating the gusts: evolutionary strategies for optimizing wind farm layouts

Maja Celeska Krstevska

Ss. Cyril and Methodius University in Skopje, Faculty of Electrical Engineering and Information Technologies, Rugjer Boshkovikj No. 18, North Macedonia,
celeska@feit.ukim.edu.mk

Abstract

The lecture gives overview on the sophisticated optimization of wind farm layout with of two fundamentally different heuristic algorithms. To do investigate such optimization, detailed real-world data from an existing wind farm in Bogdanci, North Macedonia is utilized by employing real wind farm data we are able to calibrate model adequacy and ascertain a model that will serve as a referent guidance in the planning of future onshore wind farms. The major unique feature of the research is the simultaneous optimization taking into account all major technical influence and cost factors, including: (i) detailed and advanced models for power modelling due to bivariate distribution of wind speed and direction; (ii) accurate estimation of levelized cost of energy (LCOE); (iii) analysis of the shortest electrical interconnections among wind turbines and (iv) correction of hub height on each wind turbine in the wind farm with taking also the wake effect into consideration. Different layouts were designed using sophisticated algorithms for handling the resulting high-dimensional, highly non-linear optimization problem. In particular, a non-dominated sorting genetic algorithm (NSGA) and a mixed-discrete particle swarm optimization algorithm (MD-PSO) were applied. Both optimization algorithms established bi-objective fitness functions, in particular- minimizing the levelized cost of energy and maximizing the capacity factor. By comparing the results obtained with the existing layout, it is established that both optimization algorithms are adequate in determination of wind power plant layouts. Results also show a remarkable improvement of 2.05% and 5.59% for levelized costs and capacity factor, respectively, compared to the as built wind farm layout. So, it is proven that the implementation of sophisticated optimization methods can results in essential savings during the whole lifetime of the wind farm.

1. Introduction

Optimization of wind farm layout concerning various parameters is a major point in planning and will influence the revenue for the whole life of the installation. Besides the obvious impact of wind distribution also other parameters like connection costs and levelized costs of energy influence the optimum layout and must be included in a realistic optimization algorithm.

2. Case Study

The wind farm used as a case study for this report is WF Bogdanci, located in southeast part of Macedonia. During the analysis, 16 WTs from phase one were in operation and the second phase, with additional 6 WTs was expected to be completed. The WTs used for this WF are form type SIEMENS SWT-2.3-93 (80 m hub height, 2.3 MW rated power).

3. Defined auxiliary methods and improvements

Guided by the intention to reduce to the number of different constraints or at least reduce their impact over the optimization process for the onshore WF, the authors decided to work on two separate modes of operation: binary and continuous mode. Additionally, four auxiliary methods and improvements were developed and implemented in the optimization process, in order to gain more reliable results.

i) Wind regimes for the concrete site were interpreted in unusual way by using bivariate probability density function.

ii) The power generated by a wind turbine is strongly dependent on the approaching wind speed. Here a Multimodal Wind Distribution model is used which avoids any limiting assumptions. This model is developed using multivariate kernel density estimation (KDE). The wind flow modelling calculates the reduction of energy yield on account of wake effects, caused by other turbines of the WF.

iii) Levelized Cost of Energy (LCOE) is used by project designers as a metric to evaluate the impact a change in design might have on a project. Also, it gives a basis by which projects of different technology types can easily be compared against one another. On the other hand, there are reliable researches that allocate the capacity factor (CF) of a WF as more unbiased measure (than net energy production) of the performance of the optimized WF layout. So, it is reasonable why it was decided to use these two metrics in the objective function.

iv) Euclidean Minimum Spanning Tree method was used for optimal calculation of the minimum cable length necessary to connect each WTs in a distinct WF configuration.

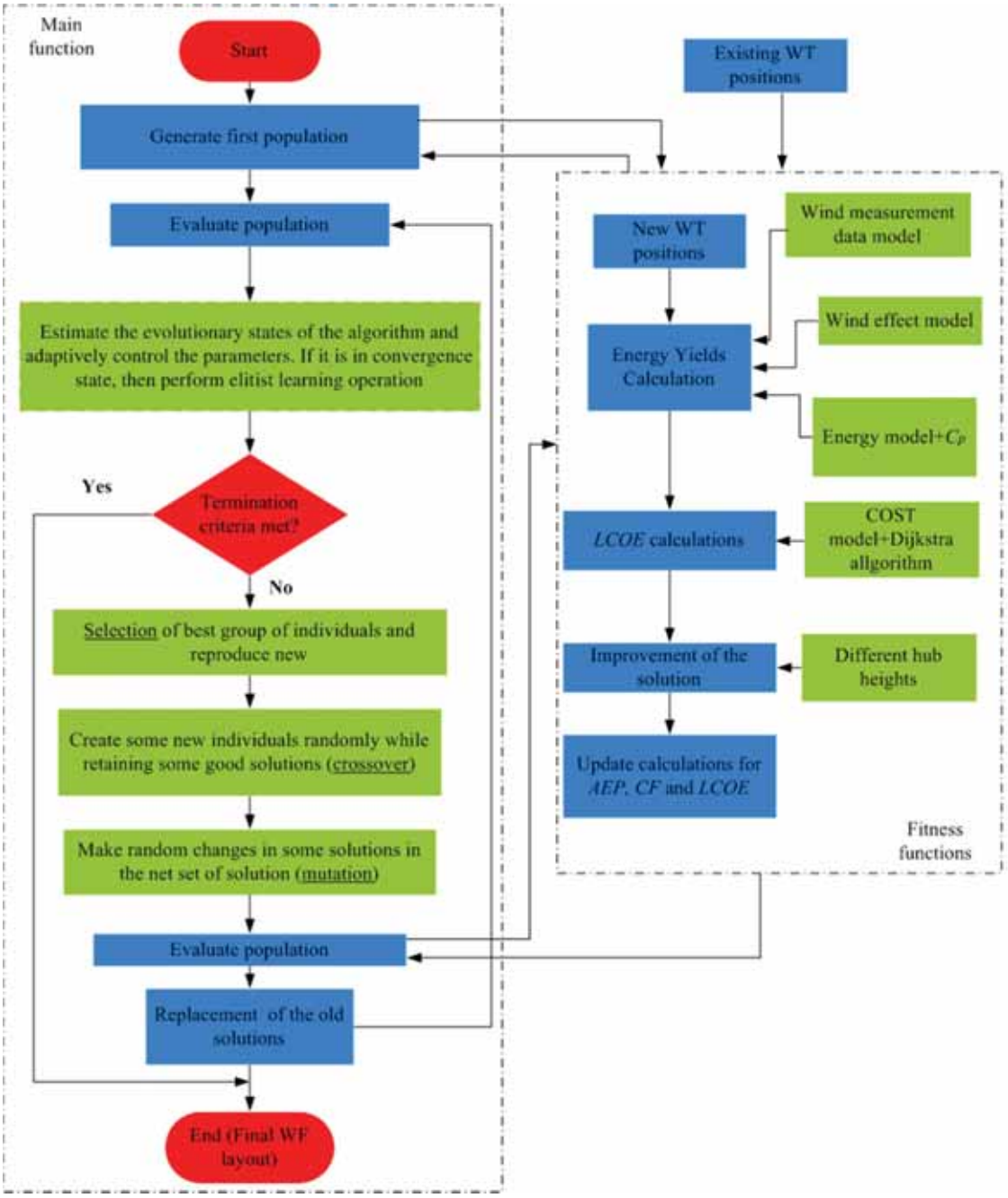

Figure 1. Flowchart of the NSGA II and MO-MDPSO optimization processes

The abovementioned methods are incorporated in an optimization algorithm in order to obtain new WF layouts. These are evaluated using the objective function, by minimization of LCOE and maximizing the CF. In particular, a nondominated sorting genetic algorithm (NSGA) and a mixed discrete particle swarm optimization algorithm (MD-PSO) were applied. For the given case study, both the NSGA and MD-PSO were carried out twice considering the different sets of constraints - binary and continuous.

4. Conclusion

Both developed optimization methods have been applied in the process of positioning wind turbines in a wind field, consisting of 22 turbines, located in a non-cultivated ground in the form of a scalene nonagon, with certain dimensions. The main four scenarios were investigated and significant improvement in the performance of the wind field was observed in each scenario, compared with the reference data for the existing wind field. The novelty that was done is the optimization of each scenario in order to increase the production of electricity from the entire wind field, through individually optimally elevating the hub-height of each wind turbine. With this phase, additional four sub-scenarios have been generated. The verification of the model was made with the data from the project according to which the Bogdanci wind farm is carried out, because until the moment of preparation of tis research in operation was only the first phase of the project. However, for further analysis to be relevant, it was preceded by calculations for the realized production and projected according to the developed model.
It is interesting to emphasize that in all scenarios the calculated LCOE is in the range 6.527 to 8.057 ¢€/kWh, that is, all scenarios have a value under the feed-in tariff of 8.9 € / kWh. At the same time, it is interesting that the value of the capacity factor during all simulation cycles did not exceed the upper limit typical of onshore wind fields (40%). All final scenarios resulted in values for the factor of utilization greater than expected on the entire wind field, that is, the improvements for this parameter are in the range of 4.1-8.64%. For an onshore wind field, such as Bogdanci, only the comparison between numerically calculated indicators and those projected values according to which the wind field is built is not relevant. Namely, it is extremely important to analyze the impact on the environment as well as all social aspects- positive and negative that are carried out by the performance of such a capital energy facility.

Short narrative biography

Maja Celeska Krstevska is currently working as an associate professor at the Ss. Cyril and Methodius University in Skopje. She holds B.Sc. (2012), M.Sc. (2014) and Ph.D (2019) degrees in electrical engineering from the same university. She carried the research for the doctoral dissertation at Graz University of Technology. She is author of more than 30 scientific publications and technical papers from the following areas: renewable energy sources, wind energy conversion, sustainable development and electromechanical energy conversion and. She is a member of IEEE technical professional organization for more than 10 years.

Knowledge distillation in Deep Learning using multimodal networks

Michał Maj[1,2], Tomasz Cieplak[2,3], Damian Pliszczuk[2], Łukasz Maciura[2]

[1] WSEI University, Lublin

[2] Netrix Link sp. z o.o., Lublin

[3] Lublin University of Technology, Lublin

Introduction

Knowledge distillation is a technique used in Deep Learning [1]. Its goal is to transfer knowledge from a larger, more complex model, called the "teacher," to a smaller, more efficient model, the "student." This enables the latter to achieve efficiency similar to the teacher model while reducing resources.
In this technique it is worth distinguishing two stages. The first one is the learning stage. In this case, training is carried out on a large dataset using the computing power of graphics cards. Therefore, you can see that there is no need to solve a given problem in real time. The second stage is the inference stage on real data. In such a case, the model no longer has access to the training data. Additionally, most of the computations will be performed on the CPU and real-time operation is required. Hence, the idea of knowledge distillation emerged, where a larger model requiring high computing power is built for training purposes. A smaller, more efficient model is then built from this model [1].

The Method

Unlike knowledge transfer, where the same model is used for training and inference and then the "head" (output from the trained network) is replaced, knowledge distillation uses two separate models. In the former case, weights are shared between models, while in the latter, generalization is achieved.
Therefore, the goal is to prepare a smaller model that performs the same tasks as the larger model, while being able to perform its work in real time. To do this, one of the elements is training on Soft Labels. The model's predictions are values in the range [0-1] representing the percentage of belonging to a given class. So for the above output (Fig. 1), the soft label has a value of 0.92. In traditional neural networks, one-hot encoding is then used to obtain a hard label. However, when training a student model, soft labels are used for knowledge distillation [1].

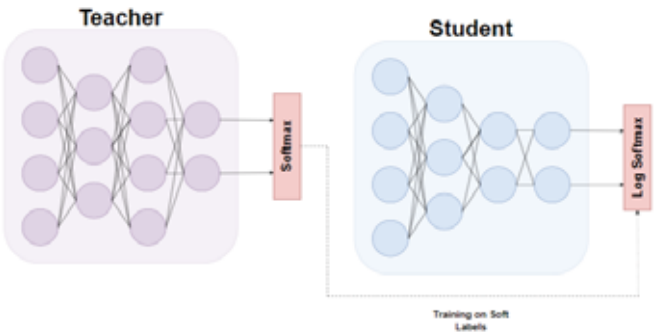

Fig. 1. Soft label training

In the learning process, the Temperature SoftMax function is used (SoftMax with temperature). It differs from the classic version in that the result of the prediction of a given class is first divided by a certain temperature value T. This technique is related to soft labels, because it allows you to notice whether a given class that was indicated during the prediction is similar to another class. Another element influencing effective knowledge transfer is the appropriate loss function for knowledge distillation.

Results

Each of the classic models and the model taught using the multimodal [2] technique were compared separately. Tests were performed on both devices. The inferential effectiveness results obtained by the teacher model are as follows (Fig. 2 a). However, the result obtained by the student model also in the task related to the classification of emotions is presented in Fig. 2 b. Additionally, the time needed to perform the inference was examined. Tab. 1 contains information on the inference time for each teacher model. Tab. 2 contains information about the inference time for individual student models. A lower value means that more image frames per second can be processed, so the less time required for inference, the more efficiently the system operates.

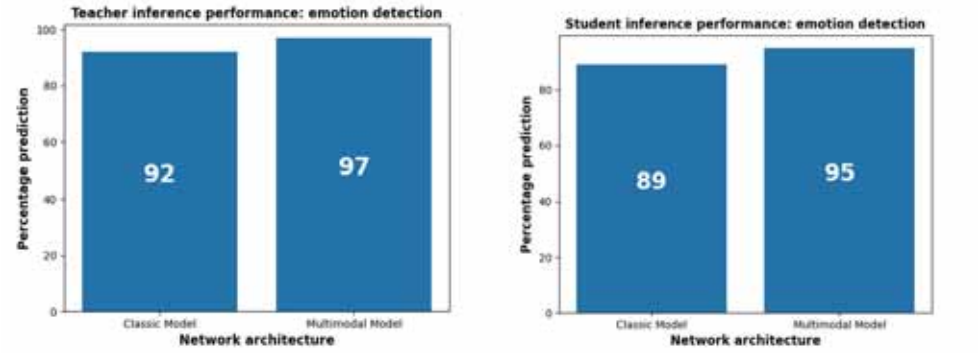

(a) **(b)**

Fig. 2. Comparison of Models Effectiveness in Emotion Detection: (a) – Teacher, (b) – Student

Teacher models / Device	Emotion Detection Model	Face Detection Model	Active User Model	Multimodal Model
Raspberry Pi	0.33s	0.09s	0.06s	0.29s
JETSON Nano	0.24s	0.08s	0.06s	0.15s

Tab. 1. Inference time in seconds for the Teacher model

Student models / Device	Emotion Detection Model	Face Detection Model	Active User Model	Multimodal Model
Raspberry Pi	0.21s	0.07s	0.03s	0.19s
JETSON Nano	0.17s	0.06s	0.01s	0.11s

Tab. 2. Inference time in seconds for the Student model

Conclusions

As presented above, the teacher models perform better in terms of percentage inference score. This is particularly visible in the case of classic models, where the result obtained by the "student" model was less than 90%. However, the "student" model of multimodal networks retained its properties and the average difference in inference was 2%, but was still greater than 92%. This is due to the fact that the multimodal technique allows achieving better results than single classic models [3].

References

[1] V. Nekrasov, T. Dharmasiri, A. Spek, T. Drummond, C. Shen, and I. Reid, "Real-Time Joint Semantic Segmentation and Depth Estimation Using Asymmetric Annotations," Sep. 2018.

[2] M. Maj, T. Rymarczyk, T. Cieplak, and D. Pliszczuk, "Deep learning model optimization for faster inference using multi-task learning for embedded systems," in *Proceedings of the 28th Annual International Conference on Mobile Computing And Networking*, New York, NY, USA: ACM, Oct. 2022, pp. 892–893. doi: 10.1145/3495243.3558274.

[3] M. Maj, T. Rymarczyk, Ł. Maciura, T. Cieplak, and D. Pliszczuk, "Cross-Modal Perception for Customer Service," in *Proceedings of the 29th Annual International Conference on Mobile Computing and Networking*, New York, NY, USA: ACM, Oct. 2023, pp. 1–3. doi: 10.1145/3570361.3615751.

Induction motor diagnostics based on electrical signals analysis using cloud technologies

Dmytro Mamchur, Oleksandr Kasich, Andrii Kalinov, Mykhaylo Zagirnyak

Kremenchuk Mykhailo Ostrohradskyi National University, Kremenchuk, Ukraine

Introduction

Induction motors are widely used in various industrial applications due to their simplicity, reliability, and low maintenance requirements. They operate on the principle of electromagnetic induction, where a rotating magnetic field is induced in the stator, causing rotor movement. They are found in pumps, compressors, fans, conveyors, and other machinery, playing a crucial role in industrial processes [1].

Induction motors are essential for driving machinery and equipment in industries such as manufacturing, mining, transportation, and agriculture. Their ability to operate under varying load conditions makes them suitable for a wide range of applications. They are efficient, durable, and cost-effective, making them indispensable for modern industrial operations.

Motor diagnostics involves assessing the health and performance of induction motors to prevent unexpected failures and downtime. Traditional methods such as visual inspection and vibration analysis have limitations in detecting early-stage faults. Electrical signals analysis offers a complementary approach, as it provides insights into the motor's internal condition by analyzing voltage, current, and power factor signals.

Electrical signals analysis plays a crucial role in diagnosing motor health because it allows for the detection of abnormalities such as rotor bar defects, winding faults, and bearing wear. By analyzing the characteristics of electrical signals, including harmonics, asymmetry, and transients, engineers can identify potential issues before they escalate into major failures. This proactive approach helps in scheduling maintenance activities, minimizing downtime, and optimizing operational efficiency.

Cloud technologies offer scalable and flexible solutions for storing, processing, and analyzing data from induction motors. By leveraging cloud platforms, organizations can centralize motor data from various locations, enabling real-time monitoring and analysis. Cloud-based analytics tools facilitate predictive maintenance by identifying patterns and anomalies in motor performance data, allowing for timely intervention and optimization of maintenance schedules. Furthermore, cloud storage ensures data accessibility and security, enabling collaboration and decision-making across multiple stakeholders.

Diagnostic techniques for induction motors

Currently, for online induction motor operability monitoring, several different approaches could be used. Traditional approach includes following methods.

Vibration Analysis. This method involves monitoring the vibration levels of the motor and analyzing frequency spectra to detect mechanical faults such as misalignment, unbalance, and bearing wear. However, it may not detect early-stage electrical faults.

Temperature Monitoring. Monitoring the temperature of critical motor components helps in identifying overheating issues caused by overload, poor ventilation, or bearing failure. Nevertheless, it may not provide insights into internal electrical faults.

Visual Inspection. Visual inspection involves examining the motor for signs of wear, damage, or contamination. While it is a simple and cost-effective method, it may not reveal hidden faults within the motor windings or rotor.

Traditional methods are effective for detecting mechanical faults but may not always identify early-stage electrical faults, leading to potential undetected issues and unexpected failures.

More advanced diagnostics imply constant diagnostic parameters monitoring, and the most easy-to-implement approaches are based on electrical signals analysis, such as motor current signature analysis (MCSA) [2] and instantaneous power signature analysis (IPSA) [3].

MCSA involves analyzing the current waveform of the motor to detect abnormalities associated with rotor defects, broken rotor bars, or winding faults. It relies on the distinctive signatures present in the current spectrum to diagnose motor health accurately.

IPSA focuses on analyzing the instantaneous power waveform to detect irregularities caused by asymmetry, unbalance, or harmonics in the motor's operation. By examining the power signature, it can provide insights into various electrical and mechanical issues affecting motor performance and could be more efficient for incipient fault diagnostics comparing to MCSA in some cases.

Electrical signals analysis, including MCSA and IPSA, serves as a complementary diagnostic technique to traditional methods. It enables the detection of early-stage faults within the motor's electrical system, enhancing the overall diagnostic accuracy and enabling proactive maintenance interventions. Additionally, it provides a non-invasive and cost-effective approach to monitor motor health, contributing to improved reliability and efficiency in industrial operations.

The use of cloud computing in induction motor health monitoring

Cloud platforms can be integrated with motor diagnostics systems to streamline data collection, storage, analysis, and visualization processes. Integration involves connecting motor sensors and diagnostic devices to cloud-based applications or platforms, allowing real-time data streaming and analysis. Such approach provides following benefits.

Real-Time Monitoring. Cloud-based platforms enable real-time monitoring of motor performance, providing instant alerts for abnormal operating conditions or potential faults detected through electrical signals analysis.

Advanced Data Analysis. Cloud-based analytics tools can process large volumes of motor data, perform advanced diagnostics, and generate actionable insights to optimize maintenance schedules and improve motor reliability.

Remote Access. Cloud-based solutions allow maintenance engineers and stakeholders to access motor diagnostic data from anywhere, using web-based interfaces or mobile applications, facilitating remote troubleshooting and decision-making.

Predictive Maintenance. By leveraging historical motor performance data stored in the cloud, organizations can implement predictive maintenance strategies, predicting and preventing failures before they occur, minimizing downtime, and maximizing equipment uptime.

In summary, cloud technologies offer numerous advantages for storing, processing, and analyzing data generated from electrical signals analysis of induction motors. Integration of cloud platforms with motor diagnostics enables real-time monitoring, proactive maintenance, and optimization of motor performance, contributing to enhanced reliability and efficiency in industrial operations.

Proposed solution

In this research authors proposed induction motors online monitoring system based on both MCSA and IPSA, using mathematical apparatus described in [3]. The system consists of 3 main parts: Field devices, Cloud Computing part and User Clients. Field devices include set of current, voltage, temperature and vibration sensors attached to controlled motor or mechanism, which send collected raw data to microcontroller for preprocessing and preliminary analysis, indicating alert signal in case harmful motor

faults detected and ensuring emergency equipment stoppage when necessary. Then preprocessed data is transferred to the cloud server where it is stored in database and used as an input for „intelligent analysis" block, where deeper analysis, based on updated and historical data, is provided, and stored in separate database. Finally, prepared results for equipment current technical conditions could be available by means of end-devices, such as smartphones, laptops, PC, etc., to end-users, summarizing current technical conditions of controlled devices, forecasting the next maintenance period and sending alerts in case of emergency situations. Block diagram of the proposed system is presented in fig. 1.

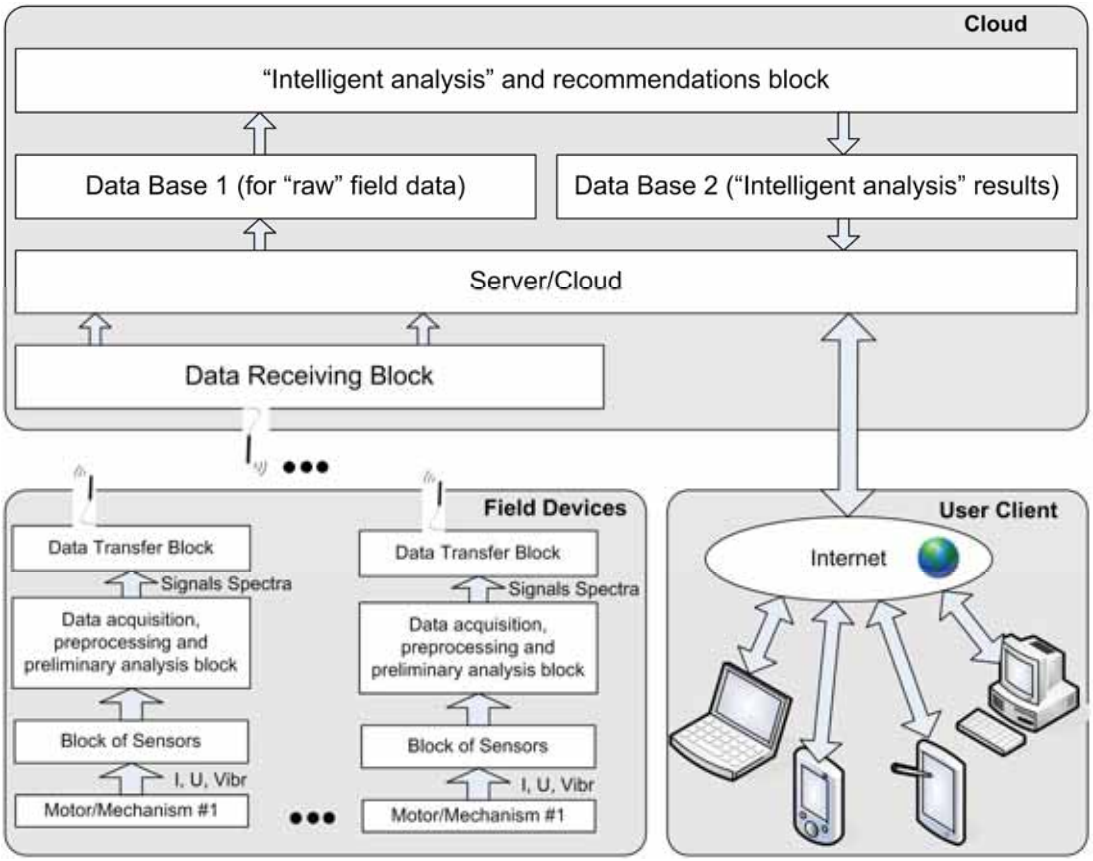

Fig. 1. The block-diagram of cloud-based induction motors monitoring systems using electrical signals analysis methods

Conclusion

In this research authors presented their own view of the induction motors cloud-based diagnostic system based on electrical signals analysis. Such approach provides possibility to create relatively cheap system which provides online equipment diagnostics without necessity to suspend manufacturing process for diagnostic procedures, allows one to detect incipient faults due to constant monitoring of diagnostic parameters along with historical data analysis. Also, proposed approach allows one to implement condition-based equipment maintenance reporting instant health condition summary to end-users by mobile and internet technologies.

References

[1] M. Yousuf, et al.: IoT-based health monitoring and fault detection of industrial AC induction motor for efficient predictive maintenance. – Measurement and Control, pp. 1–15, 2024.

[2] M. E. H. Benbouzid "A review of induction motors signature analysis as a medium for faults detection", IEEE Transactions on Industrial Electronics, vol. 47, no. 5, pp. 984–993, Oct. 2000.

[3] M.V. Zagirnyak, D.G. Mamchur, A.P. Kalinov, "Comparison of induction motor diagnostic methods based on spectra analysis of current and instantaneous power signals," Przeglad Elektrotechniczny, Iss. 12b/2012, pp. 221–224.

Assessment of electromagnetic coupling of electric power systems to pipelines using combined method of moments and transmission line theory based approach

Blagoja Markovski[1], Leonid Grcev[2]

[1] Ss. Cyril and Methodius University in Skopje, Faculty of Electrical Engineering and Information Technologies, Skopje Macedonia, bmarkovski@feit.ukim.edu.mk

[2] Macedonian Academy of Sciences and Arts, Macedonia, leonid.grcev@ieee.org

Abstract

In this paper we describe a computer model that simultaneously accounts the inductive coupling of the pipeline with power lines by utilizing the transmission line theory and the conductive coupling of the pipeline with nearby grounding systems by utilizing a full-wave electromagnetic model based on the method of moments. The paper also provides results of a case study to demonstrate the importance of such approach.

1 Introduction

Electromagnetic coupling of electric power system to nearby pipelines may result with induction of excessive pipeline-to-soil voltages that can endanger people and disrupt pipeline system safety and reliability [1]. Such voltages can be produced both in steady-state and in fault conditions of the electric power system. Accurate analysis of electromagnetic coupling of these systems is required, in order to implement proper mitigation and reduce induced voltages to safe levels.

The most complex scenario for computer modeling is when the pipeline is simultaneously subjected to inductive and conductive coupling. Then, the pipeline-to-soil voltage is calculated as a difference between the soil and pipeline potentials along the pipeline, and depending on the phase difference of these potentials they can act additive or reductive. Therefore the analysis of such scenario requires computer model that can simultaneously account for the inductive and conductive coupling of electric power system to pipelines.

This paper describes a computer model that simultaneously accounts the inductive coupling of the pipeline with power lines by utilizing the transmission line theory [2] and the conductive coupling of the pipeline with nearby grounding systems by utilizing a full-wave electromagnetic model based on the method of moments [3]. The computer model enables analysis of electromagnetic coupling of pipelines with underground or aboveground power lines and complex grounding systems, while considering soil resistivity variations and different AC mitigation techniques along the pipeline and the power system.

2 Brief description of the model

In the computer model, the pipeline and the electric power system are described by their geometrical and electrical characteristics. After importing this data, the physical system is transformed into electric circuit equivalent, as illustrated in Fig. 1. The longitudinal and transversal electrical equivalents of the power lines, pipeline, screening conductors and their mutual coupling are derived by utilizing transmission line theory. Geometry of the grounding systems, as a more complex structures, is imported

in a *.dxf format. The computer model then calculates the equivalent impedance of the grounding system and the soil potentials around the pipeline, and integrates this data into the circuit equivalent of the systems. Calculations are then performed for single line-to-ground faults for hundreds of different positions along the power system, while searching for worst-case scenario and testing the effectiveness of different mitigation methods.

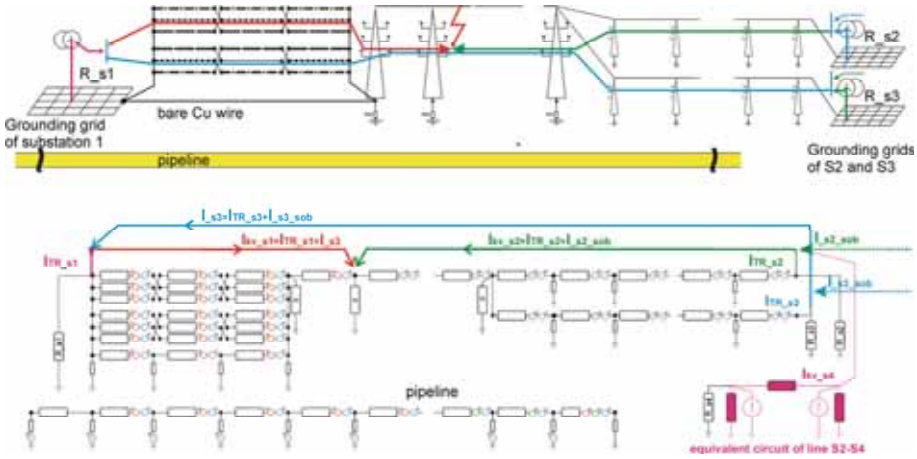

Fig. 1. Example for a physical and its equivalent circuit model of mixed overhead-underground power line and pipeline

3 Case study

In the considered case, the pipeline is subjected to simultaneous conductive coupling from 110/20 kV substation that is mutually connected by the shields of medium voltage cables with the grounding systems of 20 MW photovoltaic plant that surround the pipe. The pipeline is also subjected to inductive coupling from 110 kV overhead power line that is connected to the substation and is parallel with the pipeline. The 92 km pipeline section, soil variations along the pipeline and the existing AC mitigation devices along the pipeline are considered in the analysis. The results obtained by the model, that are provided in Fig. 2, give insight into the induced potentials from different coupling mechanisms and facilitate the choice of proper mitigation.

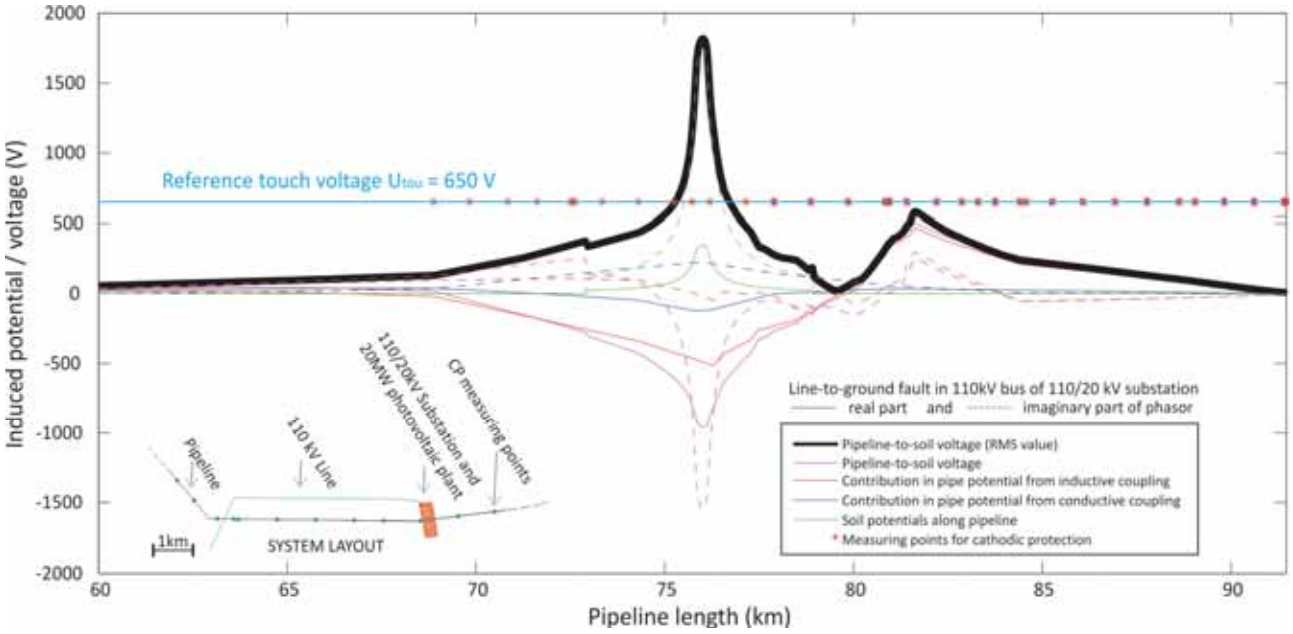

Fig. 2 Layout of the analyzed systems and results from the analysis in fault conditions

References

[1] EN 50443:2011 – Effects of electromagnetic interference on pipelines caused by high voltage a.c. electric traction systems and/or high voltage a.c. power supply systems, CENELEC, Brussels, (2011).

[2] Directives concerning the protection of telecommunication lines against harmful effects from, from electric power and electrified railway systems, Capacitive, inductive and conductive coupling: Physical theory and calculation methods – Vol. III, CCITT, Geneva (1989).

[3] B. Markovski, L. Grcev, V. Arnautovski-Toseva, (2021), "Fast and Accurate Transient Analysis of Large Grounding Systems in Multilayer Soil", *IEEE Transactions on Power Delivery*, **Vol**. 36, No. 2, pp. 598-606.

Full-wave electromagnetic model for grounding and cable analysis in multilayer earth

Blagoja Markovski[1], Leonid Grcev[2], Vesna Arnautovski-Toseva[1]

[1] Ss. Cyril and Methodius University in Skopje, Faculty of Electrical Engineering and Information Technologies, Skopje Macedonia, bmarkovski@feit.ukim.edu.mk, atvesna@feit.ukim.edu.mk

[2] Macedonian Academy of Sciences and Arts, Macedonia, leonid.grcev@ieee.org

Abstract

In case of lightning and fault conditions, hazardous voltages can be transferred to different parts of plant or distant facilities by the metallic shields of power cables. Excessive voltages can endanger people and disrupt system safety and reliability, therefore modelling of grounding systems and their connections with cable shields is of particular importance for the safety analysis. This paper presents a computer model for grounding analysis, based on a full-wave electromagnetic theory and the method of moments, that accurately accounts the electromagnetic interactions between bare and insulated conductors in a multilayer soil. The computer model is validated with published and simulated data, and used in a case-study of large and mutually interconnected grounding systems.

1 Introduction

Metallic cable shields may have significant effect on grounding system performance in case of lightning or fault conditions, since large portion of current may be led into the metallic shields and carried away to other locations. This usually improves grounding conditions at the fault location, but hazardous voltages may be transferred to other facilities and may endanger people and disrupt safety and reliability of affected systems. Therefore, analysis of grounding performance and safety, where connections of cable shields within large grounding system or between distant grounding systems exist, require computer models that can account for the mutual electromagnetic interactions between bare and insulated conductors.

In a previous paper, authors have presented computer model based on a full-wave electromagnetic theory and the method of moments (MoM), for accurate analysis of large and complex grounding systems in a multilayer soil [1]. The model was limited only in analysis of bare conductors. This paper presents an extension of that model to include both bare and insulated conductors. The paper is organized as follows: 1) description of the model, 2) validation with experimental and simulated results, 3) application of the computer model in a case study of large and mutually interconnected grounding systems.

2 Description of the model

In this computer model, the analysed grounding systems are assumed to comprise a network of N straight thin cylindrical conductors in multilayer soil, where a constant longitudinal current I_n for the n-th conductor is assumed. The current distribution in the grounding system for any type of energization is obtained by solving the following matrix equation:

$$[\,Z\,]\cdot[\,I\,]=[\,V\,] \tag{1}$$

Here, [I] is a column matrix with unknown longitudinal currents in the grounding system, [V] is related to energization of the system and [Z] is generalized impedance matrix where each Z_{mn} element describes the electromagnetic interactions between m-th illuminated and n-tn source segment. These elements are calculated by utilizing (MoM) [2] with the thin-wire approximation and the extended boundary condition [3]. For bare source segment, in the i-th layer of multilayer soil, the Z_{mn} element is calculated by Eq. (2), and for insulated source segment by Eq (3).

$$Z_{mn} = \frac{\Delta\ell_m}{4\pi}\left(j\omega\mu_0 \int_{\ell'_{n(a)}} \overline{\overline{G}}_A d\ell'_{n(a)} - \frac{1}{\underline{\sigma}_i}\frac{\partial}{\partial\ell_m}\int_{\ell'_{n(a)}} \frac{\partial}{\partial\ell'_{n(a)}} G_\Phi d\ell'_{n(a)} \right) \tag{2}$$

$$Z_{mn} = \frac{\Delta\ell_m}{4\pi}\left(j\omega\mu_0 \int_{\ell'_{n(a)}} \overline{\overline{G}}_A d\ell'_{n(a)} - \frac{1}{\underline{\sigma}_c}\frac{\partial}{\partial\ell_m}\int_{\ell'_{n(a)}} \frac{\partial}{\partial\ell'_{n(a)}} G_\Phi d\ell'_{n(a)} - \left(\frac{1}{\underline{\sigma}_i} - \frac{1}{\underline{\sigma}_c}\right)\frac{\partial}{\partial\ell_m}\int_{\ell'_{n(b)}} \frac{\partial}{\partial\ell'_{n(b)}} G_\Phi d\ell'_{n(b)} \right) \tag{3}$$

The conductor is with radius a and the insulation is with outer radius b and with conductivity σ_c. Details of the theory behind Eq. (2) can be found in [4] and the treatment of the insulating layer in Eq. (3) is based on the approach that was initially proposed in [5] for homogeneous space.

3 Case study

In the considered case, grounding systems of a 110/20 kV substation and two 10 MW photovoltaic power plants are mutually connected by the shields of medium voltage cables, as illustrated in Fig. 1. The surrounding soil can be characterized by two-layer soil model with ρ_1=120 Ωm and 2.6 m thickness of the upper layer, and ρ_2=350 Ωm with infinite thickness for the lower layer. Due to the small mutual separations, grounding systems have strong interaction and cannot be analyzed separately in safety analysis. Therefore, the presented computer model is utilized for the large (approx. 330 x 860 m) grounding system with bare and insulated conductors. The results for the conductor potentials due to single line-to-ground fault in the 110 kV bus of the 110/20 kV substation, with I_f = 6.1 kA, are presented in Fig. 1. Extensive analysis will be provided in the complete paper.

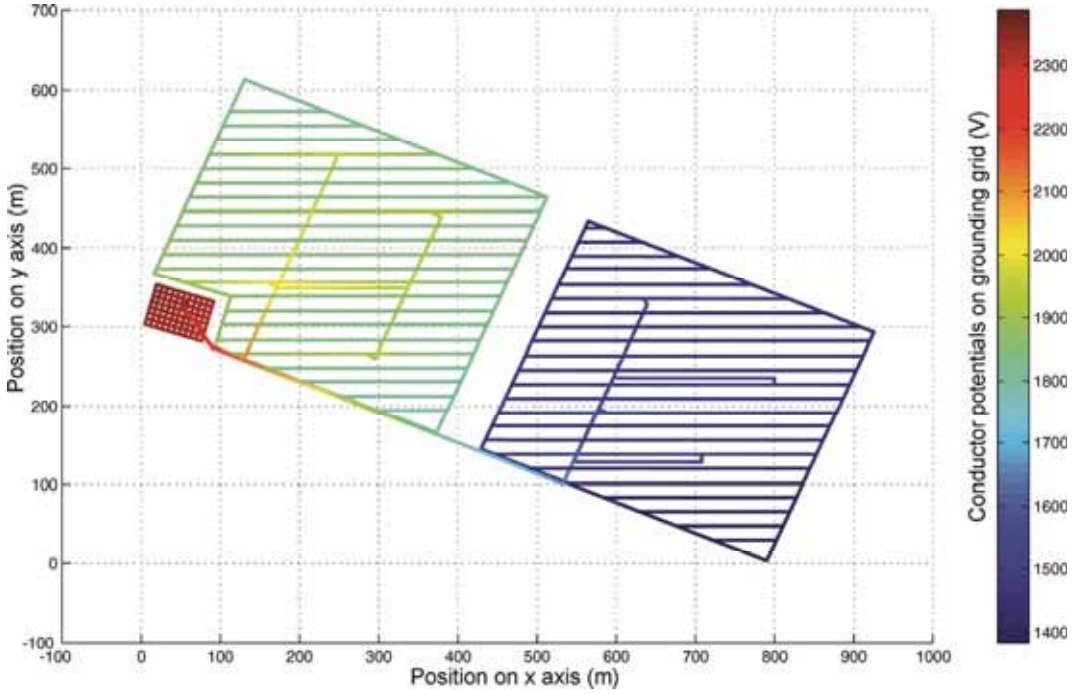

Fig. 1. Calculated conductor potentials due to single line-to-ground fault in the 110 kV bus of 110/20 kV substation

References

[1] B. Markovski, L. Grcev, V. Arnautovski-Toseva, (2021), "Fast and Accurate Transient Analysis of Large Grounding Systems in Multilayer Soil", *IEEE Transactions on Power Delivery*, **Vol**. 36, No. 2, pp. 598-606.
[2] R. F. Harrington, (1967), "Matrix methods for field problems," *Proc. IEEE*, **Vol**. 55, no. 2, pp. 136–149.
[3] B. M. Kolundzija, A. R. Djordjevic, Electromagnetic Modeling of Composite Metallic and Dielectric Structures. Norwood, MA: Artech House, (2002).
[4] L. Grcev, A. Kuhar, V. Arnautovski-Toseva, B. Markovski, (2018), "Evaluation of High-Frequency Circuit Models for Horizontal and Vertical Grounding Electrodes", *IEEE Transactions on Power Delivery*, **Vol**. 33, No. 6, pp. 3065-3074.
[5] B. D. Popovic, A. R. Djordjevic, N. M. Kircanski, (1981), "Simple method for analysis of dielectric-coated wire antennas," *Radio Electron. Eng*., **Vol**. 51. No. 3. pp. 141-145.

Maximum power point determination of bifacial PV using teaching and learning based optimization algorithm

Angela Najdoska[1], Goga Cvetkovski[1]

[1] Ss Cyril and Methodius University,
Faculty of Electrical Engineering and Information Technologies,
Rugjer Boskovic 18, P.O. Box 574, 1000 Skopje, North Macedonia,
anenajd9@gmail.com, gogacvet@feit.ukim.edu.mk

Abstract
In photovoltaic systems it has been always a challenge to determine the methodology for calculation of the maximum power point (MPP) for given system, location and atmospheric conditions. Therefore, many optimization methods are in use as well as different photovoltaic cell circuit presentations. The determination of the MPP in the process of design of a photovoltaic (PV) power plant for the dimensioning of all the applied equipment to determine is quite a challenge and can be of great importance. For that reason, in this paper the MPP will be determined using the teaching and learning optimization algorithm applied on an ideal single-diode cell model.

1 Introduction

The increased need for electricity and the strategy for application of green, clean and renewable energy sources for production of electricity encouraged the governments, the power companies and investors to orient the electricity production towards renewable energy sources. The photovoltaics are one of those sources that have been installed in the world following an exponential rate during the years. The same applies in North Macedonia with a trend more bifacial photovoltaics (PV) to be in installed in the past few years. During the past several years, by the companies dealing with design and installation of PV system, it was found out that during the design process it is very important to know the MPP of a given system for different weather conditions. This is especially important for the design and configuration of the individual elements of the PV system. In order to achieve this goal there is a need for a large number of calculation of the MPP for different solar irradiations at different seasons and temperatures. Beside those conditions the bifaciality of the PVs has to be taken into consideration. Actually the bifaciality of the PVs at some weather conditions can cause significant increase of the output power if it is not taken into consideration during the design process of a given PV plant. In order tackle this problem a good and reliable optimization algorithm should be used in which all the necessary conditions and different combinations can be taken into account. In this paper the teaching and learning optimization algorithm is applied in the optimization process.

2. Teaching and learning optimization algorithm

The optimization methods generally can be divided in two groups: deterministic and stochastic methods. On the other hand, the stochastic methods are grouped in two main groups: direct search methods and heuristic methods. Most of the heuristic methods belong to one big group of methods called nature based methods. This type of methods can be organized in four main groups: Evolutionary algorithms, swarm based algorithms, natural sciences based algorithms and human behavior related methods. The investigated teaching and learning optimization algorithm belongs to the human behavior related group of optimization methods. This algorithm belongs to the so called human related group of algorithms in

which beside TLBO algorithm also Cooperative search, Football game inspired algorithm, Cultural evolution and many others belong. Teaching and learning based optimization algorithm (TLBOA) is a population-based metaheuristic optimization technique that simulates the environment of a classroom to optimize a given objective function and it was proposed by R.V. Rao et al. in 2011 [1]. This means that the methods works on a set of members named teachers and learners and by using the metaheuristic approach which translated from Greek language means meta (beyond or high level and heuristic (greek - heuriskein or euriskein, to search). The algorithm simulates a classroom in which in the first stage the teacher puts his hard work and makes all the learners of the class to be educated. Then in the second stage the learners interact with themselves to further modify and improve their gained knowledge. In this optimization algorithm, a group of learners is considered as population and different subjects offered to the learners are considered as different design variables of the optimization problem and a learner's result is analogous to the 'fitness' value of the optimization problem. The best solution in the entire population is considered as the teacher. The design variables are actually the parameters involved in the objective function of the given optimization problem and the best solution is the best value of the objective function.

3. Maximum power point determination of a PV module using TLBOA

The objective of this research work is to determine the maximum power point of a bifacial photovoltaic (PV) module for different weather conditions. Therefore, in this work an ideal PV bifacial cell circuit presentation [2] is used in which the current through the diode is neglected. The standard mono-facial presentation is modified in order to take into account the bifaciality of the PV module which in this analysis is predefined to be 10%. The circuit presentation is shown in Fig. 1. The objective function for this optimization process is defined as absolute value of the difference between the calculated power ($P_{mpp,TLBOA}$) and the power given by the producer ($P_{mpp,catalog}$) for given conditions presented by equation (1).

$$Objective\ function = dP = \left| P_{mpp,TLBOA} - P_{mpp,catalog} \right| \quad (1)$$

Table 1. Optimization data at 1000 W/m^2 and 25°C

Variables	*Unit*	*Catalogue data*	*TLOA solution*
V_{mpp}	(V)	41.65	41.2668
I_{mpp}	(A)	13.88	14.009
ΔP	(W)	/	$5.684 \cdot 10^{-13}$
P_{mpp}	(W)	578.102	578.102

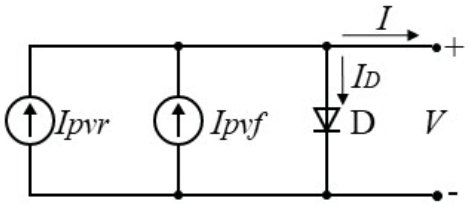

Fig. 1 Ideal bifacial PV cell model presentation

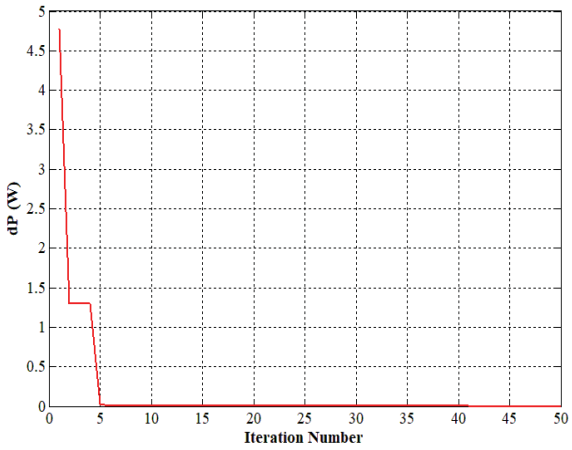

Fig. 2 Objective function change during iterations

The results from the optimization for 1000 W/m^2 and 25°C are presented in Table 1 in comparison with the catalogue data provided by the producer [3]. The change of the objective function value during the iterations is presented in Fig. 2. From the presented data it can be concluded that the applied optimization method is quite appropriate for the application, the used PV equivalent circuit model serves well and the gained results from the optimization are satisfactory.

The full version of the paper will contain a more detailed explanation of the teaching and learning based optimization algorithm. Also the equations that define all the parameters of the equivalent PV cell circuit

will also be presented. An extended number of optimizations will be realized and the data from those optimizations including the solar irradiations of 600 W/m^2 and 200 W/m^2 at the same ambient temperature of 25°C, as well as for other ambient temperatures in order to take into consideration the different seasons will be presented. The aim of the additional optimizations for other solar irradiations is to validate the model and the performance of the algorithm for different working weather conditions.

References

[1] R.V. Rao, V.J. Savsani, D.P. Vakharia, "Teaching–learning-based optimization: A novel method for constrained mechanical design optimization problems", *Computer-Aided Design*, **Vol. 43**, Issue 3, pp. 303-315.
[2] G.B. Byeong, L. Wonbin, "Power Performance of Bifacial c-Si PV Modules with Different Shading Ratios", *IEEE Journal of Photovoltaics*, **Vol 9**, No. 5, pp. 1413-1420.
[3] Jasolar, https://www.jasolar.com/uploadfile/2022/0511/20220511055529246.pdf (09.09.2023).

Optimizing energy management: a case study on hybrid energy storage systems for commercial facilities

Rosana Petrusheva[1], Maja Celeska Krstevska[1]

[1] Ss. Cyril and Methodius University in Skopje,
Faculty of Electrical Engineering and Information Technologies,
Rugjer Boshkovikj No. 18, North Macedonia,
celeska@feit.ukim.edu.mk

Abstract

This case study investigates the implementation and performance of hybrid energy storage systems (HESS) in commercial facilities, aiming to maximize energy efficiency and minimize operational costs. The paper begins by examining the motivations behind adopting HESS, including the need for reliable power supply, grid stability, and the desire to reduce carbon footprint. Key considerations in the design and deployment of HESS are discussed, including system sizing and control strategies for optimal operation. Additionally, the potential synergies between HESS and other energy management technologies, such as photovoltaic panels and smart building systems, are explored to further enhance overall efficiency and sustainability. Through this case study, valuable insights are provided for stakeholders in the commercial sector seeking to adopt HESS as a viable solution for optimizing energy management, reducing reliance on conventional power sources, and advancing towards a more sustainable future.

1. Introduction

In recent years, the integration of renewable energy source (RESs) s into commercial facilities has gained significant momentum due to environmental concerns and the pursuit of energy cost reduction. There has been a growing recognition of the significance of renewable energy sources like solar photovoltaic (PV) and wind power [1]. In response to this, microgrids have been increasingly adopted to harness these RESs more efficiently and economically, [2]. However, the inherent volatility and intermittency of RESs pose challenges such as power mismatches, voltage fluctuations, and system instability, particularly in DC microgrids. To mitigate these issues, energy storage systems (ESSs) are being deployed within DC microgrids. These ESSs play a crucial role in stabilizing the system, managing power fluctuations, and ensuring reliable energy supply, thereby enhancing the overall performance and viability of DC microgrid systems, [3,4].

2. Manuscript preparation

This study examines an object with an annual consumption of 37.6 MWh. The total roof area of the object is 1870 m^2, when a quarter of its area will be used for installed a photovoltaic power plant with a capacity of 71.68 kWp, the total annual energy production will be 98 MWh. However, given the variable nature of solar energy, it is necessary to install energy storage systems. This study will use two energy storage systems: i) Lithium-ion battery system, and ii) Hydrogen storage system, as shown in the figure below.

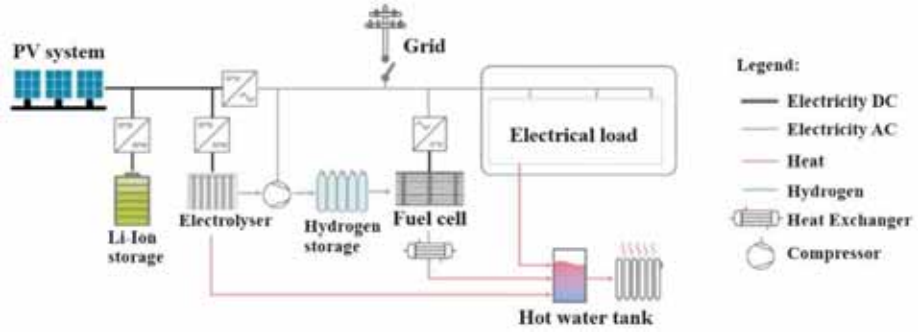

Fig. Topology of solar energy model with hybrid energy storage system

It should be noted that the object under study is a warehouse for metal products, so it has an almost constant electricity consumption throughout the year. Lithium-ion battery systems are used to meet the object's needs for shorter period of time, usually a few days. The way these batteries work is as follows: In a lithium-ion battery, lithium ions (Li+) move between the cathode and anode internally. Electrons move in the opposite direction in the external circuit. This migration is the reason the battery powers the device - because it generates electric current.

Given that the average daily consumption of the object is 103 kWh, to meet the object's needs for 3 days, two batteries need to be installed. The batteries planned for this study are manufactured by Huawei, model LUNA2000-161KWH-2H1, with a capacity of 161.3 kWh per battery.

Charging these batteries requires approximately 50 hours. Taking days with 12 hours of sunlight into account, it would take around 4 days to fully charge both batteries.

In addition to batteries, controllers are essential for regulating the battery charging and discharging processes, preventing potential damage from over-discharge or over-charge. In contrast to lithium-ion battery systems, hydrogen storage systems serve long-term energy needs. To enable the storage of hydrogen, the electrolysis process is necessary. Electrolysis is a promising option for hydrogen production without carbon from renewable and nuclear resources. Electrolysis is the process of using electrical energy to split water into hydrogen and oxygen. This reaction takes place in an electrolyzer. An alkaline electrolyzer is employed here, operating by transporting hydroxide ions (OH-) through the electrolyte from cathode to anode, while hydrogen is produced at the cathode. In this case, an electrolyzer manufactured by McLyzer, model 200-30, is used, where the hydrogen production is 200 Nm3/h, or for 12 hours, the hydrogen production is 211.2 kg. The produced hydrogen needs to be stored in cylinders, from which the hydrogen is then transferred to fuel cells to generate energy.

Fuel cells work like batteries, but they do not need to be charged or discharged. They generate electrical energy and heat as long as they are supplied with fuel. The fuel cell consists of an anode and a cathode placed around the electrolyte. The anode is supplied with fuel, such as hydrogen, while the cathode is supplied with air. The catalyst on the anode separates the water molecules into protons and electrons, which take different paths to the cathode. Electrons pass through the external circuit, creating a flow of electric energy. Meanwhile, protons pass through the electrolyte to the cathode, where they combine with oxygen and electrons to produce water and heat. In this study, fuel cells of the type FCgen®-H2PM 1.7 kW/48V are used. One fuel cell produces a power of 1.5 kW. To meet the required average daily power of 4.3 kW, 3 fuel cells are needed, which means 7.8 kg of hydrogen. Therefore, to cover the object's needs in case it is disconnected from the grid, 720 kg of hydrogen will be required for 3 months. This amount of hydrogen, produced by the electrolyzer, would be provided in 41 hours, and would require 203 cylinders of 50L for hydrogen storage.

3. Conclusion

Given that the price of electricity at noon is significantly lower compared to morning and evening hours, and it is expected to be even lower in the future during that time of day, energy storage systems will be of great importance.

References

[1] STATISTA, Solar PV - statistics & facts report, 10.01.2024, available at https://www.statista.com/topics/993/solar-pv/#dossier-chapter
[2] L. Olatomiwa, S. Mekhilef, M.S. Ismail, M. Moghavvemi (2016), "Energy management strategies in hybrid renewable energy systems: A review", *Renewable and Sustainable Energy Reviews*, **Vol. 62**, pp. 821-835.
[3] G. A. Ramos, R. C. Castelo, (2022), "Energy Management Strategies for Hybrid Energy Storage Systems Based on Filter Control: Analysis and Comparison", *Electronics*, **Vol. 11 (10)**.
[4] Y. Wang, W. Li, Z. Liu, L. Li. (2023) „An Energy Management Strategy for Hybrid Energy Storage System Based on Reinforcement Learning“, *World Electric Vehicle Journal,* **Vol. 14 (3)**.

Agrovoltaics – the integration of agricultural cultivation and electricity production

Sebastijan Seme[1,2], Eva Simonič[1], Bojan Stergar[1], Klemen Sredenšek[1]

[1] Faculty of Energy Technology, University of Maribor, Hočevarjev trg 1, 8270 Krško, Slovenia
e-mail: sebastijan.seme@um.si; eva.simonic@um.si;
bojan.stergar@um.si; klemen.sredensek@um.si,

[2] Faculty of Electrical Engineering and Computer Science,
University of Maribor, Koroška cesta 46, 2000 Maribor, Slovenia

Abstract
The paper discusses the possibility of integrating photovoltaic devices into agricultural land. This simultaneous use of land for both agriculture and electricity production from photovoltaic devices is called agrovoltaics. It represents an innovative approach to introducing renewable energy sources (primarily solar energy) and the co-use of land for agriculture to achieve the goals set out in the European Green Deal. Changes in the energy sector and the need for sustainable energy sources place photovoltaic devices at the forefront as a key part of the energy transition. At the same time, preserving agricultural land and food processing are crucial for ensuring food security. The paper presents European legislation, examples of agricultural crops, and examples of best practices in Europe and Slovenia.

1. Introduction – Description of co-located energy activities using the example of integrating agricultural cultivation and electricity production

The concept of co-located energy activities focuses on integrating various activities, in the case of agrovoltaics, it involves combining agricultural production and electricity generation, aiming to optimize resource utilization and enhance sustainability. This approach can yield greater synergies and economic benefits. Terms such as "Agrovoltaics", "Agrivoltaics", "Agro-photovoltaics", or "Agri-photovoltaics" refer to the simultaneous use of land for agriculture and electricity production from photovoltaic devices. This is a concept of co-located energy activities, such as combining agricultural processing and electricity generation. Agrovoltaics is associated with numerous policies in energy, agriculture, environment, and circular economy, as well as research and innovation supporting the goals of the European Green Deal. The aim of the European Green Deal is to achieve Europe's climate neutrality by 2050, boost the economy with green technology, create sustainable industry and transport, and reduce pollution. By turning climate and environmental challenges into opportunities, the transition will be fair and inclusive for all. Summarized from [1].
Decarbonizing the energy system is essential to achieve the European Union's (EU) climate goals by 2030 and 2050. At the same time, energy must be secure and affordable for consumers and businesses. To make this happen, member states must transform their energy systems into a fully interconnected, digitized, and competitive EU energy market, largely based on renewable energy sources. In addition to regulatory reforms, member states must enable and promote further investment in clean energy, including energy efficiency. Summarized from [1].

2. Suitable agricultural crops

The suitable agricultural crops depend, of course, on the location of cultivation and environmental needs. Agricultural crops can further be classified based on the type of farming: Crops (Crop cultivation refers

to the production of typical crops, including wheat, potatoes, maize, etc. These crops are grown annually and are highly mechanized in most countries.); Orchards and Greenhouses: (Fruits (such as apples, pears, berries, grapes), vegetables, or trees/shrubs are typically planted in rows. These crops already require protection from extreme weather conditions with hail nets, for instance.). Agricultural crops can also be classified based on the type of farming system used: open or closed farming (processing) systems. Open systems are installed in open areas between or above livestock or crops. An example of a closed agrovoltaic system is a greenhouse where solar panels are installed on the greenhouse itself. Figure 3.8 illustrates the classification of agrovoltaics and examples of their use in agricultural products or activities. Summarized from [2] and [3].

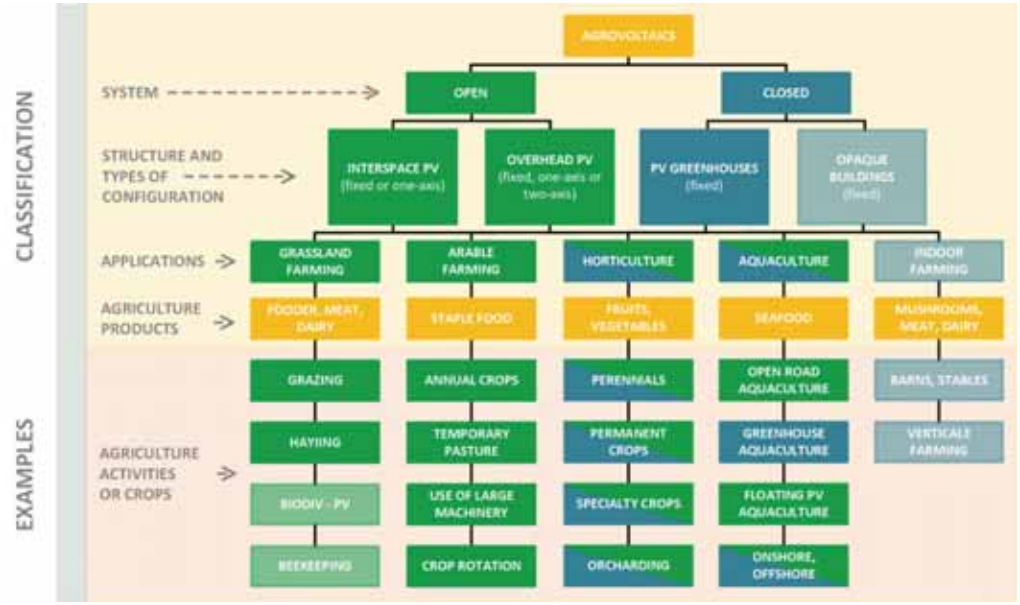

Figure 1: Classification of agrovoltaics and examples of their use in agricultural products or activities [3]

3. Conclusion

The paper presents agrovoltaics as an opportunity to use agricultural land and simultaneously produce electricity from photovoltaic devices. We find that the concept of co-located energy activities, such as agrovoltaics, represents an innovative path towards optimal resource utilization and increased sustainability. The potential of agrovoltaics in the European Union is extremely significant. According to some estimates, covering just 1% of all agricultural land could yield up to 940 GW_p of installed photovoltaic capacity, nearly five times more than the current installed capacity of all photovoltaic devices in the European Union. However, agrovoltaics faces numerous challenges, including the lack of a clear and coordinated European definition. Nevertheless, European Union member states generally express support for renewable energy sources, although the majority of strategic plans do not explicitly include support for agrovoltaics.

Acknowledgements

This APC was funded by Slovenian Research Agency under grants Applied Electromagnetics P2- 0114.

References

[1] Green transition; [Online]; available at: https://reform-support.ec.europa.eu/what-we-do/green-transition_sl#energija ; [attempt to access 15. 12. 2023].

[2] Sarr, A.; Soro, Y.M.; Tossa, A.K.; Diop, L. Agrivoltaic, a Synergistic Co-Location of Agricultural and Energy Production in Perpetual Mutation: A Comprehensive Review. Processes 2023,11,948. https://doi.org/ 10.3390/pr11030948

[3] Market research study Agrovoltaics; [Elektronski]; dostopno na: https://science.osti.gov/-/media/sbir/pdf/Market-Research/SETO---Agrivoltaics-August-2022-Public.pdf; [poskus dostopa 15.12. 2023].

Luminous flux and electrical parameters analysis in short-term stabilization duration of street luminaire

Roman Sikora[1], Przemysław Markiewicz[1], Ewa Korzeniewska[2], Alyona Nikitina[3]

[1] Lodz University of Technology, Institute of Electrical Power Engineering, Poland

[2] Lodz University of Technology, Institute of Electrical Engineering Systems, Poland

[3] Mykhailo Ostrohradskyi National University, Kremenchuk, Ukraine

Abstract

LED luminaires are currently the most frequently used luminaires in both indoor and outdoor (street) lighting. When connected, LED fixtures behave differently than fixtures with high-pressure sodium lamps. After the LED fixture is turned on, it emits a higher luminous flux and draws more power from the mains than after the thermal conditions have stabilized. Moreover, during this process, other electrical parameters of the luminaire change, such as reactive power, and as a result, the value of the power factor and the current harmonics generated by the luminaire to the power supply network change. The paper presents the results of measurements of the luminous flux and selected electrical parameters of a road LED luminaire during the thermal stabilization process.

1. Introduction

LED fixtures are currently the most commonly used fixtures in both indoor and street lighting. The luminous efficiencies of modern LED luminaires currently reach up to 250lm/W. LED luminaires, apart from many undoubted advantages, such as lower power compared to traditional luminaires (with high-intensity discharge lamps) with a comparable luminous flux value, greater durability and easy regulation of the luminous flux, also have disadvantages. The disadvantages include the generation of harmonic current into the power grid, the emission of blue light and the need to use a cooling system (radiator), which increases the weight of the fixture. In the case of LEDs, there is a relationship between the luminous flux and the LED junction temperature. After the LED fixture is turned on, it emits a higher luminous flux than after the thermal conditions have stabilized.

2. Measurement results of electrical parameters and luminous flux of street LED luminaires

A road luminaire with a rated power of 75W was selected as the research object. Before the measurements, the fixture was shined for 100 hours. The measurement time of the light flux and electrical parameters was 1 hour. The luminous flux was measured using a spherical lumen meter with a diameter of 2 m and an L-100 luxmeter. The electrical parameters were measured using a FLUKE 1760 electricity quality analyser. The tested fixture was powered by mains voltage to simulate real operating conditions. Table 1 summarizes the results of measurements of the luminous flux and electrical parameters of the tested luminaire.

Table 1. Measured electrical parameters and luminous flux

Active power P (W)	Current I (A)	Reactive power Q (var)	Displacement power factor PF_D	Distortion power factor PF_{DD}	Current Total Harmonic Distortion factor THD_I (%)	Luminous flux Φ (lm)
76.42	0.36	25.54	0.95	0.93	15.85	6997

The difference between the initial value of the luminous flux Fb and the final value of the luminous flux Fe is 9.55%. As it can be seen, the measured active power values differ slightly from the rated power. For the tested luminaire, the difference between the initial value Pb and the final value Pe is 4.67%, as it is illustrated in Figures 1 and 2. Figure 3 shows the waveforms of other electrical parameters such as: reactive power, displacement power factor, RMS current and THDI. Figure 4 shows the waveforms of selected higher current harmonics 3, 5, 7, 9 and 11.

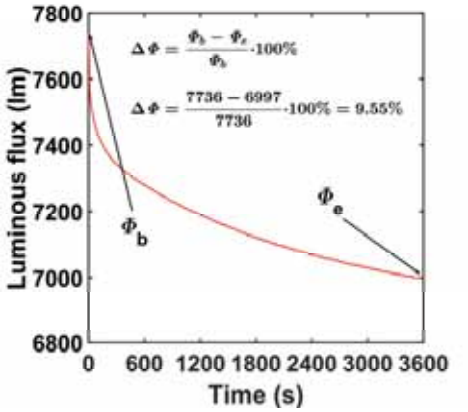

Figure 1. Short-term luminous flux depreciation of L2 luminaire

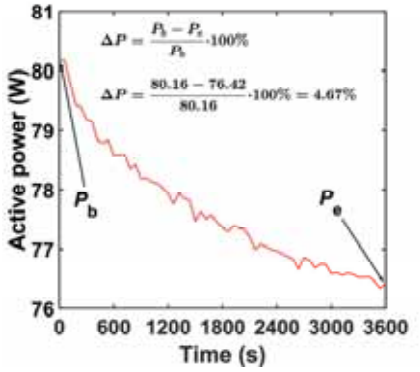

Figure 2. Active power of luminaire L2 during stabilisation of thermal conditions

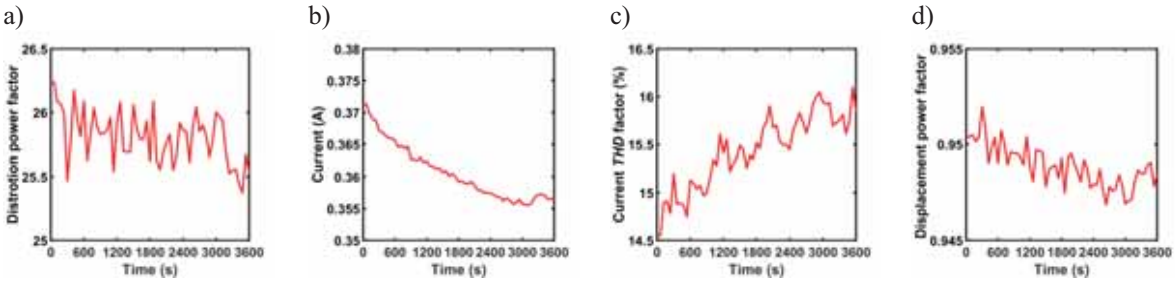

Figure 3. Measurement results of:
a) reactive power, b) RMS current, c) THD_I, d) displacement power factors PF_D

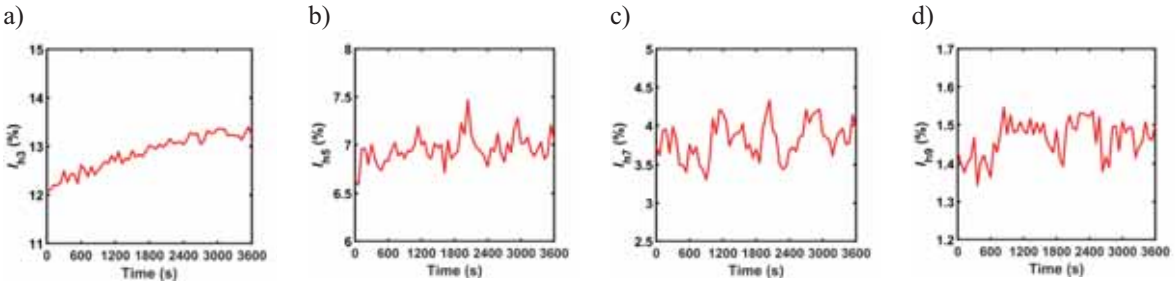

Figure 4. Selected higher harmonics of tested luminaire during stabilization of thermal conditions
a) I_{h3}, b) I_{h5}, c) I_{h7}, d) I_{h9}

Based on the measurements performed, it can be concluded that changes in electrical parameters change during the stabilization of the thermal conditions of the LED luminaire. Reactive power decreases over time. The increasing value of the THDI coefficient of the current indicates the increasing values of higher harmonics in relation to the fundamental harmonic current. The greatest increase was observed for the 3rd harmonic, the value of which increases from approximately 12% to over 13% in relation to the fundamental harmonic. The remaining analysed higher current harmonics 5, 7 and 9 change within a maximum of ±1%.

3. Summary

One of the basic requirements currently placed on lighting devices and installations is to ensure the best possible energy efficiency. This is tantamount to ensuring appropriate lighting conditions while minimizing electricity consumption. The luminous flux of the LED fixture and its other electrical parameters change as the thermal conditions stabilize. The stabilization time depends on the power of the fixture, which translates into the thermal resistance of the heat sink. During stabilization, the light flux and electrical parameters change to varying degrees. Changes in active power affect the management of reactive power, and changes in the values of higher harmonic currents may negatively affect the quality of the supply voltage.

Residential heat pump impact on distribution grid voltage amplitude: a simulation study

Eva Simonič[1], Sebastijan Seme[1,2], Karel Zupanc[3], Klemen Sredenšek[1]

[1] Faculty of Energy Technology, University of Maribor, Hočevarjev trg 1, 8270 Krško, Slovenia, eva.simonic@um.si, sebastijan.seme@um.si, klemen.sredensek@um.si,

[2] Faculty of Electrical Engineering and Computer Science, University of Maribor, Koroška cesta 46, 2000 Maribor, Slovenia,

[3] Elektro Gorenjska, d. d., Ulica Mirka Vadnova 3a, 4000 Kranj, Slovenia, karlo.zupanc@elektro-gorenjska.si

Abstract
This paper aims to explore the impact of residential heat pump operation on a low-voltage distribution grid. Simulations are conducted on a model representing a real distribution transformer feeder. Furthermore, the study investigates the integration of heat pumps with photovoltaic systems and electrical energy storage. The paper focuses on analysing daily voltage fluctuations at the consumer node furthest from the transformer. Simulation findings reveal instances of undervoltage, suggesting potential grid enhancement through the incorporation of photovoltaics and energy storage systems.

1. Introduction

The progressive shift towards electrifying sectors like heating and transportation is becoming a key objective in the pursuit of carbon-free energy systems [1-4]. The extensive adoption of heat pumps (HP) drives the widespread electrification of heating, escalating power demand and thereby impacting especially low-voltage distribution grids [2, 3]. The operational dynamics of HPs are intertwined with heat demand, a factor influenced by climatic and demographic conditions [1, 3]. Studies such as [1, 4] use various approaches to modelling grids and their participants with the use of realistic electrical energy and heat demand profiles, offering insight into grid dynamics.

2. Methodology

A simulation model of a real low-voltage grid was developed using MATLAB Simulink. The radial low-voltage distribution grid serves a rural, residential community. It is powered by a 250 kVA 20/0,4 kV transformer. For the purpose of the study, a single feeder comprising 36 consumer nodes was selected for comprehensive analyses. Consumers are assigned their smart meter time series data of electrical energy demand (and export to the grid) in the resolution of 15 minutes.

The coldest clear sky winter day of the previous three years was chosen as the meteorological scenario for the simulation: on February 13, 2021, the average daily temperature was – 5,4 °C and the daily solar irradiance was 3322 Wh/m^2. For the given weather conditions, the incorporation of new HPs is considered and executed using the Monte Carlo method. The integration process involves an examination of various HP deployment scenarios within the grid feeder. This is achieved through incremental additions of HPs to randomly selected consumers. Furthermore, each consumer newly equipped with an HP is also provided with a photovoltaic (PV) system and an electrical energy storage (EES) system. HPs are mathematically modelled to satisfy the expected thermal demand of the individual buildings. PV system mounting is implemented with respect to roof slope and azimuth.

3. Results

Fig. 1 shows the daily voltage fluctuations at the consumer node furthest from the transformer. Presently, around a third of consumers possess an HP, while the rest are gradually and randomly allocated one until all consumer nodes are equipped with an HP. Undervoltage occurrences are noted during night and morning hours, with the severity increasing as more consumers adopt HPs.

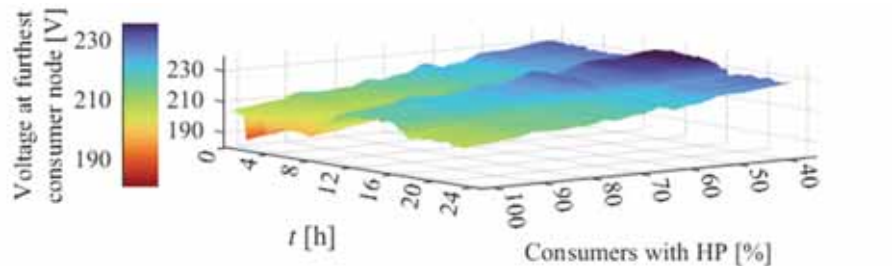

Fig. 1. Daily course of voltage at the furthest consumer node for various shares of consumers with an HP

Fig. 2 shows the daily voltage variations at the identical consumer node. In addition to HPs, PV systems and EES systems are introduced. Fewer occurrences of undervoltage are observed, along with improved uniformity of voltage over the course of the day.

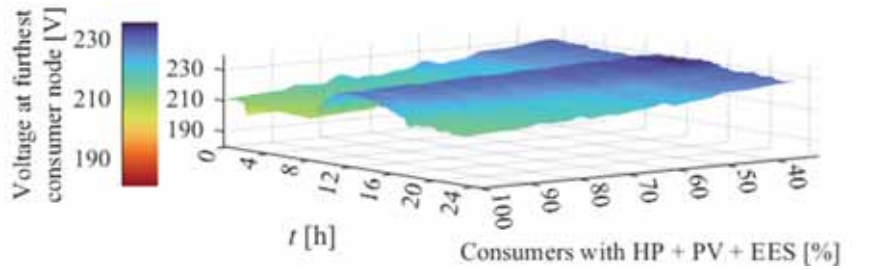

Fig. 2. Daily course of voltage at the furthest consumer node for various shares of consumers with an HP, PV, and EES

4. Discussion

This paper examines the methodology for evaluating the influence of residential HPs on a low-voltage distribution grid. Power flow simulations are performed using MATLAB Simulink, employing smart meter time series data of household electrical energy consumption and generation. The Monte Carlo method is used to randomly deploy HPs to consumers. The daily voltage profile on a cold but sunny winter day is observed at the consumer connection node furthest from the grid transformer. Undervoltage resulting from extensive HP operation is alleviated by the integration of PV systems and EES.

References

[1] C. McGarry, A. Anderson, I. Elders, S. Galloway, (2023), "A Scalable Geospatial Data-Driven Localization Approach for Modeling of Low Voltage Distribution Networks and Low Carbon Technology Impact Assessment", *IEEE Access*, Vol. 11, pp. 64567-64585.

[2] I. D. de Cerio Mendaza, I. G. Szczesny, J. R. Pillai and B. Bak-Jensen, (2015), "Flexible Demand Control to Enhance the Dynamic Operation of Low Voltage Networks," *IEEE Transactions on Smart Grid*, Vol. 6, No. 2, pp. 705-715.

[3] A. Anderson, B. Stephen, R. Telford and S. Mcarthur, (2020), "Predictive Thermal Relation Model for Synthesizing Low Carbon Heating Load Profiles on Distribution Networks", *IEEE Access*, Vol. 8, pp. 195290-195304.

[4] A. Navarro-Espinosa, P. Mancarella, (2014), "Probabilistic modeling and assessment of the impact of electric heat pumps on low voltage distribution networks", *Applied Energy*, Vol. 127, pp. 249-266.

Optimization of electrical energy production of the photovoltaic/thermal system

Klemen Sredenšek[1,2], Eva Simonič[1], Klemen Srpčič[1], Sebastijan Seme[1,2]

[1] Faculty of Energy Technology, University of Maribor,
Hočevarjev trg 1, 8270 Krško, Slovenia
e-mail: klemen.sredensek@um.si; eva.simonic@um.si;
klemen.srpcic1@um.si; sebastijan.seme@um.si,

[2] Faculty of Electrical Engineering and Computer Science,
University of Maribor, Koroška cesta 46, 2000 Maribor, Slovenia

Abstract
As the temperature of photovoltaic cells increases, the efficiency decreases due to the physical laws governing semiconductors. To counteract this thermal effect, photovoltaic/thermal modules integrate cooling mechanisms that stabilize photovoltaic cell temperatures, thereby enhancing energy conversion efficiency. This paper focuses on the optimization of electrical output from a photovoltaic/thermal system through a single-objective optimization function, which maximizes the production of electrical energy by adjusting the mass flow rate of the circulation pumps. The aim of this paper is to demonstrate how much more electrical energy can be produced using active cooling compared to a conventional photovoltaic system.

1. Introduction

The photovoltaic/thermal (PV/T) system represents a combination of commercial photovoltaic (PV) and thermal solar systems, which can simultaneously produce electrical and thermal energy. Although the PV/T system was designed to achieve higher electrical energy production through the active cooling of solar cells, it also produces a certain amount of thermal energy that can be used in various low-temperature heating systems. Fundamentally, the PV/T system comprises PV/T modules, circulation pumps, heat exchangers, valves, an inverter, and a thermal energy storage unit. To effectively operate the entire system, proper management of all components (especially the circulation pumps) is required to achieve enough electrical and thermal energy according to the end user's needs. Numerous studies [1-3] have conducted comprehensive optimizations on the PV/T system, yet these enhancements predominantly targeted specific subsystems and components. The primary objective was to refine the operational parameters to maximize electrical efficiency and enhance thermal output. Adjustments were made strategically to optimize component performance, which included modifications to the configuration of PV/T modules, recalibration of circulation pumps, and improvements in heat exchanger efficiency. The PV/T system presented in this paper consists of ten PV/T modules with an electrical power of 3,3 kW_p and a thermal energy storage tank with a volume of 500 liters, separated by a heat exchanger and two circulation pumps. The first circulation pump is responsible for the active cooling of the PV/T modules, while the second circulation pump transfers the heat from the PV/T modules to the thermal energy storage tank.

2. Methodology and results

Based on the mathematical model of the PV/T system described in [4], an optimization of the electrical energy production was performed for six sunny and six cloudy days in the year 2023. The criterion function, which is used to determine the optimal electrical energy production of the PV/T system, is presented as equation (1).

$$f_{\text{ele.}} = \sum_{n=1}^{D} E_{\text{ele.}} \tag{1}$$

Where n represents the day of the year, D is the number of days in the year, and $E_{ele.}$ is the produced electrical energy. Fig. 1 presents the cumulative production of electrical energy for six sunny and six cloudy days in 2023.

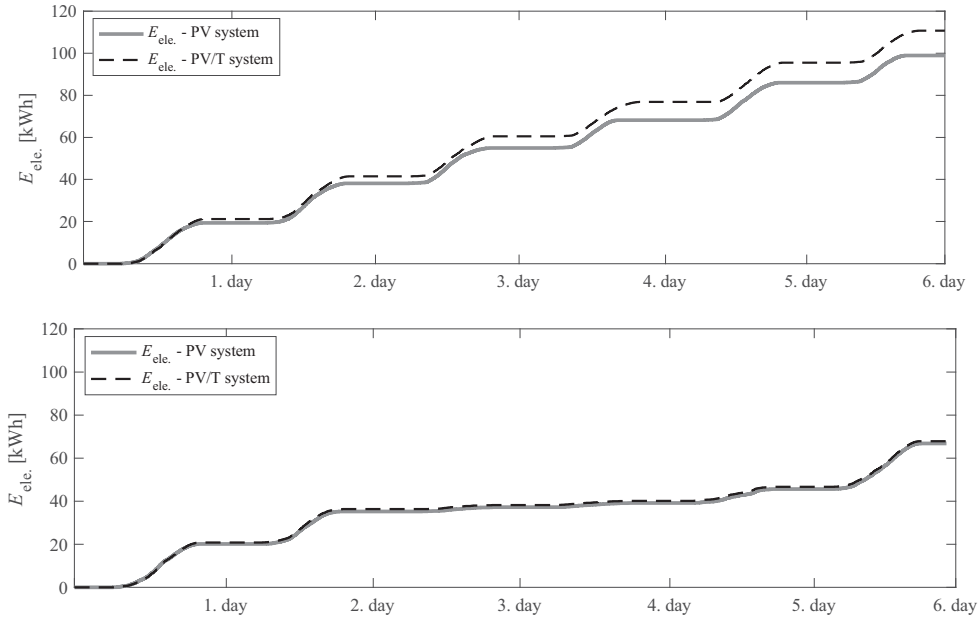

Figure 1: Cumulative production of electrical energy $E_{ele.}$ for PV/T systems (optimization aimed at maximizing the production of electrical energy) and PV systems (typical operation) for six sunny days and six cloudy days

Fig. 1 clearly demonstrates that optimizing the electrical energy $E_{ele.}$ output across six consecutive sunny days and six cloudy days results in the additional generation of 11,812 kWh (11.9 %) and 1,088 kWh (1.13 %) of electrical energy, respectively, compared to a PV system without active cooling. The data indicates that active cooling of PV cells markedly enhances their energy conversion efficiency, thereby substantially increasing the electrical output, particularly during periods of higher ambient temperatures.

3. Conclusion

This paper presents the advantages of the PV/T system and its optimization of electrical energy production. The study showcases how active cooling markedly improves electrical energy production by optimizing the mass flow rate. The results reveal an increase in electrical energy production by 11.9 % and 1.13 % for sunny and cloudy conditions, respectively, compared to traditional PV systems. These findings highlight the critical role of thermal management in enhancing the efficiency of solar energy systems. Consequently, implementing active cooling can lead to more sustainable and effective photovoltaic installations that are capable of meeting higher energy demands. Ultimately, this research provides a compelling case for the broader adoption of PV/T systems to improve the viability and performance of renewable energy systems.

References

[1] Tamayo Vera, J.; Laukkanen, T.; Sirén, K. Multi-objective optimization of hybrid photovoltaic-thermal collectors integrated in a DHW heating system. *Energy and Buildings* 2014, 74, 78–90.

[2] Tamayo Vera, J.; Laukkanen, T.; Sirén, K. Performance evaluation and multi-objective optimization of hybrid photovoltaic-thermal collectors. *Solar Energy* 2014, 102, 223–233.

[3] Saeedi, F.; Sarhaddi, F.; Behzadmehr, A. Optimization of a PV/T (photovoltaic/thermal) active solar still. *Energy* 2015, 87, 142–152.

[4] Sredenšek, K.; Seme, S.; Štumberger, B.; Hadžiselimović, M.; Chowdhury, A.; Praunseis, Z. Experimental Validation of a Dynamic Photovoltaic/Thermal Collector Model in Combination with a Thermal Energy Storage Tank. *Energies* 2021, 14, 8162.

Classification lung diseases with electrical impedance tomography

Barbara Stefaniak[1], Amelia Kosior-Romanowska[1], Paweł Tchórzewski[1], Anna Iwanicka-Maciura[1], Dariusz Wójcik[1,2], Tomasz Rymarczyk[1,2]

[1] Research and Development Center, Netrix S.A., Lublin

[2] WSEI University, Lublin

Introduction

The article describes the research results related to the work on a medical diagnostic system project based on electrical impedance tomography. One of the solution's key features is its help to diagnose respiratory diseases, with a particular focus on chronic obstructive pulmonary disease (COPD), acute respiratory distress syndrome (ARDS) pneumothorax (PTX), pneumonia (PNA), bronchospasm and pulmonary hypertension (PHTN). Diagnosing medical conditions often involves conducting multiple intricate tests, leading to prolonged waits for accurate diagnoses. The objective of presented approach is to minimize the number of necessary tests for an accurate diagnosis, resulting in time savings. The article compares two classification models designed to distinguish individuals with a disease and healthy ones.

Methods

Numerical models were constructed to include a broad range of both diseased and healthy cases [1-6] (see Figure 1 - 7). Next, material parameters for the human body were identified [7]. Several stages of disease progression were considered, with three stages for ARDS and four for the remaining conditions. To prepare the dataset, simulations of electrical impedance tomography measurements were performed using the finite element method.

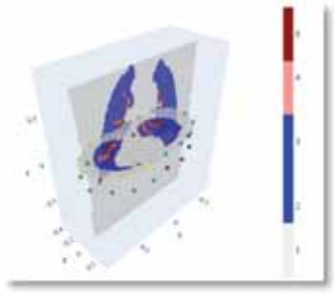

Figure 1. Model of healthy case

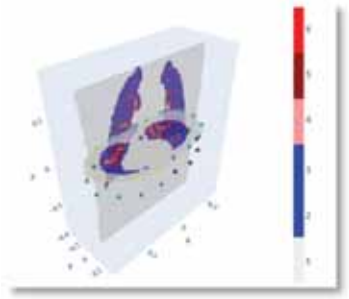

Figure 2. Model of ARDS disease

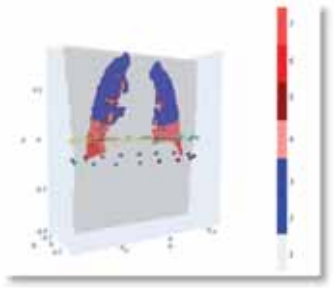

Figure 5. Model of pneumonia disease

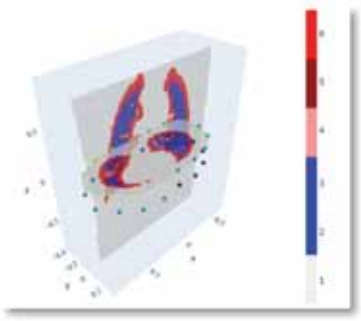

Figure 2. Model of COPD disease

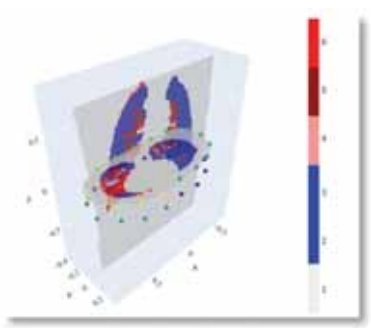

Figure 4. Model of PTX disease

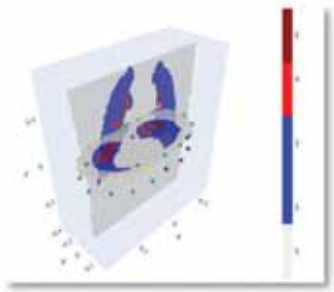

Figure 6. Model of bronchospasm disease

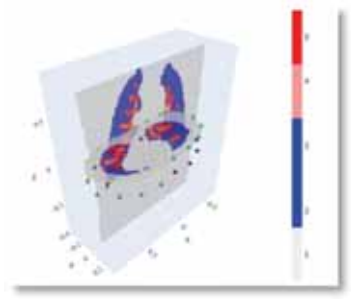

The models consist of at most seven components: 1 – torso without lungs, 2 – left lung without bronchi and blood vessels around the bronchi, 3 – right lung without bronchi and surrounding blood vessels, 4 – bronchi, 5 – blood vessels surrounding the bronchi, 6 – region with lesions corresponding to the disease, 7 – area showcasing a secondary lesion (specifically utilized for pneumonia).

Figure 7. Model PHTN disease.

Two classification models, namely a Multi-layer Perceptron classifier (MLP) and Gradient Boosting Classifier, were developed and compared for their effectiveness in distinguishing between individuals with respiratory diseases and healthy subjects. The models were trained on a comprehensive dataset encompassing various stages of disease progression. EIT data frames were simulated by the finite element method.

Each classification model was evaluated based on its accuracy in diagnosing specific lung conditions, with the MLP achieving an accuracy of 87.5% and the Gradient Boosting Classifier achieving 80.5%. The study showcases the potential of EIT-based diagnostic systems in enhancing the efficiency and accuracy of respiratory disease diagnosis, thus offering promising avenues for future research and clinical implementation.

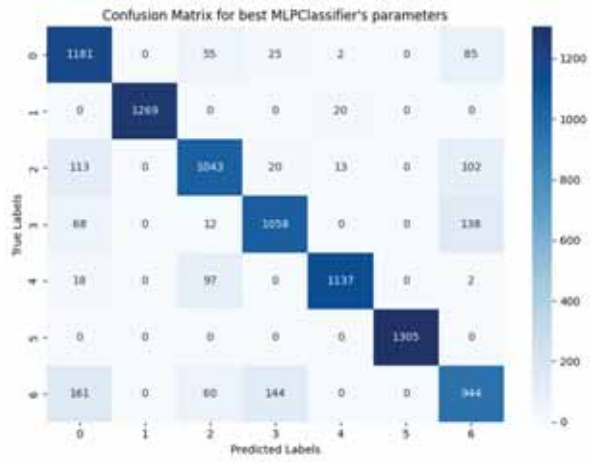

Figure 8. Confusion matrix for MLP

Figure 9. Confusion matrix for Gradient Boosting

References

[1] E. Jassem, D. Górecka. Ciężka i terminalna postać przewlekłej obturacyjnej choroby płuc, Severe and terminal chronic obstructive pulmonary disease. neumonol. Alergol. Pol. 2009, 77, 411–416

[2] Zespół ostrej niewydolności oddechowej (ARDS) - European Lung Foundation. Available online: https://europeanlung.org/pl/information-hub/lung-conditions/zespol-ostrej-niewydolnosci-oddechowej-ards/ (accessed on 27th July 2021)

[3] Odma opłucnowa | Pulmonologia. Available online: http://www.mp.pl/social/article/150463 (accessed on 18th October 2016).

[4] Pneumonia - Wikipedia. Available online: https://en.wikipedia.org/wiki/Pneumonia (accessed on 24th November 2023).

[5] Bronchospasm: Symptoms, Treatment; What it Is. Available online: https://my.clevelandclinic.org/health/diseases/22620-bronchospasm (accessed on 18th March 2022).

[6] M. Wieteska-Miłek. INFORMATOR DLA PACJENTÓW. Wszystko o Tętniczym Nadciśnieniu Płucnym; M. Wieteska-Miłek, Klinika Krążenia Płucnego, Chorób Zakrzepowo-Zatorowych i Kardiologii CMKP, Europejskie Centrum Zdrowia Otwock Wydanie IV, Warszawa, 2018.

[7] P.A. Hasgall, F. Di Gennaro, C. Baumgartner, E. Neufeld, B. Lloyd, M. C. Gosselin, D. Payne, A. Klingenböck, N. Kuster, "IT'IS Database for thermal and electromagnetic parameters of biological tissues," Version 4.1, Feb 22-nd, 2022.

Scalability of interior permanent magnet motors for electric vehicles: design remarks

Bojan Štumberger[1,2], Zdravko Praunseis[1], Miralem Hadžiselimović[1,2], Brigita Ferčec[1], Amor Chowdhury[1], Sebastijan Seme [1,2], Iztok Brinovar[1]

[1] University of Maribor, Faculty of Energy Technology,
Hočevarjev trg 1, 8270 Krško, Slovenia,
bojan.stumberger@um.si, zdravko.praunseis@um.si, miralem.h@um.si,
brigita.fercec@um.si, amor.chowdhury@um.si,
sebastijan.seme@um.si, iztok.brinovar1@um.si

[2] University of Maribor, Faculty of Electrical Engineering and Computer Science,
Koroška cesta 46, 2000 Maribor, Slovenia

Abstract
The paper deals with the scalability limitations of the interior permanent magnet synchronous motors (IPMSMs) for Electric Vehicles (EVs) when the scaling laws are not strictly followed. Efficiency and power capability performances of IPMSMs with similar motor design but with different stator diameter to rotor diameter split ratio over a wide-speed range are presented on the basis of the finite element analysis (FEA).

1. Introduction

It is evident that IPMSMs dominate the drive systems for electric vehicles (EVs) [1-4]. The maximal peak power level of motors for EV propulsion systems has been increasing from year to year [1], and it is currently in the range of 70 to 250 kW with the battery system voltage from 350-800 V. In general, electric motors for EVs require a certain speed range with continuous torque, a certain speed range with maximal overload torque and a certain speed range with constant power. Due to the variety of different torque and power demands, scaling of the successful motor design is frequently used as a solution for early design stage. Although scalability of IPMSMs is useful and accurate [5-7], the scaling laws cannot always be strictly followed.

2. Results

Efficiency and power capability performance of IPMSMs with different peak power level is presented on the basis of the finite element analysis. Cross-sections of IPMSMs with 36 stator slots and 8 poles taken into consideration are presented in Fig. 1. All motors have similar stator and rotor design but different stator diameter to rotor diameter split ratio and equal one-side air-gap width (1 mm). The same quality of the active material is accounted for in the FEM analysis for all motors. In the presented results, equal DC link voltage level (720 VDC) for all motors design is taken into consideration. Motor power characteristics for different maximal peak values of phase current are presented in Fig. 2, while the efficiency map characteristics in dependency on speed and torque are presented in Fig. 3. Results of the designed liquid-cooling system and the limits of motor operation with continuous output power load will be presented in the full paper.

Acknowledgements
This work was supported in part by the Slovenian Research and Innovation Agency (ARIS) under the research grant for research programme Applied Electromagnetics P2-0114.

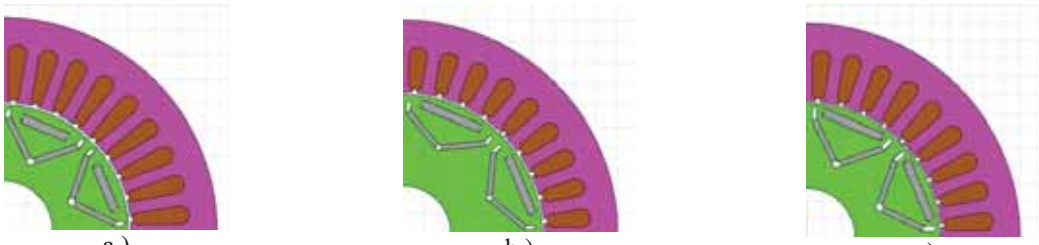

a.) b.) c.)

Fig. 1. Cross-section of IPMSM (36 stator slots and 8 rotor poles, D-type rotor configuration), outer stator diameter/outer rotor diameter: a.) 170/100 mm; b.) 200/130 mm; c.) 240/150.

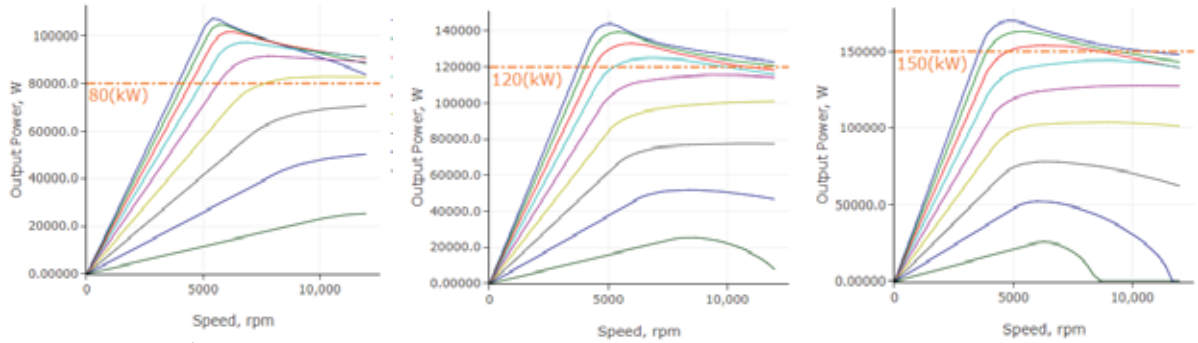

a.) b.) c.)

Fig. 2. Motor power characteristics for different maximal peak values of phase current, from 50 Apk to 450 Apk with step 50 Apk: a.) Dout_s/Dout_r=170/100 mm; b.) Dout_s/Dout_r=200/130 mm; b.) Dout_s/Dout_r=240/150 mm. Core length for a.), b.) and c.) is equal to 140 mm.

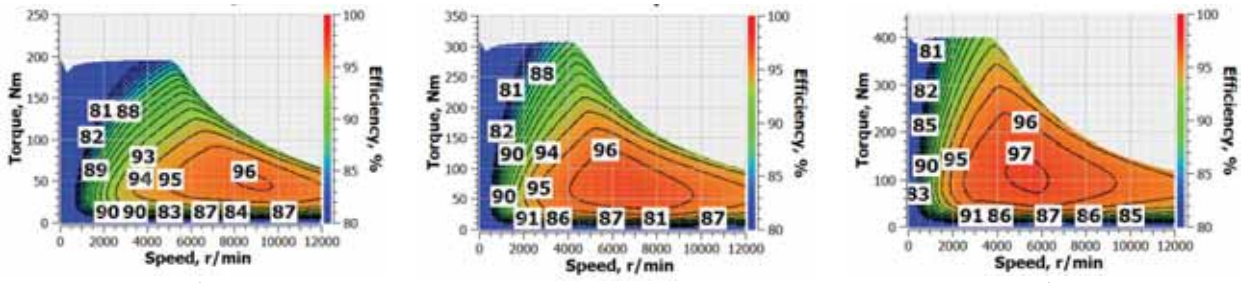

a.) b.) c.)

Fig. 3. Efficiency characteristics in dependency on speed and torque: a.) Dout_s/Dout_r=170/100 mm; b.) Dout_s/Dout_r=200/130 mm; b.) Dout_s/Dout_r=240/150 mm. Core length for a.), b.) and c.) is equal to 140 mm.

References

[1] https://www.evspecifications.com/

[2] Z. Wang, T. W. Ching, S. Huang, H. Wang, T. Xu (2020), "Challenges Faced by Electric Vehicle Motors and Their Solutions", *IEEE Access*, DOI 10.1109/ACCESS.2020.3045716.

[3] L. Shao, A. E. H. Karci, D. Tavernini, A. Sorniotti, M. Cheng (2020), "Design Approaches and Control Strategies for Energy-Efficient Electric Machines for Electric Vehicles a Review", *IEEE Access*, DOI 10.1109/ACCESS.2020.2993235.

[4] V. I. Vlachou, G. K. Sakkas, F. P. Xintaropoulos, M. S. C. Pechlivanidou, T. D. Kefalas, M. A. Tsili, A. G. Kladas (2024), "Overview on Permanent Magnet Motor Trends and Developments", *Energies* 2024, 17, 538, DOI 10.3390/en17020538.

[5] S. Stipetic, D. Zarko, M. Popescu, "Ultra-fast axial and radial scaling of synchronous permanent magnet machines", *IET Electr. Power Appl.*, 2016, Vol. 10, Iss. 7, pp. 658–666.

[6] S. Stipetic , D. Zarko , M. Popescu , "Calculation of Efficiency Maps Using a Scalable Saturated Model of Synchronous Permanent Magnet Machines", *IEEE Transactions on Industry Applications*, Vol. 54, No. 5, September/October 2018, pp. 4257-4266.

[7] A. Aroua, W. Lhomme, F. Verbelen, M. N. Ibrahim, A. Bouscayrol, P. Sergeant, K. Stockman (2023), "Impact of scaling laws of permanent magnet synchronous machines on the accuracy of energy consumption computation of electric vehicles", *eTransportation* 2023, DOI 10.1016/j.etran.2023.100269.

Application of temporal analysis of high-frequency signals in a distributed asset management system

Michał Styła[1], Dominik Gnaś[1], Przemysław Adamkiewicz[1,2]

[1] Information Technology Research & Development Centre (CBRTI sp. z o.o.), Rzeszów

[2] WSEI University, Lublin

Abstract

This thesis addresses the use of temporal analysis of ultra-wideband signals in a real-time localisation system (RTLS). The main focus is on tag hardware solutions, miniaturisation and energy optimisation. It also addresses the algorithms responsible for estimating the user's location, how to manage the acquired data, and the methodology for its transfer and processing. The type of location network presented can find application in all kinds of WMS systems, as well as an alternative to in-building navigation based on cyclic RSSI measurements.

Development of the hardware layer

The envisaged structure of the equipment network included two types of elements: so-called anchors and markers. Anchors are elements with a known and fixed position in space, and with permanent and unrestricted access to the building's power supply and local network. Tags, on the other hand, are elements attached to objects tracked and localised by anchors. Both types incorporate the use of Qorwo's DWM microcontrollers and the nRF52832 (Bluetooth 5) wireless microcontrollers supporting them in non-localisation data transmission. Other types of data transmitted outside the UWB band can be considered as readings from environmental sensors installed on each tag. The only exception is the accelerometer, whose signal is only used to wake the device from deep sleep in order to save the tag's built-in battery. This is a crucial procedure as it prevents the battery from being consumed in the absence of object movement. The accelerometer's trip threshold is adjustable over a wide range depending on the application conditions. Other key features include an integrated UWB antenna optimised for 6.5 GHz centre frequency (channel 3) and 500 MHz bandwidth, a series of power and signal filters, and a separate transmission line with matching circuits and antenna for 2.4 GHz band operation. The final appearance of the devices is shown in Figure 1.

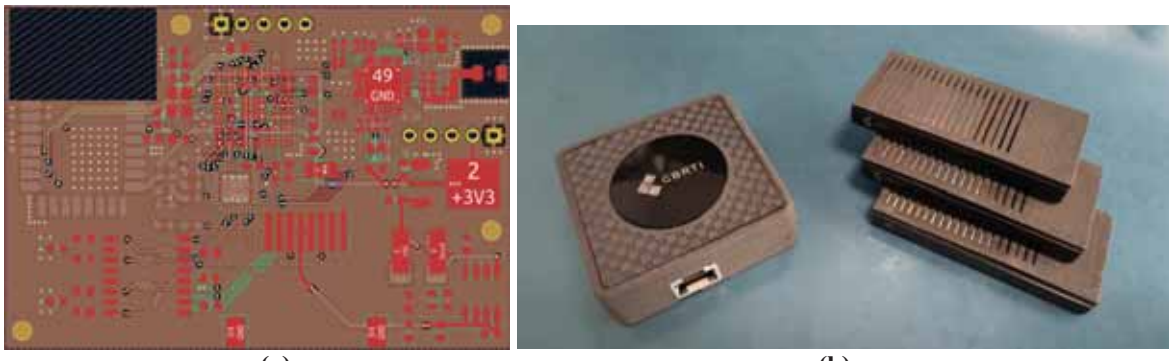

(a) **(b)**

Fig. 1. Author's coupling solutions created in the project: (a) – mosaic of electrical connections of the ultra-wideband anchor, (b) – actual prototypes of the UWB anchor (left) and UWB tags (right)

Comparison of positioning algorithms & results

Two newly developed algorithms with a reference point in the form of a trilateration method for determining points in space using a system of triangles (trilateration) are analysed. The first can be called machine learning-assisted trilateration (MLET), while the second is localisation by optimisation (LBO). The method using MLET takes each pair of anchors and their corresponding distances and then finds the corresponding circle intersections. An unsupervised machine learning algorithm - DBSCAN - then takes the set of intersections and divides the points into relevant and outliers. The centre of the relevant cluster is the localised position returned by the method. The second method - LBO - uses a different approach. It constructs a goal function from the distance equations of each anchor. Ideally, this function would completely disappear for the solution. However, it should be stressed again that the algorithm is dealing with noisy data, so the global minimum of the objective function corresponds to the best approximation of the user's position. Figure 2 shows a summary of the positioning error values for a series of 80 samples. The resulting diagrams clearly show that trilateration returns worse results than the other two methods. The error reaches up to 50 cm for trilateration, while MLET and LBO do not exceed 30 cm. In turn, Table 1 summarises the averaged error values for all measurement series and calculation algorithm types. These show a 25% advantage of the MLET and LBO algorithms over traditional trilateration.

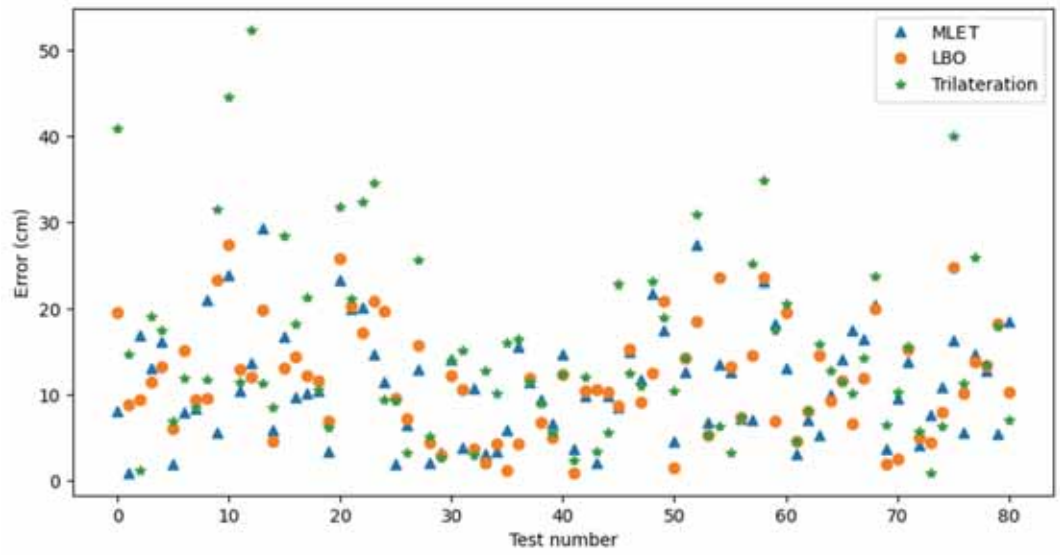

Fig. 2. Position errors - distance between actual and calculated position of the device for the three selected methods

Table 1. Comparison of mean error values obtained from the operation of the three selected algorithms.

Method	Trilateration	MLET	LBO
Mean error (cm)	15.21	11.31	11.66

References

[1] Fernandes J. R., Wentzloff D.: Recent Advances in IR–UWB transceivers: An overview, Proceedings of 2010 IEEE International Symposium on Circuits and Systems, 30 May 2010 - 02 June 2010, 2010.

[2] Sasaki N., Kimoto K., Moriyama W., Kikkawa T.: A Single-Chip Ultra-Wideband Receiver With Silicon Integrated Antennas for Inter-Chip Wireless Interconnection, IEEE Journal of Solid-State Circuits, vol. 44, no. 2, pp. 382–393, 2009.

[3] Gnaś D., Adamkiewicz P.: Indoor localization system using UWB, Informatyka, Automatyka, Pomiary W Gospodarce I Ochronie Środowiska, vol. 12, no. 1, pp. 15–19, 2022.

[4] Saeidi T., Ismail I., Wen W. P., Alhawari A. R. H., Mohammadi A.: Ultra-Wideband Antennas for Wireless Communication Applications, International Journal of Antennas and Propagation, 2019.

[5] Lee Y., Kim J. Lee H., Moon K.: IoT-based data transmitting system using a UWB and RFID system in smart warehouse, 2017 Ninth International Conference on Ubiquitous and Future Networks (ICUFN), 04-07 July 2017, 2017.

Implementation of reflective methods for microwave frequency signal processing in radio tomography

Michał Styła[1], Dominik Gnaś[1], Przemysław Adamkiewicz[1,2]

[1] Information Technology Research & Development Centre (CBRTI sp. z o. o.), Rzeszów

[2] WSEI University, Lublin

Abstract

The project consisted of using electromagnetic waves in the 5.8 GHz range and radio tomography technology to detect occupants indoors using reflective methods. Activities included the creation of a concept for the hardware layer, the structure and hierarchy of the data transfer network, as well as a method for processing the acquired waveforms into usable information. The acquired data (in the form of samples of the reflected signal) were transferred to a location engine located on the test server and then converted into location information of the users. Methods for the possible amplitude and frequency analysis of signals for human factor detection, the structure of the PCB and microwave antenna, and methods for the efficient management of data samples in order to make a system close to RTLS (Real Time Location System) speed served as the basic issues to be solved.

Design of the device

The focal point of the device is the MAX2828ETN+ transceiver, which is a front-end system, i.e. without an internal control unit in the form of a microcontroller, but controlled externally by means of registers and the bit/flag values contained therein. The transmit and receive paths are separated from each other and independently controlled. The master control functions are provided by a WSoC nRF52832 microcontroller. It performs the additional function of transporting readings from environmental sensors via Bluetooth 5. The rest of the components used are complex HF filtering and conditioning circuits, as well as integrated reference signal sources for timing or synthesis of other signals. The carrier frequency signal can be derived and fed into the circuit is via a quad-patch microwave antenna, which is attached to the PCB via an SMA connector or by a 'sandwich' method with the help of spacers via special transceiver line terminations. The final device parameters settled on a laminate with a size of 106 x 80 x 1.6 mm, radiated power of 10 mW and an effective range of 10 metres. The final appearance of the device is shown in Figure 1.

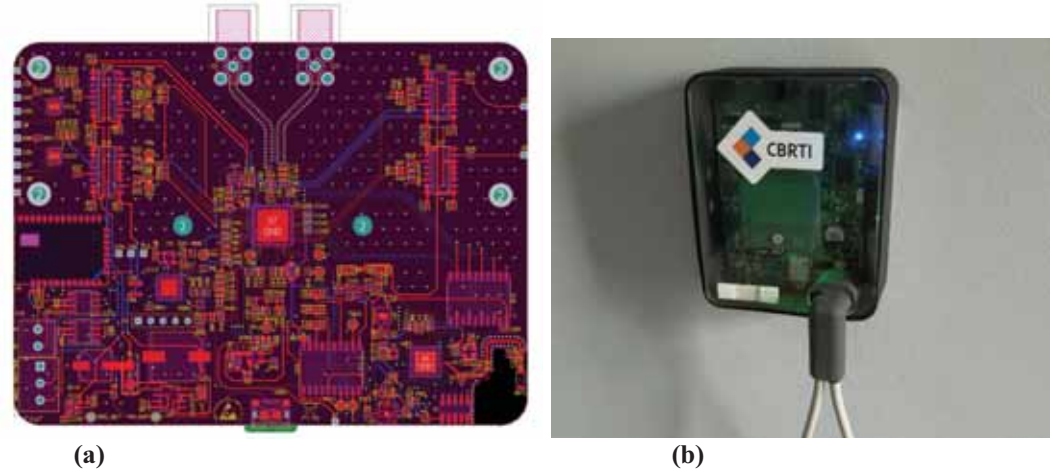

(a) **(b)**

Fig. 1. Radio reflection probe prototype: (a) – patchwork of electrical connections, (b) – genuine specimen

Signal processing and results

The user's position information was determined from a transmitter network of 16 reflection probes in a room-bound arrangement, which is characteristic of tomography. Waves reflected from objects returning to the detector were amplified and filtered, and then passed to a circuit that reduced their frequency so that they could be successfully sampled by the ADC. A CAN bus and an access gateway with access to the building's local network were responsible for transporting the data to the location engine located on the computing server. Each packet containing a signal sample was equipped with probe number information, as well as a time stamp to maintain synchronisation/consistency of the data sets. Example visualisations obtained from the amplitude and frequency analysis of the signals are presented in Figure 2. One starting point for the signal processing was to relate the amplitude to the distance from the detector/presence at the detector, and the other was to the use of the Doppler phenomenon for object movement. Extreme unfavourable cases of movement parallel to the detector were counterbalanced by readings from other probes where the movement shown was more unambiguous. The disappearance of motion below a certain threshold caused the last known position of the object to be remembered and resumed when the oscillograms fluctuated again. The maximum response from the reflection probes was induced within the radiation pattern of their microwave antennas, i.e. 45 degrees horizontally and 30 degrees vertically, resulting in a final accuracy of 40 to 50 cm, depending on the prevailing conditions.

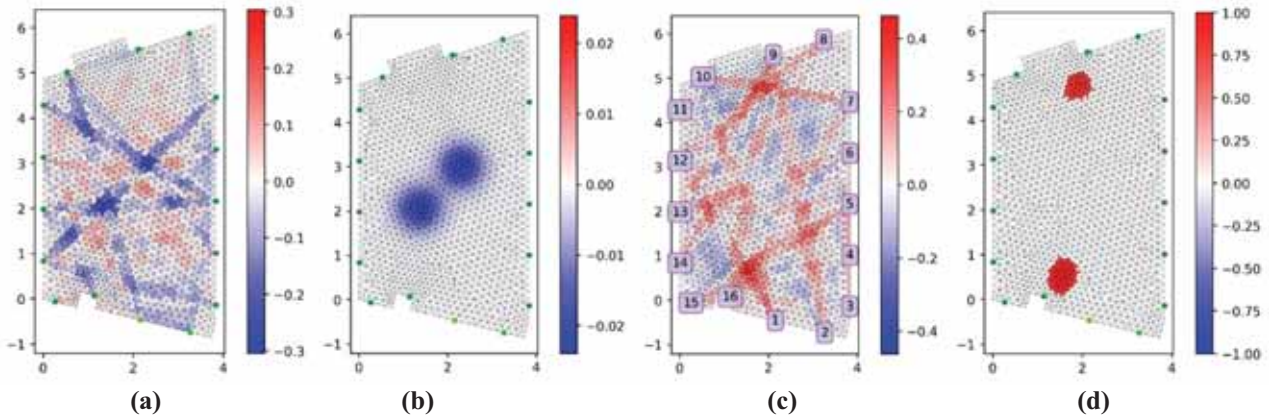

Fig. 2. Visualisation of users positions based on amplitude and frequency analysis of waveforms (relative units): (a) – TSVD direct result (static scenario I), (b) – direct TSVD result with Gaussian filtration (static scenario I), (c) – TSVD direct result (static scenario II), (d) – direct TSVD result with Mexican Hat filtration (static scenario II).

References

[1] Brodeski D., Bilik I., Giryes R.: Deep Radar Detector, 2019 IEEE Radar Conference (RadarConf), 22–26 April 2019.

[2] Wnuk M., Chudy Z.: Pomiar mocy impulsu elektromagnetycznego mikrofal, Przegląd Elektrotechniczny, vol. 90, no. 8, pp. 239–242, 2014.

[3] Bilik I., Bialer O., Villeval S., Sharifi H., Kona K., Pan M., Persechini D., Musni M., Geary K.: Automotive MIMO radar for urban environments, 2016 IEEE Radar Conference (RadarConf),02–06 May 2016

[4] Zhang C., Luo W., Urtasun R.: Efficient Convolutions for Real Time Semantic Segmentation of 3D Point Clouds, In Proc. International Conference on 3D Vision (3DV), 2018.

[5] Styła M., Kiczek B., Kłosowski G., Rymarczyk T., Adamkiewicz P., Wójcik D., Cieplak T.: Machine Learning-Enhanced Radio Tomographic Device for Energy Optimization in Smart Buildings, Energies, vol. 16, no. 1, p. 275, 2022.

Scientific communication in engineering sciences – a need or a bother…

Witold Sygocki

Central Institute for Labour Protection – National Research Institute,
Warsaw 00-701, Czerniakowska 16, Poland,
wisyg@ciop.pl

Abstract
Contemporary scientific communication is not only domain of specialist from scientific libraries, information and documentation centres of university as was before. Every scientist should knew the way how scientific communication works, what are the best tips for scientist, institution, organisation. Institution in Poland use different various tools for both indexing and presenting scientific achievements. Outside institutions, publishers of bibliographic and abstract databases present extensive profiles of scientists in Web of Science CC, Scopus for example. This material signals the complexity of the scientific communication process and proposes verifying the correctness and completeness of data in authors' profiles in the indicated resources such as ORCID.

Key words: *scientific communication, author and institution profile, Web of Science, Scopus, SciVal, InCites, ORCID*

Sources of information about researchers output

Resources available in the network environment include those related e.g. to publishers: Scopus (Elsevier), organizations: ORCID, database publisher: Web of Science (companies Thomson Reuters/Clarivate Analytics). It is worth remembering that access to Scopus and WoS CC in Poland is related to a national license. ORCID, - Open Researcher and Contributor ID, is a global, not-for-profit organization sustained by fees from our member organizations, was created in 2010. They are community-built and governed by a Board of Directors representative of our membership with wide stakeholder representation. That unique, persistent identifier free of charge to researchers [1]. It consists of 16 digits divided into 4 parts, e.g.: 0000-0002-2541-9380. What we see as scientific achievements depends on what has been indexed by the publisher, institution or author. It is the author who should update information about publications in ORCID. ORCID is used by publishers to verify author data and his/her achievements. This is especially important when we have authors with the same name and surname: like Jan Kowalski. For that first/family name has 2573339 results, on 51467 pages in ORCID. Putting "John Kowalski" in quotation marks gets 40 results, 29 of them have no affiliation, which makes it impossible to identify the author. Example below:

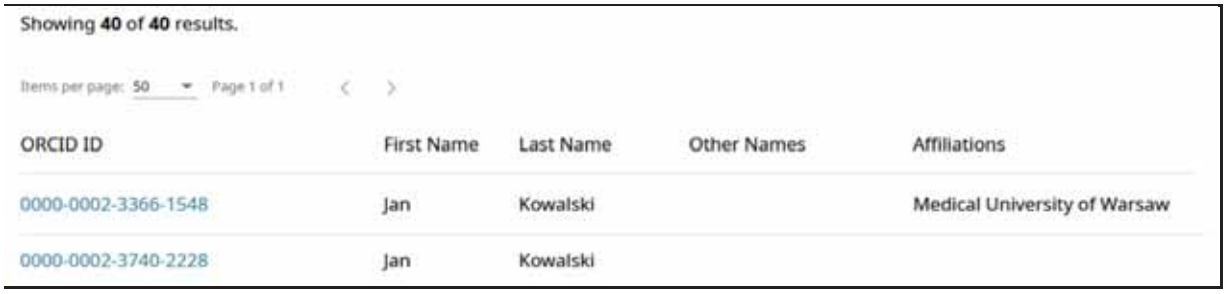
Showing **40** of **40** results.

Items per page: 50 Page 1 of 1

ORCID ID	First Name	Last Name	Other Names	Affiliations
0000-0002-3366-1548	Jan	Kowalski		Medical University of Warsaw
0000-0002-3740-2228	Jan	Kowalski		

Fig. 1. Fragment of the view in ORCID for the question about the author "Jan Kowalski" (accessed: April 14, 2024).

That show how important in ORCID is to update your profile, along with affiliation and public access for everyone, without log in. ORCID is required by recognized publishers (e.g. Springer, Elsevier, Wiley). It may happen that without the author's ID, the publication will not be accepted for processing by the publisher. Currently, ORCID is not mandatory in Poland, but only recommended. The identifier appears in the profiles of scientists in the PBN (Polish scientific bibliography) database, in profiles in WoS CC, Scopus and other base - resources of individual universities.

The information in the ORCID system depends on the scientist, while the information in the databases - in the profiles available there - depends on the journals indexed in WoS and Scopus, respectively. The number of records and author profiles in WoS CC and Scopus are different, that is the result of the difference in the number of indexed journals and conference materials. WoS CC indexes approximately 21,000 scientific journals, and Scopus over 29,000 [2]. In Web of Science CC are 92,341,095 records, in Scopus more than 94 million [3]. The table no.1 below presents some examples of information about publication output and the numerical differences in each resource.

Tab. 1. Number of indexed publication (all publications/ open access) in different resources and H-index for each author (categorized also in engineering sciences) WoS CC, Scopus, ReserchGate, ORCID*

Authors	WoS CC		Index H in WoS CC	Scopus		Index H in Scopus	ReserchGate	ORCID
	All	Open Access		All	Open Access			
A	97	36	17	136	23	20	124	117
B	7	0	1	14	0	3	25	24
C	107	4	10	70	0	8	176	no
D	178	47	25	256	80	30	291	286

*data accessed: 15.04.2024.

Example below – author's profile in WoS – each profile has a Web of Science Researcher ID: ……., as well as the previously mentioned ORCID:

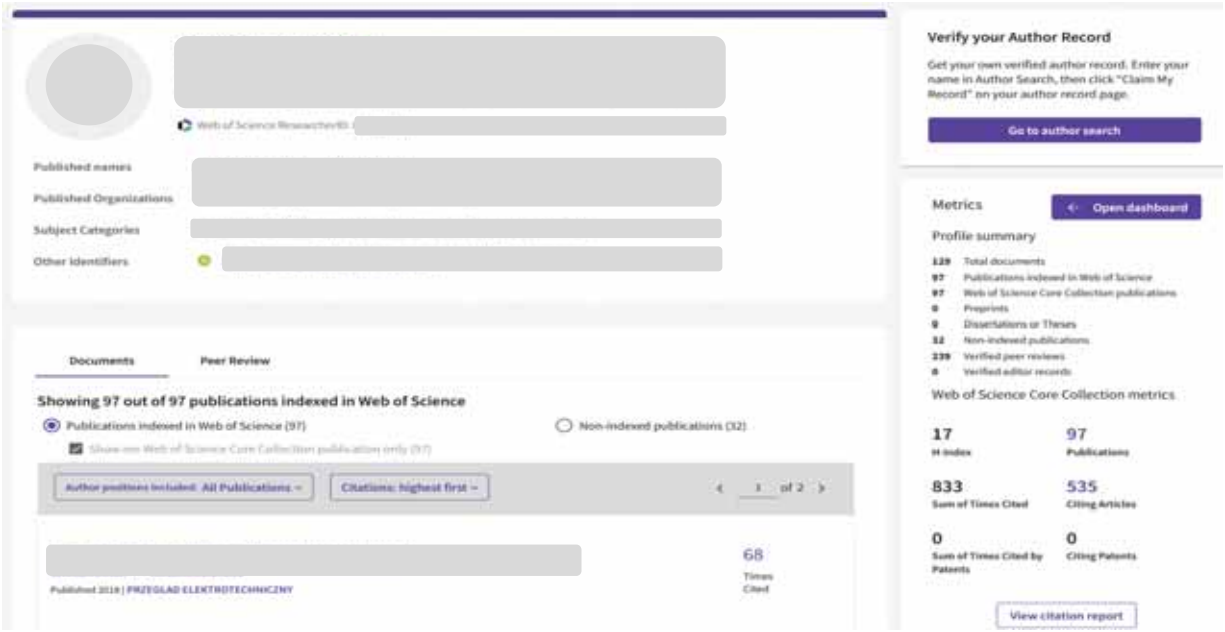

Fig. 2. Author's profile in Web of Science CC (accessed: April 14, 2024)

Scopus Author Identifier is a unique number that matches authorship to groups of documents. Documents that cannot be confidently matched are grouped separately. In this case, you may see more than one entry for the same author [4].
When Scopus does not have an ORCID identifier, Scopus allows you to link the author profile to the ORCID identifier. This can be done from the author's profile by clicking the "Add to ORCID" link.

Example below – author's profile in Scopus - each profile has a Scopus Author Identifier: ……, as well as the previously mentioned ORCID:

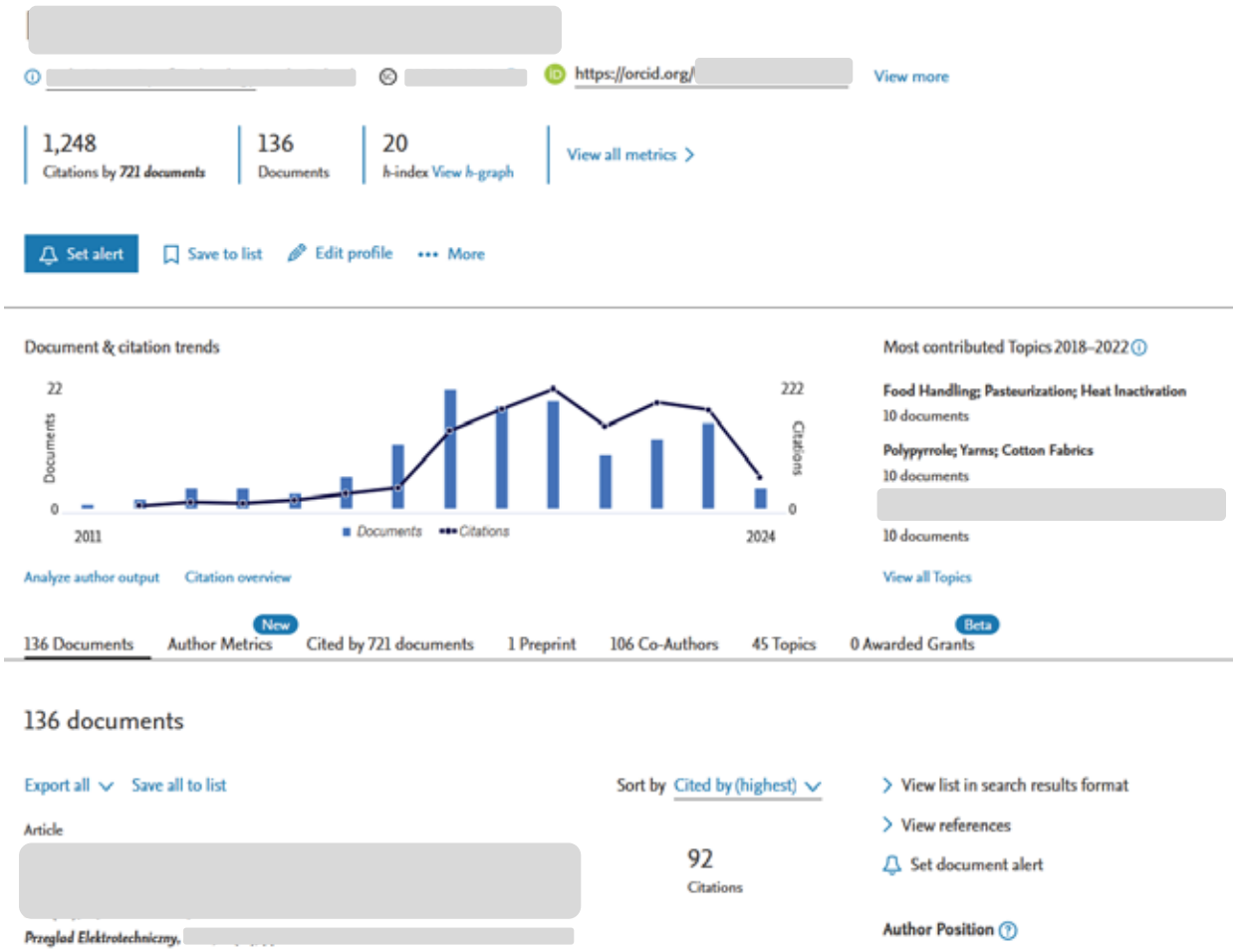

Fig. 3 Author's profile in Scopus (accessed: April 14, 2024)

It is worth remembering that each author should verify the correctness of data indexed in the WoS and Scopus databases - which is important for the quality of the profile.

Correlated tools: Scopus_Elsevier (SciVal) and WoS CC_Clarivate (InCites)

Publishers of bibliographic and abstract databases have made available analytical tools enabling the analysis and comparison of the achievements of scientists, institutions and presenting the journal's position in comparison to others, e.g. within engineering disciplines.

SciVal is a tool provided by Elsevier, it has been available in Poland since 2018 [5]. It operates on the Scopus bibliographic database platform. It is used to conduct analyses, comparisons and

visualizations of scientific achievements, which are created on the basis of daily updated data from over 230 countries and over 99,000 affiliation profiles. Each user who wants to use that tool must have a personal account for Elsevier websites. In addition to the achievements of the author and institution, as well as the ability to check national and international activity and cooperation, InCites allows you to generate reports about publishers and single journals and present position in relation to other. Example below – Przeglad Elektrotechniczny:

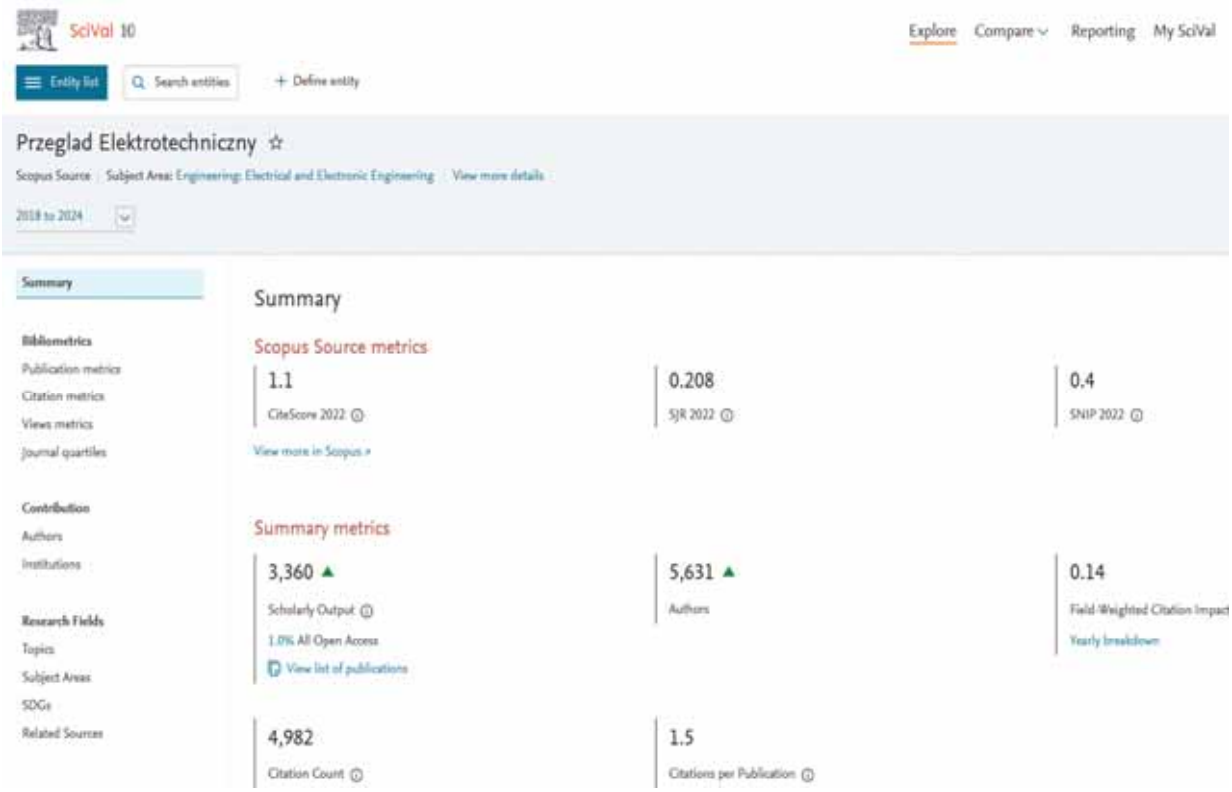

Fig. 4. Report for Przeglad Elektrotechniczny in SciVal, indicators: SJR, SNIP – fragment (accessed: April 15, 2024).

The Scopus, and therefore SciVal, contains information about bibliometric indicators: CiteScore, SCImago Journal Rank, Source Normalized Impact per Paper (SNIP). These metrics are updated annually, just as the Impact Factor is updated by Clarivate Analytics.

Another tool - InCites - the author can define and determine the impact of his scientific achievements as well as establish cooperation with scientists from other universities or choose an appropriate source for publishing the results of his research [6]. That analytical system is used to visualize scientific and bibliometric data and conduct cross-sectional analyzes in various areas. The bibliometric data visible in the InCites system use records from the Web of Science, dating back to 1980. Each user who wants to use InCites must have a personal account on the Web of Science platform. That tool provided by Clarivate Analytics, it has been available in Poland, since 2018.

Example below – Fig. 5 - from InCites - present the micro citation topic word cloud based on the researcher profile, searched using ORCID identifier (period of publications 2018-2023).

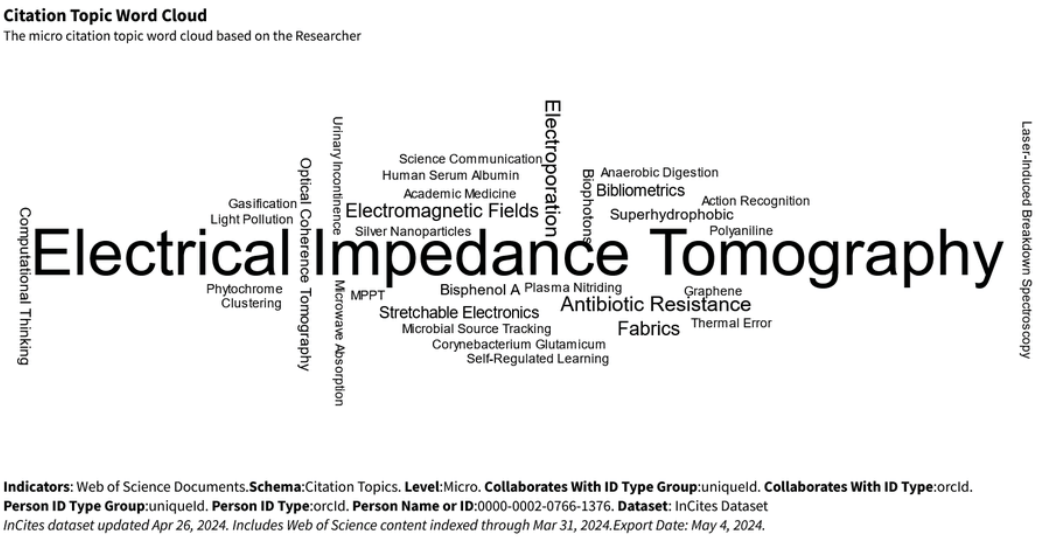

Fig. 5. Citation Topic Word Cloud, part of report for researcher identified by ORCID: 0000-0002-0766-1376 in InCites (accessed: 4 May, 2024).

Scientific communication for scientist - as a summary

- Open website resources make it possible for anyone to get to know the achievements at any place and at any time - the question is whether we use known sources of informations
- Some universities and research institutions in Poland have own system for indexing and reporting achievements (e.g. Most Wiedzy, Baza Wiedzy) - many of them provide information about ORCID and citations from WoS, Scopus, or Google Scholar in single resercher profile
- a scientist's profile with bibliometric data, shows publication and conference activity - they present the achievements and at the same time provide information for business about the role it plays in a given discipline
- SviVal and InCites allow you to generate reports, e.g. for a scientist or institution
- In cooperation with the library, a scientist should ensure the validity and correctness of e.g. publication data in ORCID, WoS CC, Scopus or even publishers site
- some scientists have and update profiles, e.g. on ReserchGate, Academia.edu - which is not related to the affiliated institution
- solicitude of information about achievements is now equally important for the scientist and the institution
- every scientist should be convinced whether it is worth informing the world of science, business and society about his/her achievements, or whether it is unnecessary...

References

[1] Information about ORCID. Access in WWW: https://info.orcid.org/what-is-orcid/ (Access: 13.04.2024.)
[2] Information about Web of Science CC. Access in WWW: https://clarivate.com/products/scientific-and-academic-research/research-discovery-and-workflow-solutions/#resources (Access: 13.04.2024.)
[3] Information about Scopus_Elsevier. Access in WWW: https://www.elsevier.com/__products/scopus/content?dgcid=RN_AGCM_Sourced_300005030 (Access: 13.04.2024.)
[4] Information about Scopus. *Scopus Your brilliance connected. Content. Coverage. Guide.*.Access in WWW: https://assets.ctfassets.net/o78em1y1w4i4/EX1iy8VxBeQKf8aN2XzOp/c36f79db25484cb38a5972ad9a5472ec/Scopus_ContentCoverage_Guide_WEB.pdf (Access: 13.04.2024.)

[5] SciVal provides strategic insights to help your research programs thrive. Access in WWW: https://www.elsevier.com/products/scival (Access: 13.04.2024.)
[6] Information about InCites provided by Clarivate: What's New, Getting Started (Explore Data. Create Tiles. Save & Share), Training Videos, Indicators Handbook. Access in WWW: phttps://incites.help.clarivate.com/Content/home.htm (Access: 13.04.2024.)

Acknowledgements
This paper was created (and published)* on the basis of results of a research task carried out within the scope of the 6th stage of the National Programme "Governmental Programme for Improvement of Safety and Working Conditions", funded by state services of the Ministry of Family, Labour and Social Policy (under the name of the Ministry of Family and Social Policy prior to December 12th, 2023). *Task no. 7.ZS.06, entitled:* "Scientific communication (regarding the safe functioning of humans in the working environment) for increasing the effectiveness of research works". The Central Institute for Labour Protection – National Research Institute is the Programme's main co-ordinator.

Impact of high order harmonics on the motor copper losses and short-circuit characteristics

Ivan Temelkovski, Goran Rafajlovski, Goga Cvetkovski, Mihail Digalovski

Ss. Cyril & Methodius University,
Faculty of Electrical Engineering & Information Technologies,
Rugjer Bošković bb, P.O. Box 574, 1000 Skopje, N.Macedonia
e-mail: ivant@feit.ukim.edu.mk, goran@feit.ukim.edu.mk,
gogacvet@feit.ukim.edu.mk, mihaild@feit.ukim.edu.mk

Abstract
In this paper, a three-phase low-voltage squirrel cage induction motor is considered. From the short-circuit test, the operating characteristics are obtained in two different ways: once when the induction motor is connected directly to the network and another when the motor is inverter fed. Furthermore, an analysis of the high order harmonics is given and the copper losses that occur during the no-load test of the induction motor are determined. A qualitative analysis of the results is given and the significant impact of the inverter on the copper losses is highlighted.

1. Introduction

Nowadays the effects that power electronics cause on the power quality, and also on the operation of the induction motors can no longer be ignored. This is due to the increased use of power electronics, but also due to the feedback effects of the power grid. For that reason, the analysis of the high order harmonics that occur in induction motors is of great importance for the electric power industry [2].
Induction motors are electrical machines that are usually designed to operate at a nominal sinusoidal voltage. Because of this, any distortion of the voltage waveform and the presence of high order harmonics impact on their operation and efficiency. Thus, voltage harmonics increase the power losses in the magnetic circuit of the induction motors, while current harmonics increase the power losses in their windings. These increased power losses contribute to additional heating of the electric machine, thereby reducing its life. Therefore, there is no doubt that the presence of higher harmonics should be subject to a more detailed analysis.

2. Copper losses

The copper losses are given in relation of the first harmonic current component according to this relation [1]:

$$\Delta P_{js(1)} = 3R_{s(1)} \cdot I_{s(1)}^2 \tag{1}$$

Assuming that the winding is normally composed from wiring conductors, it is clear that the skin-effect influence on stator resistance $R_s(h)$ will be insignificant [1]:

$$R_{s(h)} = R_{s(1)} + \sum_{h=2}^{N} R_{s(h)} \approx R_{s(1)} \tag{2}$$

The relationship based on the relative performance unit considering the harmonics influence is given as [1]:

$$p_{js,\Sigma h}(\%) = \frac{\sum_{h=2}^{N} R_{s(h)} \cdot I_{s(h)}^2}{R_{s(1)} \cdot I_{s(1)}^2} \cong \frac{\sum_{h=2}^{N} I_{s(h)}^2}{I_{s(1)}^2} \tag{3}$$

The total stator coper losses in respect of the harmonics are given as [1]:

$$\Delta P_{js(1)} = \Delta P_{js(1)}(1 + p_{js,\Sigma h}) \tag{4}$$

3. Results of the measurements

The stator winding resistance was measured by the help of a Wheatstone bridge and found to be 0.7 Ω. Based on the measured current harmonics, the stator copper losses of the motor are determined. From the short-circuit test in laboratory conditions at reduced voltage, the total power losses were obtained. All parameters relevant to power quality such as phase and line voltages and currents, active, reactive and apparent power, total voltage and current harmonic distortion, power factor, harmonic spectrum up to 50th harmonic were obtained during the measurements by the Omni-quant instrument.

3.1 Impact on the Copper Losses

For the same supply voltage that is applied to the motor, knowing the value of the resistance of the stator winding, the following results were calculated for the copper losses:
P_{sc}=92,4 (W) - when induction motor is supplied from the grid by the help of an autotransformer
P_{sc}=172 (W) - when induction motor is inverter fed
Taking into account the results, it can be seen that the total power losses in the case when the induction motor is inverter fed during the short-circuit test approximately 1.86 times higher than the power losses obtained when the motor is connected directly to the network.

3.2 Impact on the Total Harmonic Distorsion

A huge impact of the electronic components can also be seen by the obtained results for the total harmonic distortion. As can be seen from the picture, the total voltage harmonic distortion increases by about 50%, while the total current harmonic distortion by about 100% in the cases when the induction motor is inverter fed. These figures clearly show that the impact of harmonics occurred in the motors should not be neglected.

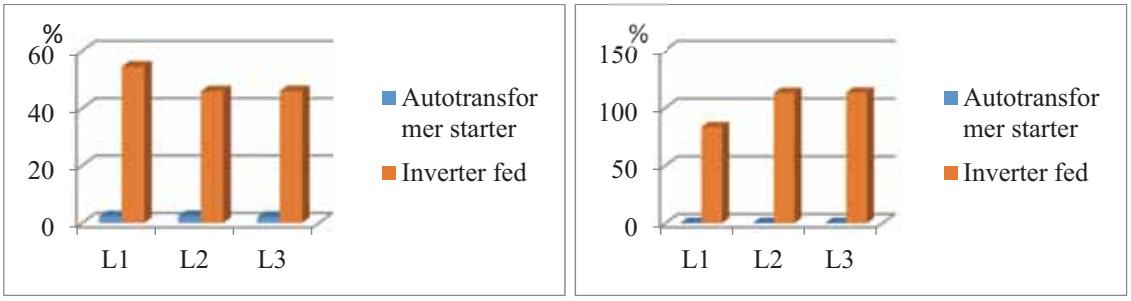

(a) (b)

Fig. 1 Total harmonic voltage (a) and current (b) distorsion

4. Conclusion

From the results it can be concluded that the application of the induction motor in different circumstances can greatly affect both its working characteristics and power losses. Of course, if these impacts are not taken into account, the induction motor may be damaged as a result of the unexpected power losses that would occur in some cases. That is one of the main reasons why a qualitative analysis of the different cases has been made, which will enable the proper use of the right induction motor in the right cases.

References

[1] Otýpka J., Pečínka P., Orság P., Stýskala V., "*The Influence of Nonharmonic Voltage Source on Losses in Induction motor*", Conference paper 2017, DOI: 10.1109/EPE.2017.7967246

[2] Y.Birbir and S.Nogay, "*Voltage and Current Harmonic Variations in Three-phase Induction Motors with Different Stator Coil Pitches*", International Journal of Energy, Issue 4, Vol. 1, 2007

[3] Mihail Digalovski, Krste Najdenkoski, Goran Rafajlovski, *"Impact of current high order harmonic to core losses of three-phase distribution transformer"*, Proceedings of EUROCON 2013 (IEEE, Region 8), pp. 1531-1535, Zagreb, Croatia.

Transformer tank losses

Mislav Trbušić, Anton Hamler, Marko Jesenik

University of Maribor, Faculty of Electrical Engineering and Computer Science,
Koroška cesta 46, 2000 Maribor, Slovenia,
mislav.trbusic@um.si

Abstract
A simple loss model of the tank wall is presented in the article to evaluate transformer tank losses numerically. The calculation is based on a quasi-analytical approach where the 2D Finite Element Method obtains the magnetic field while the analytical formula evaluates the losses.

1. Introduction

The transformer's losses substantially impact the transformer design and cost. The losses are generally generated in windings, core, and other constructional parts, including flitch plates, tank walls, tank cover, etc. By good loss estimation, the design can be improved, which leads to lower costs and a more energy-efficient solution. Therefore, the transformer's design process should adopt a reliable loss model. The theory and practical computation procedures cover the winding and core losses quite well while estimating the tank losses is still arduous without advanced computer programs. However, the key issue is knowing the magnetic field distribution at the tank's wall. Once this question is solved, the procedure for tank loss determination is straightforward. For practical reasons, the computational time in the task must be comparable with the one needed to estimate the winding losses. Nowadays, a widely used approach to loss estimation in electromagnetic devices is through the Finite element method (FEM). Such an approach could relate to the 2D or 3D technique, where the latter is more accurate but requires much more CPU time. Thus, it is reasonable to put some effort into developing a concept relying on the 2D FEM technique. The tank loss model revealed here is brought on the quasi-analytical way, where the 2D FEM software computes the magnetic field distribution along the tank's wall while the losses are evaluated through the pseudo-analytical equation derived from the magnetic conductive plate. When handling tank losses in everyday design practice, it is feasible to know the total amount of losses rather than the spatial distribution of losses in the tank. According to this fact, the calculations can be simplified significantly.

2. Tank's wall model

To obtain the suitable loss model of three phase – three limb type transformer, the tank's wall can be divided into seven segments as is shown in Fig 1-a. Adopting a presumption that the magnetic field effectively enters the wall only in the width area of the windings the losses can be determined by summing up the losses in the individual segments. Due to symmetry, it is sufficient to calculate losses only for the half-segment and then multiply it by two for the whole segment (Fig 1-b, c).

3. Magnetic field distribution

The magnetic field causing the losses is the stray field that induces the eddy currents within the tank's wall. Thus, numerical evaluation of the field at the wall is essential for the task here. By the 2D axisymmetric approach, the required field distribution is attainable by the FEMM 4.2 software solution relatively fast and efficiently. A typical field distribution along the transformer's tank wall is given in Fig 2. However, in the simplified model given here a mean magnetic field value is taking place in the loss equation.

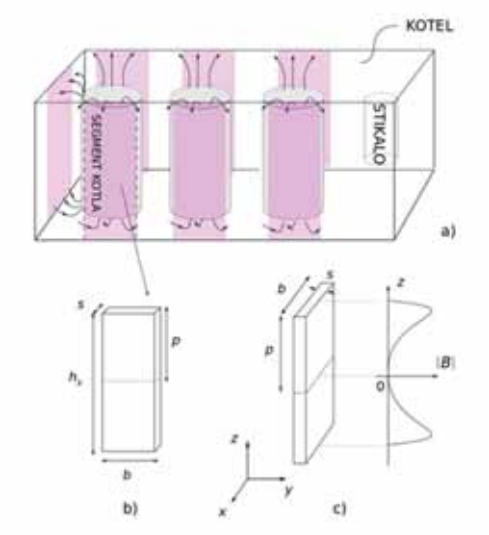

Fig. 1: Transformer tank wall model

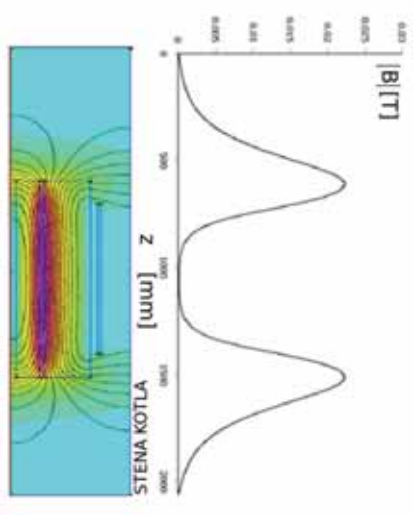

Fig. 2: The magnetic field distribution at the tank's wall

4. Results and discussion

The presented method has been evaluated on the three-phase transformer unit RT 25000 kVA – 33/6,3 kV, whose main design parameters were taken from the reference [3]. The case study in [3] includes 3D FEM calculations and measurements of the transformer losses that were crucial for the data comparison given in Table 1. Even though the relatively high discrepancy in tank loss estimation between 2D and 3D calculations can be observed (34%), the overall losses pertaining to the tank losses and other losses arising in the constructional parts match relatively closely (7%). In contrast, both numerical approaches give approximately 10% lower values than were measured on the specified transformer unit. However, the numerical evaluation of the tank losses is a rather complex task, and the simplified model presented here could be a convenient way when the fast estimation of losses in the constructional parts is desired.

Table 1: Comparison of losses concerning case study in [3]

	2D computation	3D computation	Measured values	Description
P_k [W]	118730	N.A.	120000	Short circuit losses
I^2R [W]	92640	N.A.	90700	DC winding losses
P_{dod} [W]	9160	N.A.	11500	Winding losses due to the stray magnetic field
P_{kon} [W]	2670	5000	N.A.	Other losses in the constructional parts e.q. fitch plates, tank cover, winding leads, …
P_{kot} [W]	**13347**	**9970**	N.A.	Tank wall losses
P_v [W]	16017	14970	17800	Total losses in constructional parts
$P_v = P_k - I^2R - P_{dod}$ $P_v = P_{kon} + P_{kot}$				

Acknowledgements
This work was supported by the Slovenian Research Agency under Grant P2-0114.

References

[1] Transformer handbook 3th ed.«, ABB, 2007.
[2] K. Karsai, D. Kerényi, L. Kiss, Large Power Transformers, Budapest: Académia Kiadó, 1987.
[3] L. Kralj, Izgube v kotlu in konstrukciji transformatorja zaradi stresanega polja, Diplomsko delo, UL-FE, Ljubjana, 2010 (Slovene language only)
[4] D. C. Meeker, Finite Element Method Magnetics, Version 4.2
[5] A. Jurman, Razsipano magnetno polje in lasnosti transformatorja, Magistrsko delo, UL-FE, Ljubljana, 2008. (Slovene language only)

Optimisation of two parameters of a spherical magnetorheological actuator

Jakob Vizjak, Marko Jesenik, Anton Hamler

University of Maribor, Faculty of Electrical Engineering and Computer Science,
Koroška cesta 46, 2000 Maribor, Slovenia,
email: jakob.vizjak1@um.si; marko.jesenik@um.si; anton.hamler@um.si

Abstract
A spherical magnetorheological model was built and analysed with the combination of Matlab and Opera software, consisting of a spherical rotor, a stator, a magnetorheological fluid between them, a non-magnetic ring, a couple of seals and a coil. Typically, many models must be built during optimisation, consuming much time. Due to this, the goal was to introduce a method that requires fewer models, and, consequently, less time. An approach combining a grid search and fit functions was compared to one using only the grid search. A suitable fit function selection achieved a comparable result to the grid search while being significantly faster.

1. Introduction

In recent years, more and more devices have been developed that use the so-called smart fluids. One such fluid is the Magnetorheological (MR) fluid [1]. Its most prominent property is the MR effect, which manifests as a viscosity increase in the presence of a magnetic field. In this publication, this property of the MR fluid was used to model a spherical MR actuator intended for haptic applications.

The actuator model was built as a spherical joint, and consists of a spherical rotor, a stator, a non-magnetic ring, a coil inside the stator and upper and lower seals. The MR fluid is in the gap between the rotor and the stator.

The goal was to model the actuator using the Finite Element Method (FEM), and optimise the geometry to maximise the breaking torque of the actuator and minimise the size. The difficulty with typically used optimisation processes, such as evolutionary algorithms or grid search, is the time consumption of the process due to the number of models that need to be built. For this reason, an optimisation approach combining a reduced grid search and a fit function was used to optimise two free parameters: the radius and height of the actuator's stator.

2. Methods

First, several fixed and free parameters were defined, to model the actuator based on the geometric and magnetic requirements. There were two free parameters: the radius of the actuator and the height of the actuator's stator. The whole geometry of the actuator was parametrised based on the fixed and free parameters.

The model was parametrised using Matlab software. The model was built and analysed using Opera software. A COM interface was utilised to connect Matlab and Opera to build and analyse the model.

With FEM, a magnetostatic analysis was performed, to get the magnetic conditions in the actuator, or, more specifically, in the MR fluid. Based on the magnetic conditions, the available breaking torque was calculated using the Bingham plastic model and yield stress dependency on the magnetic field curve provided in the fluid's datasheet [2]. The Bingham plastic model is used commonly in MR fluids applications [3,4].

Two actuator torques were calculated, the first for the rotation of the rotor around the vertical axis (T_z), and the other for rotation around a horizontal axis (T_{xy}).

For the optimisation, an OF was constructed with the help of a reference model, as in [5]. The aim was

to minimise the actuator's size and maximise its breaking torque. The OF was composed as shown by the following equation:

$$OF = w_1/2\ ((T_{zref} - T_z)/T_{zref} + ((T_{xyref} - T_{xy})/T_{xyref}) + w_2/2\ ((R - R_{ref})/R_{ref} + ((H_{ref} - H_{ref})/H_{ref}) \quad (1)$$

Here, w_1 and w_2 are the weights for each part of the OF, R is the actuator's radius, and H is the stator's height. T_{zref}, T_{xyref}, H_{ref} and R_{ref} are the torques, height and radius of the reference actuator. Priority was given to the actuator size with $w_1 = 0.25$ and $w_2 = 0.75$.

A grid of models was built for different combinations of R and H values. For R, values between 30 mm and 50 mm with a step of 4 mm were used, while, for H, values between 37 mm and 50 mm were used, with a step of 2.6 mm. The OF value was calculated for each model, and a two-variable polynomial function was fitted to the result. The minimum of the polynomial represented the optimised model. R and H values at the minimal polynomial value were used to build the final model.

The results were compared to a grid search, with the step between R values reduced to 2 mm and the step between H values reduced to 1.3 mm.

3. Results

The reference model was built first. The resulting values were: $T_{zref} = 2.7329$ Nm, $T_{xyref} = 2.2631$ Nm, $R_{ref} = 40$ mm, and $H_{ref} = 43.5$ mm. 38 models were built, including the reference model, 36 in the grid, and the final model. The time required to build 38 models was around 403 min (~6.7 h). The computer used has an Intel Xeon W-2245 (3.90 GHz) processor and 64 GB of memory. The best model from the grid was OF = - 0.1101 at $R = 32$ mm and $H = 37$ mm. Two fit functions were used. First, a third-degree polynomial predicted the best model at $R = 30.32$ mm and $H = 37$ mm, with the value OF = - 0.1103. The final model was built with predicted R and H values that gave OF = - 0.1105. Second, a fourth-degree polynomial predicted the best model at $R = 36.19$ mm and $H = 37$ mm with the value OF = - 0.1133. The final model gave OF = - 0.1128.

The results were compared to the grid search results. The total number of models built during the sweep was 122 (reference model plus 121 models in the grid). The time required was around 1300 min (~21.7 h). The best model had the value OF = - 0.1130 at $R = 36$ mm and $H = 37$ mm. The approach using a fit function took significantly less time to complete (less than a third of the time required for the parameter sweep). All the approaches gave the same H value of 37 mm. The grid search gave the best resulting OF value at $R = 36$ mm. The second fit function came close at $R = 36.19$ mm (~0.5 % difference), and the first fit function was at $R = 30.32$ mm (~16 % difference to grid search).

4. Conclusions

The grid search gave a slightly better result than the fitting approach. A significant advantage of the fitting approach is the time consumption, which was around 69 % better than the grid search, satisfying the goal of faster optimisation. A weakness of the fitting approach is selecting a suitable fitting function. Selecting an unsuitable function can lead to impractical results.

For the future, the goal is to combine the fitting approach with an Evolutionary Algorithm.

References

[1] H. Eshgarf, A. Ahmadi Nadooshan, A. Raisi, (2022), "An overview on properties and applications of magnetorheological fluids: Dampers, batteries, valves and brakes", *J. Energy Storage, vol. 50, p. 104648, doi: 10.1016/j.est.2022.104648.*

[2] Arus MR Tech`, "MAGNAFLO." Accessed: Mar. 21, 2023. [Online]. Available: https://arusmrtech.com/wp-content/uploads/2021/11/MAGNAFLO.pdf

[3] D. Senkal, H. Gurocak, (2009), "Spherical Brake with MR Fluid as Multi Degree of Freedom Actuator for Haptics", *J. Intell. Mater. Syst. Struct.*, vol. 20, no. 18, pp. 2149–2160, Dec. 2009, doi: 10.1177/1045389X09348925.

[4] K. Karakoc, E. J. Park, A. Suleman, (2008), "Design considerations for an automotive magnetorheological brake", *Mechatronics*, vol. 18, no. 8, pp. 434–447, doi: 10.1016/j.mechatronics.2008.02.003.

[5] J. Vizjak, A. Hamler, M. Jesenik, (2023), "Design and Optimization of a Spherical Magnetorheological Actuator", *Mathematics*, vol. 11, no. 19, doi: 10.3390/math11194098.

Regarding the issue of computing the magnetic field effect on an energized ferromagnetic conductor

Mykhaylo Zagirnyak

Kremenchuk Mykhailo Ostrohradskyi National University

Introduction

Currently, various methods exist for computing the constant magnetic field impact on magnetically responsive bodies. These methods include integrating the force density over the volume of the body determined by models such as molecular currents (denoted as $\bar{j}_m = rot\bar{M}$) or magnetic charges (denoted as $\rho_m = -\mu_0 div\bar{M}$) distributed within the substance. Here $\bar{M}$ – the vector of the magnetization of the substance, μ_0 is the magnetic constant. Both methods yield equivalent results when calculating the total magnetic force on bodies devoid of electric conduction currents within their volume.

The purpose of the paper

The purpose of the paper is to show by way of a simple example that the integral equivalence for the indicated methods of modeling the magnetized state of a substance is not preserved if conduction electric currents flow in the volume of the body on which the force action of a constant magnetic field is determined.

Problem statement

Let us examine a linear energized conductor composed of a material possessing magnetic properties. This conductor is positioned within a uniform magnetic field characterized by induction $\bar{B}_0$, which is directed perpendicular to the conductor axis (Fig. 1).

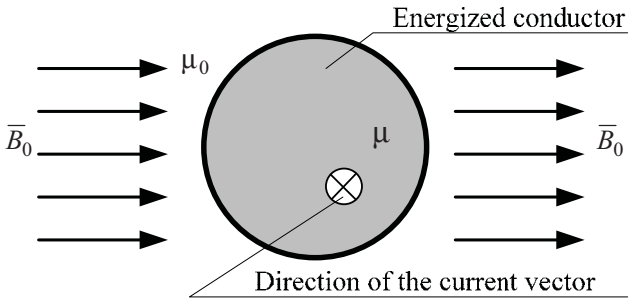

Fig. 1. A conducting material possessing magnetic properties and subjected to a uniform magnetic field while carrying an electric current

For any arbitrary external magnetic field, it is evident that the overall force acting on an alive magnetic conductor within an external magnetic field (referred to as force $\bar{F}_\Sigma$) can be decomposed into two distinct forces: $\bar{F}_1$, which represents the force exerted on the electric current within the conductor, and

$\overline{F}_2$, which signifies the force acting on the magnetized substance of the conductor. The purpose of this paper is to tackle the calculation of this force component for two different models characterizing the magnetized state of matter – the model of equivalent magnetizing currents and the model of equivalent magnetic charges – in order to compare the resultant outcomes.

Determining the force exerted on a magnetized substance using both the model of equivalent magnetic charges and the model of equivalent magnetizing currents

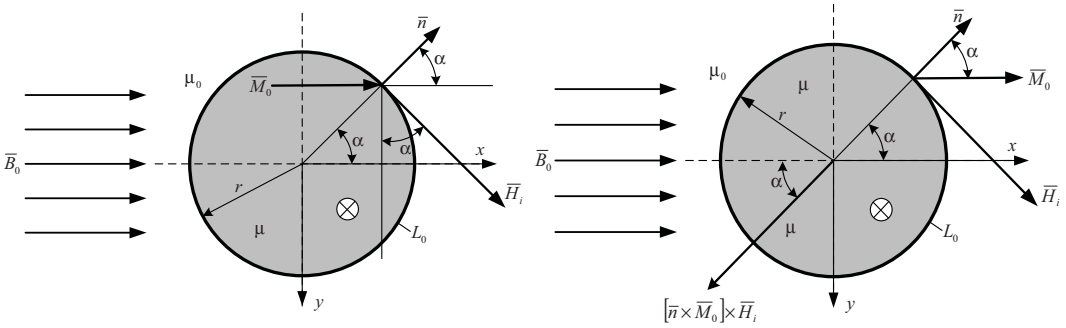

Fig. 2. Regarding the computation of the force acting on a magnetic substance based on both the model of equivalent magnetic charges (a) and the model of equivalent magnetizing currents (b)

The consideration of the components of the force on the magnetic substance of the conductor on the side of the magnetic field of the current makes it possible to get the expression for the magnetization of the conductor

$$\overline{M}_0 = 2\frac{\mu-\mu_0}{\mu_0(\mu+\mu_0)}\overline{B}_0 .$$

Using several mathematical representations this formula allows obtaining the following expressions for the considering forces on the magnetized substance of the conductor according to both models:
equivalent magnetic charges

$$f_y = iB_0\frac{\mu-\mu_0}{\mu+\mu_0}, \tag{1}$$

equivalent magnetizing currents

$$f_y = -iB_0\frac{\mu-\mu_0}{\mu+\mu_0} . \tag{2}$$

Discussion of the obtained results

Based on the preceding discussion, both the model of equivalent magnetizing currents and the model of equivalent magnetic charges reveal a non-zero force on the magnetic substance within the researched conductor. Furthermore, as follows from equations (1) and (2) for both models, the force density (specific force) acting on the magnetic substance is identical in magnitude but opposite in direction. This indicates a lack of integral equivalence when determining the overall force on a body made of magnetic material, a condition noted in the Introduction to occur in the absence of electric currents within magnetic substances. Consequently, given the expectation of both models yielding the same result for the total force on the energized conductor, the computation of the force on the current within the conductor using these models will produce divergent outcomes, ensuring the balance of forces acting on the current and the magnetic substance. The acknowledgment of conflicting formulas, as highlighted in [1], leaves the inquiry into the physical origins of electromagnetic forces in magnets unresolved. Hence, the query posed by A. Einstein [2] regarding the methodology for determining the force on current within a magnetic substance remains pertinent.

Conclusion

Integral equivalence between models representing the magnetized state (specifically, equivalent magnetizing currents and equivalent magnetic charges) is found not to be maintained when assessing the overall force on a magnetized substance within a body carrying an electric current. Consequently, addressing the impact of the magnetic field force on an electric current within a body composed of magnetized material necessitates an additional solution to the problem.

References

[1] Tsybulevskii F.I., On the calculation of the forces acting on energized magnetics in a magnetic field, Russian Electromechanics. (1991), No. 1, 5-11. (Rus)

[2] Einstein A., On ponderomotive forces acting on ferromagnetic energized conductors in magnetic field: Einstein A. Collection of research papers. In 4 v. V. 3. M.: Nauka, 1966. P. 240-241. (Rus).

Prospective designs of traction motors in new concepts of electric cars

Mykhaylo Zagirnyak[1], Viacheslav Prus[1], Mohamed Zaidan QAWAQZEH[2]

[1] Kremenchuk Mykhailo Ostrohradskyi National University, Kremenchuk, Ukraine

[2] Al-Balqa' Applied University, Al-Salt, Jordan

Introduction

The peculiarity of the development of modern automotive industry consists in the environmental aspect, which, first of all, involves participation in the general striving of mankind for the reduction of carbon emissions. Such a task can be fully solved only by means of effective generation during the production of electric energy and its effective transformation during consumption. Providing the necessary conditions for recycling cars and their structural parts is the second important issue.

The greatest reduction in CO_2 emissions is ensured, all things being equal, when using electric cars. Compared to gasoline analogues, it makes from 27.2% when electricity is generated exclusively from fossil fuels to 54.4% when using mixed sources of generation for the conditions of the European Union. The trend towards their further reduction implies an increase in the percentage of components from nuclear generation (a decrease of 98.4%) and wind energy (today it is considered a point of zero emission) in the total production of electricity [1].

In terms of energy use, the further increase of electric car efficiency in the main operating modes is the task of creating new concepts. At the same time, the electric car must preserve the advantages inherent in this type of transport, such as instant access to the maximum value of the torque and its easy control, the possibility of recuperating braking energy, the low weight of the traction electric motor, its high controllability, low noise level and others.

From this position, when developing new concepts of modern electric cars and improving hybrid models, the main attention should be paid to the justification, calculations and design of electric traction motors, which develop the mentioned advantages and in a certain way compensate for the shortcomings of existing solutions [2]. This is the purpose of this paper.

Materials and research results

DC and AC electric motors are used as traction motors in various models of electric cars. Among them, induction, synchronous with permanent magnets excitation, DC brushed motors and controlled by power switches, brushless motors are primarily distinguished. Their main advantages and disadvantages are summarized in Table 1.

According to the results of a comparative analysis of the main types of traction motors of electric cars, two promising designs were identified, the improvement of which has prospects in terms of development and improvement when working as part of the central drive: IMSCR and permanent magnet synchronous reactive motor (PMaSynRM) [3]. The direction of development of the first design is determined by the transition to the combined winding of the "slavyanka" type, which allows a significant increase of the torque and the equivalent efficiency of the motor, that is, compensation for its main shortcomings. This requires recalculations of electric and magnetic circuits for the indicated type of winding. The basic design of PMaSynRM involves the use of strong NdFeB magnets, which contain expensive rare earth materials. Therefore, its modernization pursues the goal of optimizing the magnetic system in order to replace or reduce the specific weight of such magnets in the structure. Such a solution requires an increase in the supply voltage, which will negatively affect the current density in the stator and rotor windings and lead to a deterioration of the motor's thermal mode. This determines the need for

calculations of component losses, energy indicators and temperature modes and fields. These measures make it possible to improve the simplest designs of traction motors in order to improve their energy efficiency and reliability [4].

Table 1. Comparative characteristics of the main types of traction motors of electric cars

Traction motor type	Advantages of use in electric motors	Disadvantages of use in electric motors	Scope of application
Induction motor with a short-circuited rotor (IMSCR)	Simplicity of design; low price; high manufacturability; high reliability; long service life; low weight	Low starting torque; high starting current; low efficiency at underload (30-35%);	Traction motor of modern electric cars models with control from a frequency converter (Tesla S and others)
Synchronous motor with permanent magnets (SM)	High overload capacity by moment; high efficiency (over 90%); the possibility of adjusting the reactive current in the presence of the excitation winding; longer service life; high reliability; maximum recovery of braking energy; complete safety when towing	The presence of expensive rare earth magnets; low inductance of the stator winding; the presence of a sensor of the absolute position of the rotor; complex control system; the use of a high-speed inverter	A promising traction motor of modern models of electric cars (Tesla X and others)
DC brushed motor (DCM)	Wide adjustment range; high overload capacity; ease and smoothness of adjustment	Low reliability; high overall indicators; the lowest performance indicators	As part of the combined traction unit of the first concepts of modern electric cars, for energy-saving movement outside the city
DC/AC brushless motor (BLDC/PMSM)	The largest resource; unpretentiousness in service; high speed in transient modes; the widest adjustment range; high starting torque and overload capacity; low starting current and no-load current; the best mode indicators of energy efficiency (more than 90%)	Complex control algorithms; uncertainty of the system in the event of a malfunction of the rotor position sensors; high cost and low reliability	Mainly in motor-wheel drives of electric cars and city transport of low relative power (Subaru, Toyota Bz 4 X, Lexus EV and others)

Conclusions

In the course of the research, prospective designs of traction motors of electric cars were substantiated and ways of their further improvement were determined in order to improve energy efficiency and reliability indicators under the condition of reducing the cost price.

References

[1] Global EV Outlook 2024, Moving towards increased affordability International Energy Agency Report, https://www.i.e.a.org/reports/global-ev-outlook-2024/trends-in-electric-cars
[2] John M. Miller, Propulsion Systems for Hybrid Vehicles. IET, 2004.
[3] Gianmario Pellegrino, Thomas M. Jahns, Nicola Bianchi, Wen L. Soong, Francesco Cupertino, The Rediscovery of Synchronous Reluctance and Ferrite Permanent Magnet Motors. Springer International Publishing, 2016.
[4] Ned Mohan, Siddharth Raju, Analysis and Control of Electric Drives: Simulations and Laboratory. Wiley, 2021.

9th International Symposium on Applied Electromagnetics SAEM 2024

ISBN 978-83-88131-07-3